Lawrence Berkeley Laboratory
UNIVERSITY OF CALIFORNIA

Materials & Molecular Research Division

STUDIES ON ZINC NODULES ELECTRODEPOSITED FROM ACID ELECTROLYTES

R. Anderson* and C.W. Tobias
(*M.S. Thesis)

December 1984

Prepared for the U.S. Department of Energy under Contract DE-AC03-76SF00098

LBL-18646

STUDIES ON ZINC NODULES ELECTRODEPOSITED FROM ACID ELECTROLYTES

Rolfe Anderson

with Charles W. Tobias

Materials and Molecular Research Division
Lawrence Berkeley Laboratory
and
Department of Chemical Engineering
University of California
Berkeley, California 94720

This work was supported by the Assistant Secretary for
Conservation and Renewable Energy,
Office of Energy Systems Research,
Energy Storage Division of the U. S. Department of Energy
under Contract No. DE-AC03-76SF00098

TABLE OF CONTENTS

STUDIES ON ZINC NODULES ELECTRODEPOSITED FROM ACID ELECTROLYTES

Rolfe C. Anderson

with Charles W. Tobias

Materials and Molecular Research Division
Lawrence Berkeley Laboratory
and
Department of Chemical Engineering
University of California
Berkeley, California 94720

ABSTRACT

The development of morphology of electrodeposited zinc was investigated by studying the initial stages of deposition. Zinc was deposited galvanostatically from 1.0 M $ZnCl_2$ electrolyte ($0.7 < pH < 4.6$) on rotating disc electrodes at current densities from 5 to 130 ma/cm^2. Pine glassy carbon, Union Carbide pyrolytic graphite, Gould pyrolytic graphite, Exxon graphite loaded polymer, and platinum substrates were used. The number densities of nodules (diameter greater than 1 μm), typically encountered during incipient morphological development, were measured using scanning electron microscopy, and image analysis. Nodule densities up to 7×10^4 $nodules/mm^2$ were measured. Results may be summarized as follows:

1) Nucleation processes were discernable through cyclic voltammetry.

2) Potential step kinetic measurements yielded exchange current densities on the order of 1 ma/cm^2.

3) The nodule density increased with surface overpotential at a rate from 200 to 1000 $nodules/mm^2 \times mv$.

4) The potential between the working and reference electrodes exhibited a transient potential peak during the first few seconds of deposition. The relative magnitude of the peak potential is inversely related to the number of available nucleation sites.

5) A parallel exists between the magnitude of this peak and the number density of nodules on a given substrate. Substrates rank in order to decreasing activity towards zinc nucleation:

- Union Carbide HOPG pyrolytic graphite
- platinum
- Gould pyrolytic graphite
- Exxon graphite loaded polymer and Pine glassy carbon

I. INTRODUCTION

I.A. Purpose of Study

Convection causes a flow imprint on the macromorphology of many electrodeposited metals. Striated or grooved deposits are formed by copper, silver, nickel, and zinc during electrodeposition in the presence of forced convection (1). The impetus behind this study originates from similar morphological problems encountered in zinc halide secondary batteries. Striations in the direction of flow are formed during battery charging—or zinc deposition. Details concerning zinc halide secondary batteries are given by Faltemier (2), while observations of striated deposits have already been reported by Jaksic (51), Tsuda (6) and Faltemier (2).

In general morphological development is a complex phenomenon which often results in intricate three dimensional shapes. Electrodeposits are therefore difficult to characterize quantitatively; often researchers are limited to qualitative methods. It is the goal of this study to advance a more quantitative understanding of the development of surface textures during electrodeposition of zinc from acid electrolytes.

I.B. Background

It is often difficult to form smooth electrodeposits of metals. Most metals will form rough deposits if plated for a long enough time (1). Severe roughness may take the form of dendritic and/or striated (grooved) deposits. The current development of acid zinc battery systems lends particular importance to zinc electrodeposition from acid electrolytes (for details see Faltemier's thesis) (2,3,4,21). In such

batteries, zinc deposits on the negative electrode during battery charging and dissolves during discharge. The formation of dendrites and striae can limit the battery's capacity and cycle life (i.e., cause shorting). In this battery system the electrodeposition and dissolution take place in the presence of forced convection.

The effect of convective flow on metallic electrodeposition has been investigated in this laboratory since the 1950's. Beginning in 1976 Jaksic, followed by Faltemier, Kommenic, and Tsuda performed numerous flow cell and rotating disk electrode experiments involving electrodeposition from $ZnCl_2$ electrolytes. Jaksic, and later Faltemier, varied zinc concentration, pH, amount of charge passed, Reynolds number, and current density during electrodeposition on rotating disc electrodes and in a flow cell and observed the consequences on deposit development and appearance (2). They noted that striae, or grooves, formed in the direction of flow when the current density was below 80 ± 10 ma/cm^2 for 1M $ZnCl_2$ electrolyte and below 15 ± 2 ma/cm^2 for 1 M $ZnSO_4$ electrolyte. The $ZnCl_2$ concentration was varied between 0.5 and 4 M and the pH varied from 1.9 to 5.0 by addition of HCl. Also, $ZnSO_4$ was used as the electrolyte to investigate morphology in the absence of ionic complexing. It was found that zinc concentration, electrolyte type (complexing/non-complexing), pH, substrate and surface preparation each had only weak effects on the evolution and final appearance of the deposit. An increase in the Reynolds number caused the striae to develop and propagate more rapidly along the electrode. Faltemier employed in-situ photography and used long (30 cm) electrodes to investigate consequences of leading edge effects. Smooth deposits were obtained through the use of

pulsed current electrodeposition by both Faltemier and Tsuda.

The evolution of striations was studied by varying time of deposition. Figure 1.1 shows the steps observed during morphological development from nodule formation (A), preferred growth (B), and finally propagation of striae in the direction of flow (C).

This author determined the striation densities from photographs of deposits formed in flow cell experiments of Faltemier et al. (2). With increasing time of deposition, coalescence or melding of the striae occurs; this effect is shown in Figures 1.2 and 1.3. Striation densities corresponding to various current densities are shown in Figures 1.4 and 1.5. Striation density unquestionably increases with current density, although the data are too sparse to make a detailed conclusion. Yee and Jorne (5) reported more detailed results from experiments with rotating disc and rotating hemisphere electrodes. They found that the striation density increased significantly with current density. These authors used a Chernov bulk diffusion model to elucidate the relationship between current density and striation density by considering only mass transport to line sinks.

In this laboratory from 1980 to 1981 Tsuda (6) studied the effects of current density, rotation speed, pulsed current, and concentration of lead ions on acid zinc electrodeposition using rotating disc electrodes. His results were in general agreement with previous workers in this laboratory. Tsuda noticed no variations in the shape or number of spirals formed with the addition of lead ions but observed that the induction time (before spirals became visible) decreased as the concentration of lead ions was increased. More importantly he found that lead

ions inhibited nucleation of zinc on a platinum substrate; the average size of initial protrusions increased but their number over a given area decreased. Also, Tsuda noted that as the current density increased the number of initial protrusions over a given area increased, accompanied by a decrease in their average size.

McBreen and Gannon (7) studied zinc electrodeposition from both $ZnBr_2$ and $ZnCl_2$ electrolytes. They carried out their studies in very high purity electrolytes prepared from 99.9999% zinc and in a cell which was specially designed to assure uniform current distribution. They deposited zinc potentiostatically on glassy carbon and found that the resulting current transient could be fit to a model involving instantaneous nucleation of three-dimensional centers followed by growth of right circular cones under kinetic control. McBreen and Gannon defined the term "nucleation overvoltage," as the lowest overpotential which, when stepped to, results in a current response within a 30 minute period (8). The nucleation overvoltages were reported to be 17 mv for 3 M $ZnCl_2$ and 12 mv for 3 M $ZnBr_2$ on glassy carbon. No nucleation overvoltage was observed when zinc was used as the initial substrate. Also, they noted a decrease in the growth rate constants by as much as two orders of magnitude in response to an addition of 10^{-4} M lead or bismuth ions. McBreen and Gannon reported a current efficiency of $\approx$100% from weight measurements.

Landau, Cahan, and Selman issued a major report covering theoretical and experimental aspects of electrodeposition from $ZnCl_2$ and $ZnBr_2$ electrolytes (1). This report focuses on the formation and propagation of dendrites. Although the growth mechanisms of dendrites and striae

undoubtably differ, it is likely that the roughening process leading to their initiation is the same. According to these authors the induction time before a dendrite becomes visible is a strong function of overpotential; this delay approaches infinity as the overpotential is decreased towards what is defined as the critical overpotential. This threshold, or critical overpotential decreases with increasing exchange current density but increases in the presence of additives or dendrite inhibitors. One plausible explanation of this considers the effects of ionic hydrogen discharge on the kinetics of zinc electrodeposition.

The codeposition of hydrogen is an interesting explanation for the mechanisms of dendrite inhibition and/or promotion. Although hydrogen evolution accounts for only about 0.2% of the charging current in zinc chloride batteries (9), it might play a dominant role in zinc electrodeposition kinetics. Trace amounts of iron promote hydrogen evolution and dendrite growth. Conversely lead acetate, copper, antimony, and organic surface additives inhibit hydrogen evolution in addition to suppressing dendrite formation. This is borne out by Tsuda's results according to which lead ions inhibited the formation of initial protrusions. Other researchers have reported evidence indicating the incorporation of hydrogen in the electrodeposited zinc lattice (10,11).

The possibility of hydrogen codeposition may explain disagreements in the literature over the Butler-Volmer kinetic parameters for this system. Landau et al. (1) reported experimental work performed to determine mass transport and kinetic parameters in this system. Working with Landau, Ashtok and Lee investigated the kinetics of electrodeposition from $ZnCl_2$ and $ZnBr_2$ electrolytes using both relaxation and steady

state methods in a rotating hemisphere system. Despite considerable care taken to establish well defined conditions, the results were inconclusive. They estimated the exchange current density and cathodic transfer coefficient for deposition from both $ZnCl_2$ and $ZnBr_2$ solutions as follows:

$$i_o \approx 1 \text{ to } 5 \text{ ma/cm}^2$$

$$\alpha_c \approx 0.5 \qquad (1.1)$$

This exchange current density is much lower than some literature values. Table 1.1 shows the kinetic parameters for zinc electrodeposition reported by various investigators.

Selman, Namjoshi and Lee also investigated mass transport properties of the zinc ion. A dropping mercury electrode was used to measure the effective ionic diffusivity of zinc in various KCl supported electrolytes. Electrolyte concentrations from 0.1 to 3.0 M $ZnCl_2$ and $ZnBr_2$ in 3 M KCl gave effective ionic diffusivities of 14.1 to 3.3×10^{-6} cm^2/s. These values may be compared to others in the literature shown in Table 1.2. Rajhanbah et al. (120) used limiting current measurements on a rotating disk electrode to determine effective ionic diffusivities of the zinc ion in $ZnCl_2$ electrolytes; these results are also shown in Table 1.2.

The electrocrystallization of zinc is not well understood. In particular, it is not known what factors determine the evolving surface morphology. Work in this laboratory has focused on characterizing conditions in which striae are formed and determining the mechanisms involved in their formation. Several proposed mechanisms are described in

Faltemier's thesis (2). The most plausible hypothesis was forwarded by Jaksic and Tobias (45,46,47) and later Tsuda (6). In this mechanism, disturbance of the concentration field in the wake of a principal nodule results in enhanced nucleation and surface roughening. This occurs because of a modest increase in the surface overpotential inside the wake. Growth of these roughness elements is further enhanced due to both mass transfer and ohmic effects. Tsuda (6) showed a strong influence of current density on the frequency of initial protrusions on platinum. The central purpose of this work is to establish a relationship between surface overpotential and number density of nodules for the electrodeposition of zinc from $ZnCl_2$ electrolytes.

I.C. Scope of Study

The electrodeposition of zinc from acid electrolytes in the presence of forced convection results in the formation of grooved, or striated deposits over a wide range of experimental conditions. This investigation addresses the dependence of the formation of nodules, precursors to the developing macro morphology, on current density, overpotential, and nature of substrate.

The primary goal of this study is to experimentally determine the number density of zinc nodules electrodeposited from 1.0 M $ZnCl_2$ electrolyte and relate this to current density and surface overpotential. Grown nuclei, or nodules, deposited on platinum, pyrolitic graphites, glassy (vitreous) carbon and a proprietary graphite loaded polymer (Exxon) are photographed using Scanning Electron Microscopy (SEM). The SEM photographs are subsequently processed by an image analyzer to measure the nodule number densities. Cyclic voltammetry, potential step, and

galvanostatic experiments are performed to further characterize the zinc electrodeposition process and the relative activities of various substrates with respect to zinc deposition.

Table 1.1. Kinetic parameters for the electrodeposition of zinc from halide solutions.

Reference	Anion	pH	i_o or i^*_{oo} at 1 M (ma/cm^2)	α_c
Hurlen (13)	Cl^-	3	io_{oo} = 700	0.5
Alcazar and Harrison (14)	Cl^-	3.5	i_o = 0.52 at 0.01M	0.5-1
Kim and Jorne (15)	Cl^-	2	i_{oo} = 1.75	~0.5
Edmund and White (16)	?	?	i_{oo} = 44	~0.5
Ashtok and Lee (1)	Br^- Cl^-	3.5 4.9	i_o = 0.5 to 12	~0.5
Hauser and Newman (17)	Cl^-	0	i_o** = 3.8	~0.5

*$i_{oo} = i_o \times c'/(c_{ox}^{\alpha} \times c_{red}^{1-\alpha})$; where c' is unit concentration (48).

**Corrosion current on a rotating zinc disc in 1.0 M HCl.

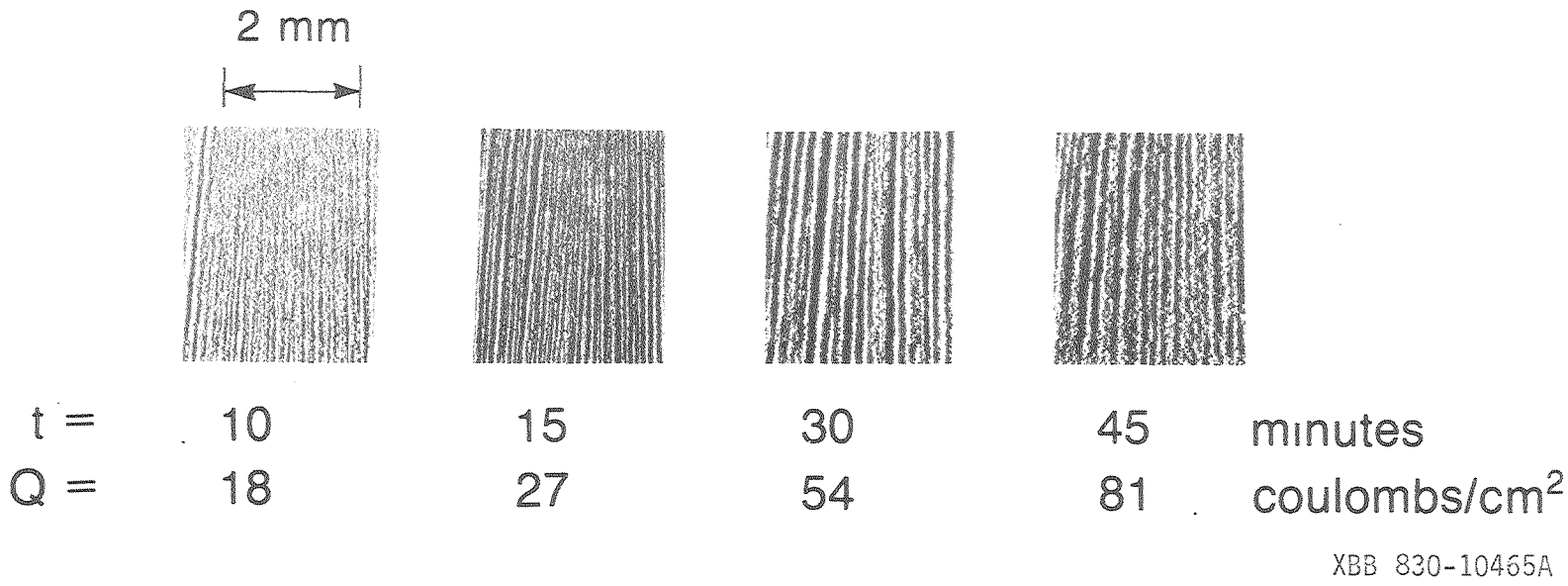

Fig. 1.2 Effect of time of deposition on the number density of striations (from experiments by Jaksic and Faltemier).

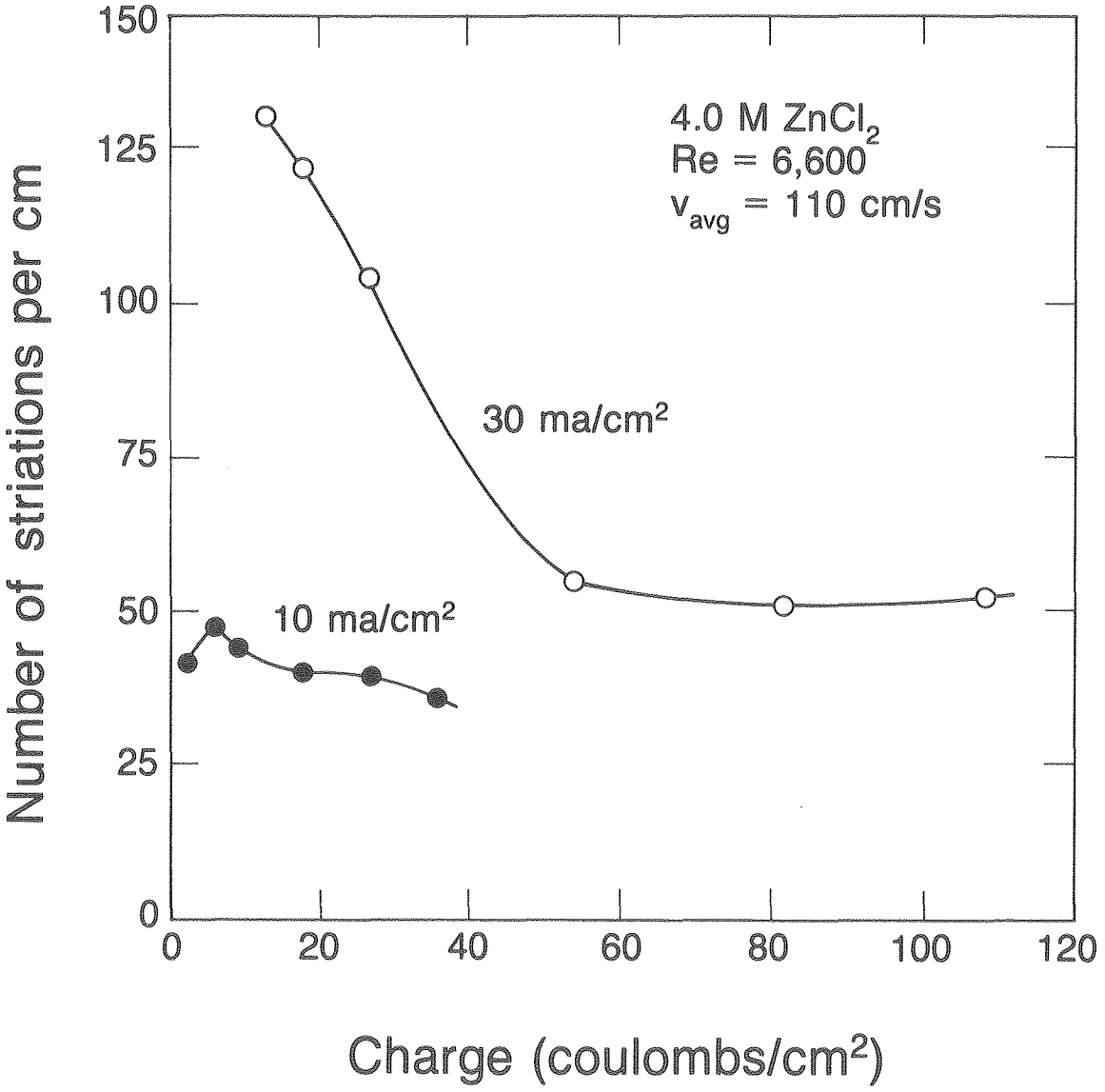

XBL 8311-7348

Fig. 1.3 Effect of time of deposition on the number density of striations (from experiments by Jaksic and Faltemier).

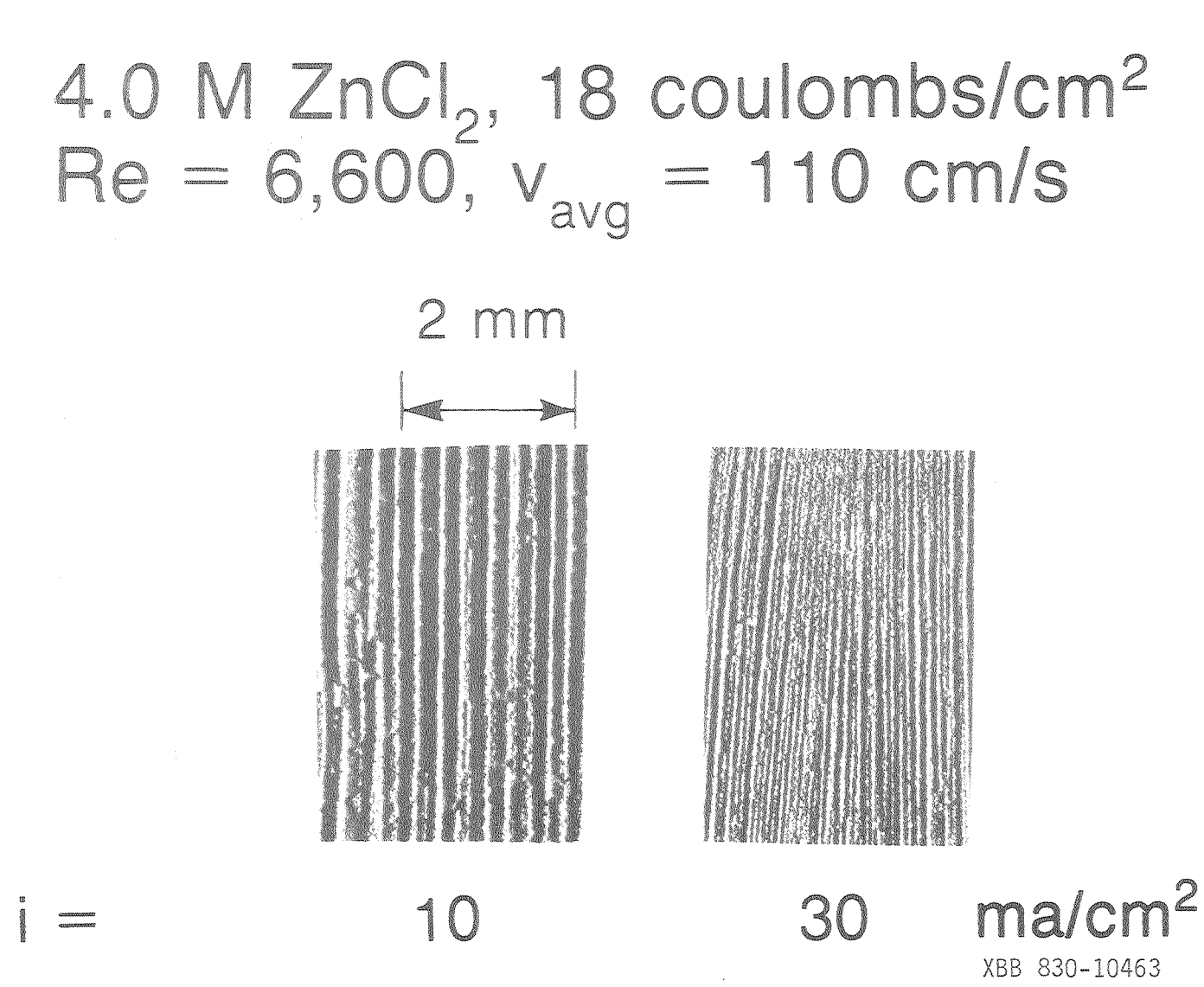

Fig. 1.4 Effect of current density on the number density of striations (from experiments by Jaksic and Faltemier).

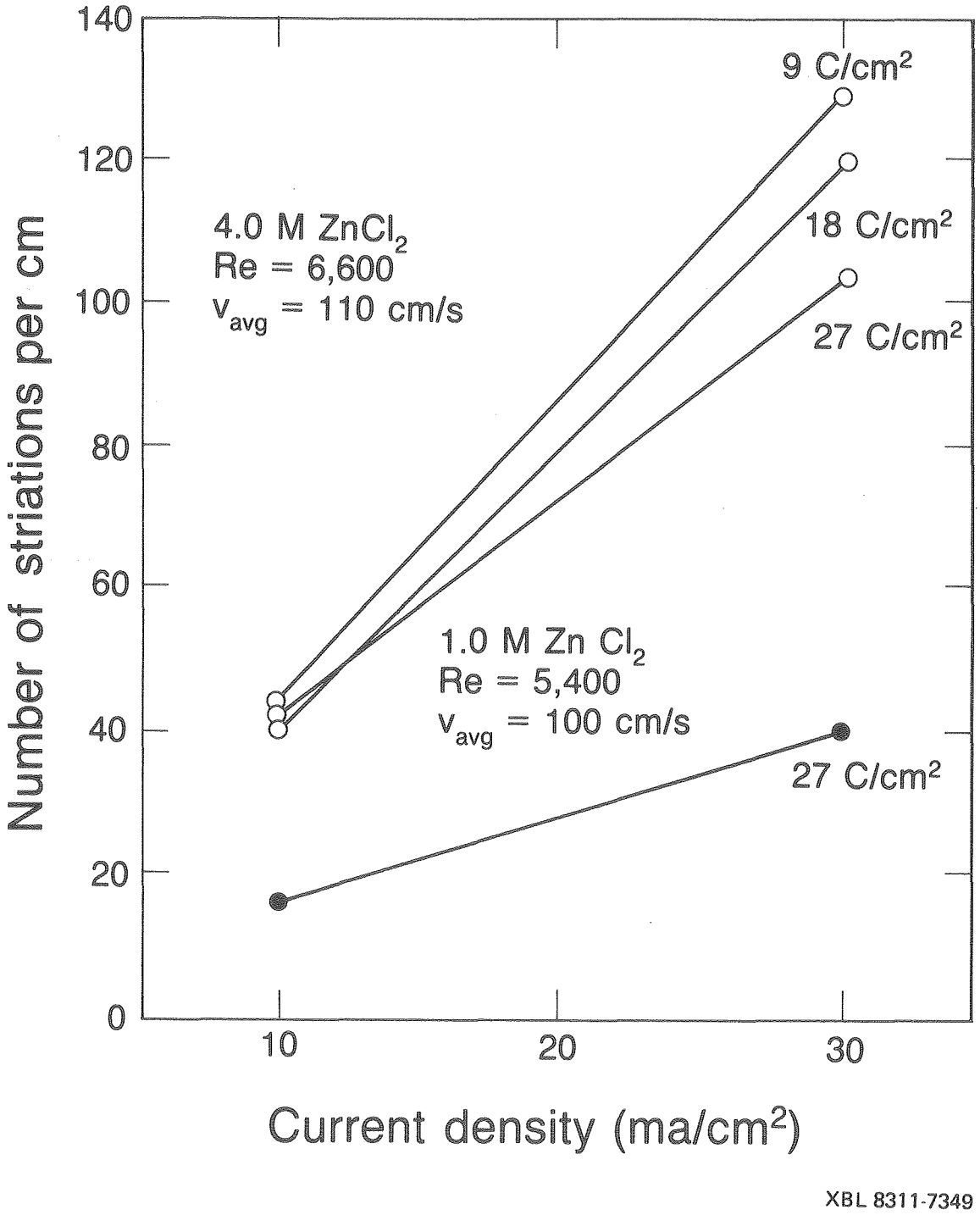

Fig. 1.5 Effect of current density on the number density of striations (from experiments by Jaksic and Faltemier).

II. EXPERIMENTAL

II.A. Apparatus and Materials

II.A.1. Electrolysis Cell

The electrochemical cell employed in these studies is shown in Figure 2.1. This Pyrex glass cell consists of two compartments connected by a Pyrex fritted glass plug. A platinum foil counter electrode occupies the smaller compartment; this separation helps to avoid any possible contamination of the main chamber and to isolate chlorine bubbles from the working electrode during deposition. The rotating disc working electrode is located face down in the main chamber. A Luggin tip capillary in the main compartment provides a bridge to a beaker containing a saturated calomel reference electrode. The same electrolyte was used in each of the three chambers.

II.A.2. Instrumentation

The experiments were conducted using the equipment listed below.

1. PAR Model 371 Potentiostat-Galvanostat with Model 178 Electrometer Probe
2. PAR Model 175 Universal Programmer
3. Keithly Model 173A Digital Multimeter
4. Gould Model 7056 XY Recorder
5. Tektronix Model 5111 Storage Oscilloscope
6. Pine ASR2 Analytical Rotator and Speed Controller
7. AIS Model BA-1 Reference Electrode Buffer Amplifier

8. A dual reed switch circuit, constructed in house, which was used in conjunction with the Universal Programmer and Potentiostat-Galvanostat to provide automatic switching between potentiostatic and galvanostatic modes.

9. Corning Model 130 pH Meter

10. PAR Model 173 Potentiostat-Galvanostat with Model 179 Digital Coulometer Module.

11. Polaron Model E5100 SEM Coating Unit

12. Varian Model VE10 Vacuum Evaporator

13. ESI Model 253 Impedance Meter with Yellow Springs Model 3403 Conductivity Cell

14. Corning Model 476001 Saturated Calomel Reference Electrode

II.A.3. Electrolyte

The electrolytes were prepared using one or more of the following reagents and water distilled in a Corning Water Distillation Apparatus (Model AG-21).

1. $ZnCl_2$: Mallinckrodt, Analytical Reagent

   lot analysis given:

   Fe passes test
   Pb 0.001%

   independent chemical analysis:

   Fe less than 0.001 ug/cc
   Pb 0.7 ug/cc

   (see Appendix H for a more complete independent chemical analysis of reagent)

2. $ZnCl_2$: MCB Reagents, EM Industries

   maximum impurity levels given:

   Fe 0.001%
   Pb 0.005%

   independent chemical analysis:

   Fe less than 0.01 ug/cc
   Pb 0.3 ug/cc

3. HCl: J.F. Baker Chemical, Analytical Concentrate Dilute-It (1 N HCl)

4. KCl: Mallinckrodt, Analytical Reagent

II.A.4. Electrodes

Experiments were performed on the following substrates: platinum, single crystal zinc, pyrolytic graphite, glassy (vitreous) carbon, and graphite loaded polymer. The terms designating different types of carbonaceous materials have led to some confusion in industry and the literature. Brief descriptions of these materials are given below (22).

graphite

Lattice structure involves layer stacking—material is anisotropic.

pyrolytic graphite

Graphite powder and a phenolic resin binder are graphitized by heating. Material is non-porous; its qualities depend upon the binder used.

glassy (or vitreous) carbon

Cyclization and ring fusion polymers of phenol aldehyde, novolac, and resole types (high degree of crosslinking) are degraded while compressed at temperatures up to 2000°C. Extensive crosslinking prevents rearrangement. Material is black, nonporous, extremely hard, and resistant to oxidation.

graphite loaded polymers conductive carbon plastics

Graphite powder is added to a polymer and extruded (23).

Details concerning the various substrate discs shown in Figure 2.2 are given below.

traphite loaded polymer

D = 11.1 mm; A = 0.97 cm^2

Exxon Research and Engineering provided these samples which are identical to those currently used in their $ZnBr_2$ batteries. Oversized discs were punched from sample sheets and machined on a lathe to the final diameter.

pyrolitic graphite

Union Carbide HOPG: D = 11.4 mm; A = 1.02 cm^2

Gould: D = 11.2 mm; A = 0.98 cm^2

The Union Carbide pyrolytic graphite electrodes were previously fabricated in this lab. Gould Research and Development provided different pyrolytic graphite samples which were equivalent to zinc electrodes used in their batteries. Small hexagons cut from the brittle sheets were machined to a round shape on a lathe.

platinum

D = 14.5 mm ; A = 1.65 cm^2

The platinum rotating disc electrodes were fabricated by Tsuda in this laboratory.

glassy carbon

D = 7.8 mm ; A = 0.48 cm^2

The glassy carbon electrode was fabricated by Pine Instruments Inc.

single crystal zinc

D = 9.2 mm; A = 0.64 cm^2

Discs were cut using an EDM (Electrical Discharge Machine) and a circular cutting tool from a 99.999% zinc slab which was previously oriented in the 1000 plane also using the EDM. (Orion Chemical Co.) (24).

Two types of mounts, fabricated in house, are depicted in Figure 2.3. In the first type the substrate disks were silver epoxied to a threaded brass mount. This was then set into non-conducting epoxy which was oven cured and subsequently machined to the appropriate size and shape on a lathe. All substrates except graphite loaded polymer were mounted in this manner.

The second type of mount was designed for replaceable substrates. This was necessary for the graphite loaded polymer samples which were not amenable to mechanical polishing. A tapered brass mount was used as a dummy while the epoxy was molded. It was later removed and replaced by a shorter brass mount on which a substrate disk was silver epoxied. A tight rubber seal was complimented by the use of insulating lacquer for a leak-free electrode.

II.B. Procedures

II.B.1. Electrolyte Preparation

1.0 M $ZnCl_2$ electrolyte was prepared from MCB reagent salt and used in cyclic voltammetry studies and in the early phases of the nodule studies. The pH of this electrolyte was 4.6. Also, 3.0 M $ZnCl_2$ solutions were used in some of the cyclic voltammetry experiments. It was later

suspected that Mallinckrodt Analytical Reagent contains lower levels of lead and iron impurities than MCB reagent; in reality these impurity levels are roughly equivalent for both reagents (see above and Appendix H). Nonetheless the Mallinckrodt reagent salt was used for the remaining studies. When diluted this reagent salt exhibited cloudiness from zincate formation and therefore required pH adjustment through the addition of HCl. At a pH of 2.08 the cloudiness disappeared. Consequently a 1.0 M solution of this pH was used for the remaining studies except those investigations concerning the effect of ionic hydrogen concentration. In these experiments pH values were varied from from 0.7 to 2.1. Different concentrations of $ZnCl_2$ and additions of KCl were employed in some of the open circuit potential drift studies (see Appendix A).

II.B.2. Electrode Preparation

All substrates except the graphite loaded polymer were polished using 600 grit sandpaper, then 6 μm diamond paste, and finally 1 μm diamond paste. Samples were cleaned between each polishing step in an ultrasonic bath of Liqui-Nox detergent and distilled water; this ensured that particles were not carried to successive polishing steps.

Nodule formation has been proven to be very sensitive to surface contaminants—especially organics and surfactants (see Appendix E); consequently the preparation of a clean electrode is critical. Platinum was electropolished in a solution of 1M KOH and 1M K_2HPO_4 at 300 ma/cm^2 for 30 minutes. Glassy carbon and pyrolytic graphite were soaked in 10% KOH for at least 12 hours, dipped in concentrated nitric acid for one second, rinsed well, and pre-anodized in-situ at +1.0 volts versus SCE for 3 minutes. The single crystal zinc samples were electropolished in a

1:1 solution of 80% phosphoric acid and ethanol for 5 minutes, thoroughly rinsed, and dipped in concentrated phosphoric acid for 1 second. Graphite loaded polymer was washed with ethanol, dipped in concentrated nitric acid, rinsed, and pre-anodized under the same conditions as glassy carbon and pyrolytic graphite. All substrates were rinsed with copious amounts of distilled water and allowed to drain immediately prior to deposition.

II.B.3. Details of Operation

The principal experimental method involved galvanostatic electrodeposition of 0.05 to 1.8 coulombs/cm^2 zinc on a disc electrode rotated at 1000 rpm. Experiments were carried out in a cell open to air and at room temperature (20-25°C). Current densities from 5 to 130 ma/cm^2 were maintained. The potential of the working electrode versus a saturated calomel reference was recorded as a function of time. Figure 2.4 shows the electrical schematic of the interconnection of instruments. Unfortunately when the PAR Model 371 Potentiostat-Galvanostat is used in galvanostatic mode the electrometer probe is disabled. To overcome this difficulty, a high input impedance voltage follower, or buffer was required to monitor the potential. The Universal Programmer was used to provide noise-free stepping of the control current. After deposition the electrode was gently submerged in distilled water, rinsed, and carefully dried with dichlorodifluoromethane.

The PAR Model 173 Potentiostat-Galvanostat and Model 179 Digital Coulometer Probe were used in the kinetic studies. The set-up shown in Figure 2.5 produced the plots of charge passed versus current in the Kinetic Measurement Section.

II.B.4. Examination of Deposits

Photographs of the dried electrode surface were taken using either the AMR Model 1000 or ISI Model DS 130 Scanning Electron Microscope (SEM). Typical magnifications were nominally 300× and 1000×; these translate to objective areas of about 0.06 and 0.003 mm^2 respectively. The majority of the photographs were taken at the disks' center (±0.5 mm).

A Laue x-ray diffractometer was used to test the single crystal zinc substrate after electropolishing.

II.B.5. Estimation of Ohmic Drop

Ohmic potential drop can often obscure electrochemical measurements if not corrected for. In this system, the ohmic overpotential accounted for as much as 80% of the total overpotential between the working and reference electrodes. This ohmic overpotential was mainly due to resistance in the electrolyte between the Luggin tip and the working electrode. It is clear that measured overpotentials must be carefully adjusted for ohmic effects. The value of the ohmic resistance to a disc can be estimated by various methods.

Newman provides theoretical expressions for the resistance between a disc electrode imbedded in an infinite insulating plane and a hemispherical counterelectrode located infinitely far away (27). He derived this value for both primary and uniform current distributions.

in general: $R = (\varepsilon)/(4kr_o)$

where k = solution conductivity (mho/cm),

and r_o = radius of disc.

for primary: $\varepsilon = 1$

for uniform: $\varepsilon = 1.28$ (at center of disc) (2.1)

In a typical experimental situation the resistance would lie somewhere between these two values (27, 28). Tables 2.1 and 2.2 give measured solution conductivities and calculated primary resistances for various substrate discs.

II.B.6. Special Considerations for Nodule Experiments

Experimental nucleation rates are usually either inferred from electrochemical transients or estimated by counting microscopic nodules. To use the former method one must make assumptions concerning nucleus shape and type of growth control. For example Fletcher et al. (25) modelled the electrochemical deposition and growth of hemispherical nuclei under convective diffusive control in response to a potentiostatic step. Clearly this type of method is subject to limitations imposed by the model used.

In contrast, direct observation of microscopic nodules provides straightforward assessment of actual surface developments. Notably, Lacman et al. studied the nucleation of copper on single crystal platinum electrodes (26). Here the nucleation rate must be determined from more than one experiment. In this study direct observation was the method of choice because it requires fewer assumptions.

The choice of the rotating disc electrode brought with it certain complications. In particular the nonuniform current distribution, discussed in the Kinetic Measurement Section, obscured the results. Fortunately, a current density plateau exists at the center of the disc electrode. This is true even for a primary current distribution, the most severe case of nonuniform current density. For this reason the choice was made early in this study to focus attention on the nodules at the center of the disc.

Table 2.1. Measured Solution Conductivities.

Solution	k (mho/cm)
1.0M MCB	0.082
1.0M Mallinckrodt (pH = 2.1)	0.079

Table 2.2. Calculated Resistances to Rotating Disc Electrodes.

Substrate	r_o (mm)	a (cm^2)	PRIMARY RESISTANCE (ohms) (reagents:) MCB	Mallinckrodt
glassy carb.	3.9	0.48	7.8	8.1
s.c. zinc	4.6	0.66	6.6	6.9
graphite loaded polymer	5.6	0.98	5.4	5.7
Gould pyrolytic graphite	5.6	0.98	5.4	5.7
Union Carbide pyrolytic graphite	5.7	1.0	5.3	5.6
Platinum	7.2	1.6	4.2	4.4

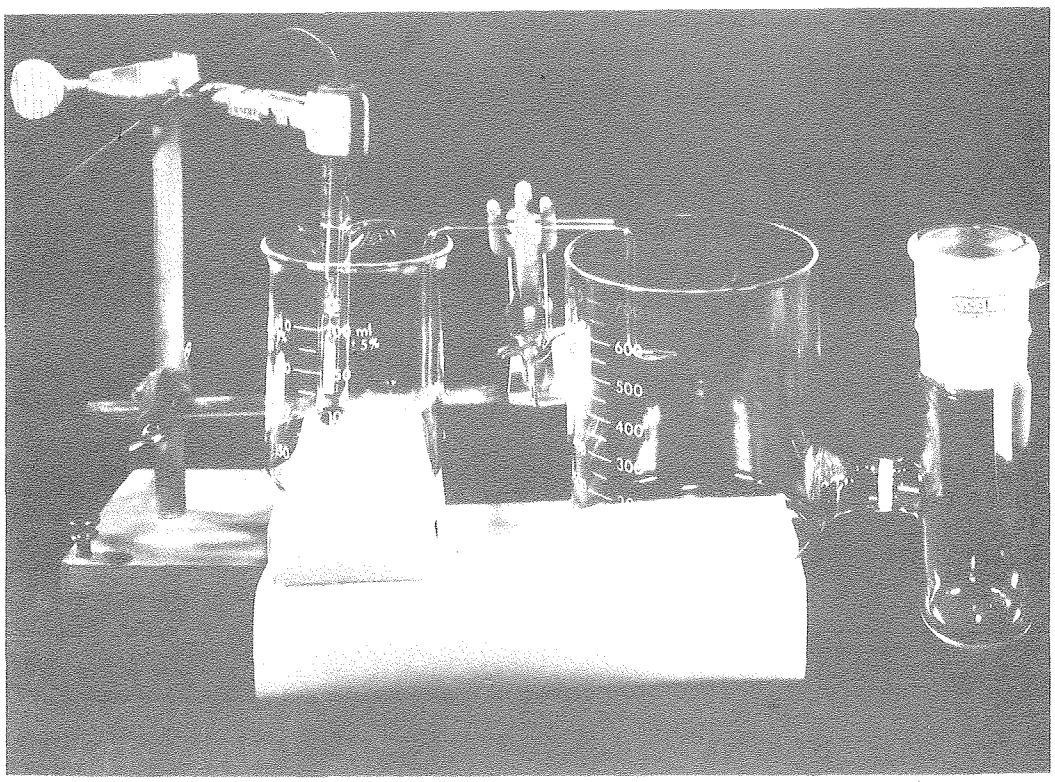

XBB 847-5002A

Figure 2.1 Electrolysis cell

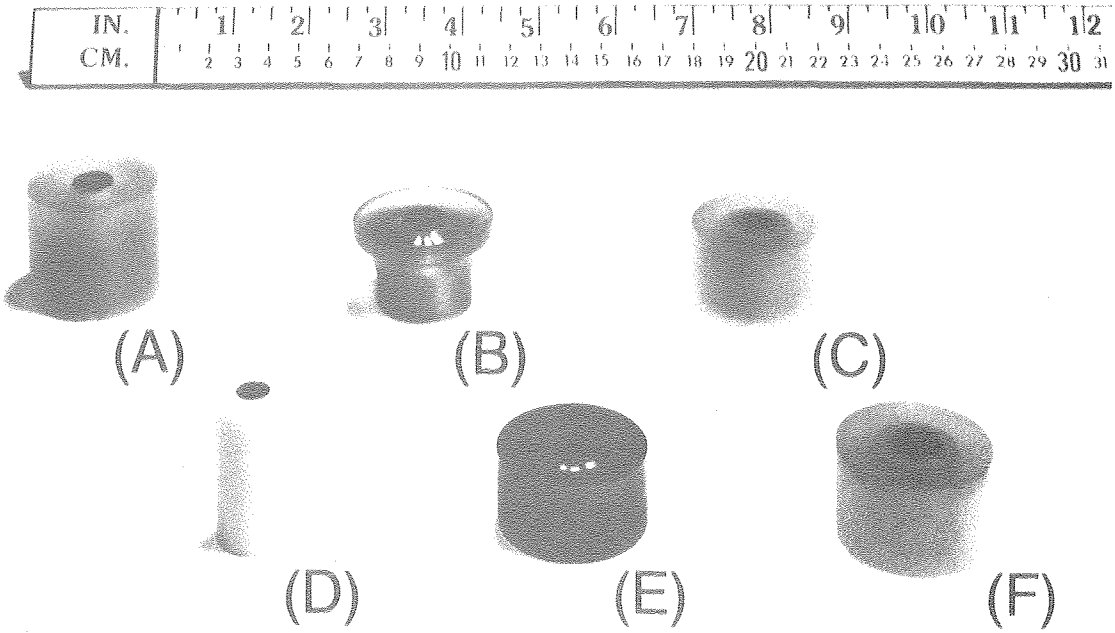

XBB 847-5003A

A) Exxon graphite loaded polymer disc on replaceable substrate mount

B) Union Carbide pyrolytic graphite electrode

C) single crystal zinc electrode

D) Pine glassy carbon electrode

E) platinum electrode

F) Gould pyrolytic graphite electrode

Fig. 2.2 Rotating disc working electrodes used in electrolysis.

Type 1: Standard

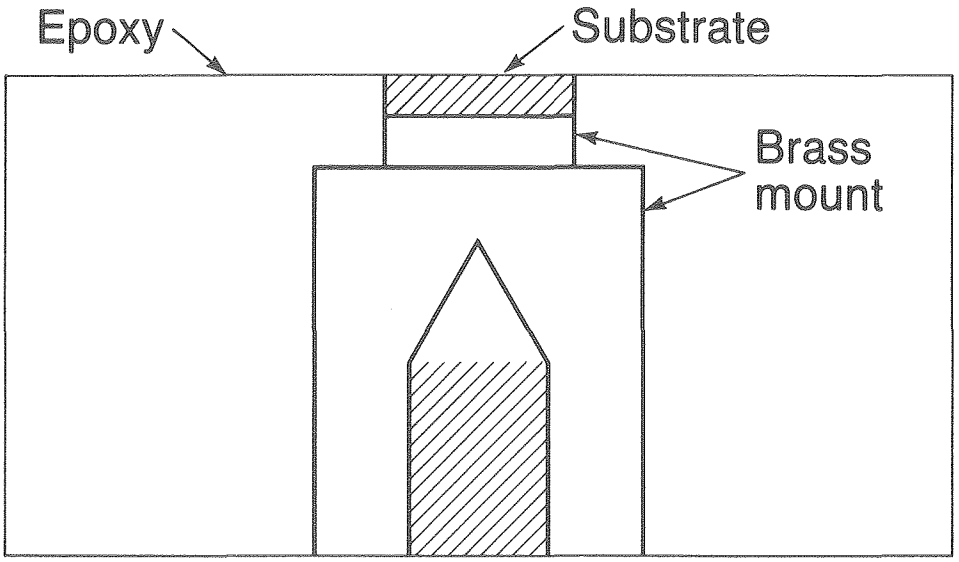

Type 2: Replaceable substrate

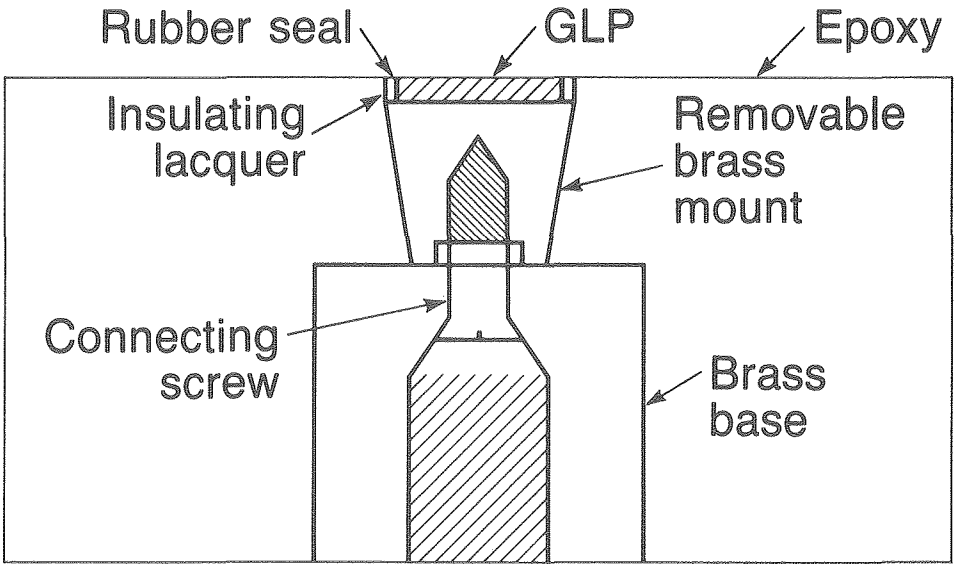

Figure 2.3 Types of Electrode Mounts

XBL 8410-4598

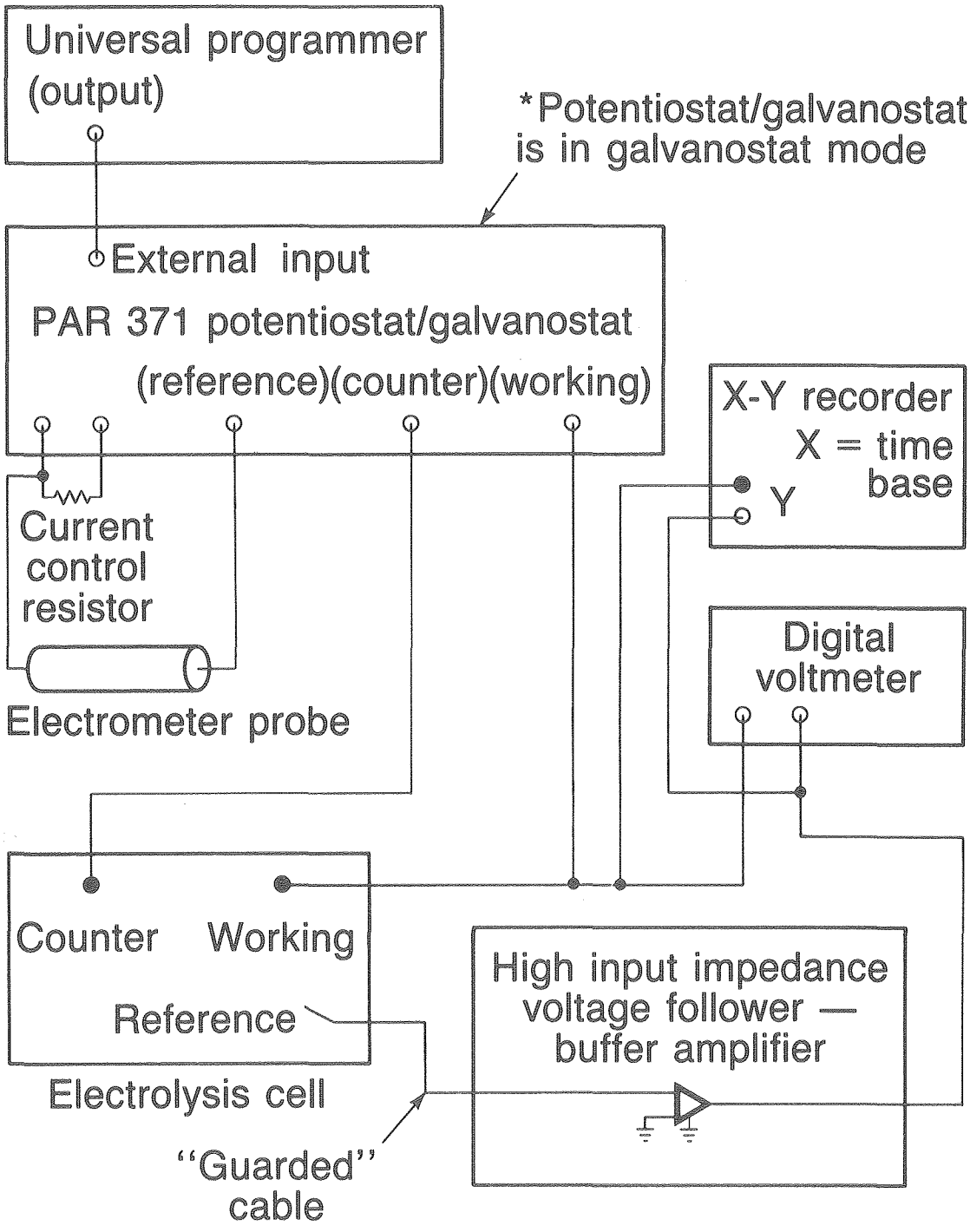

Figure 2.4 Equipment Interconnections for Primary Experimental Setup

XBL 849-10779

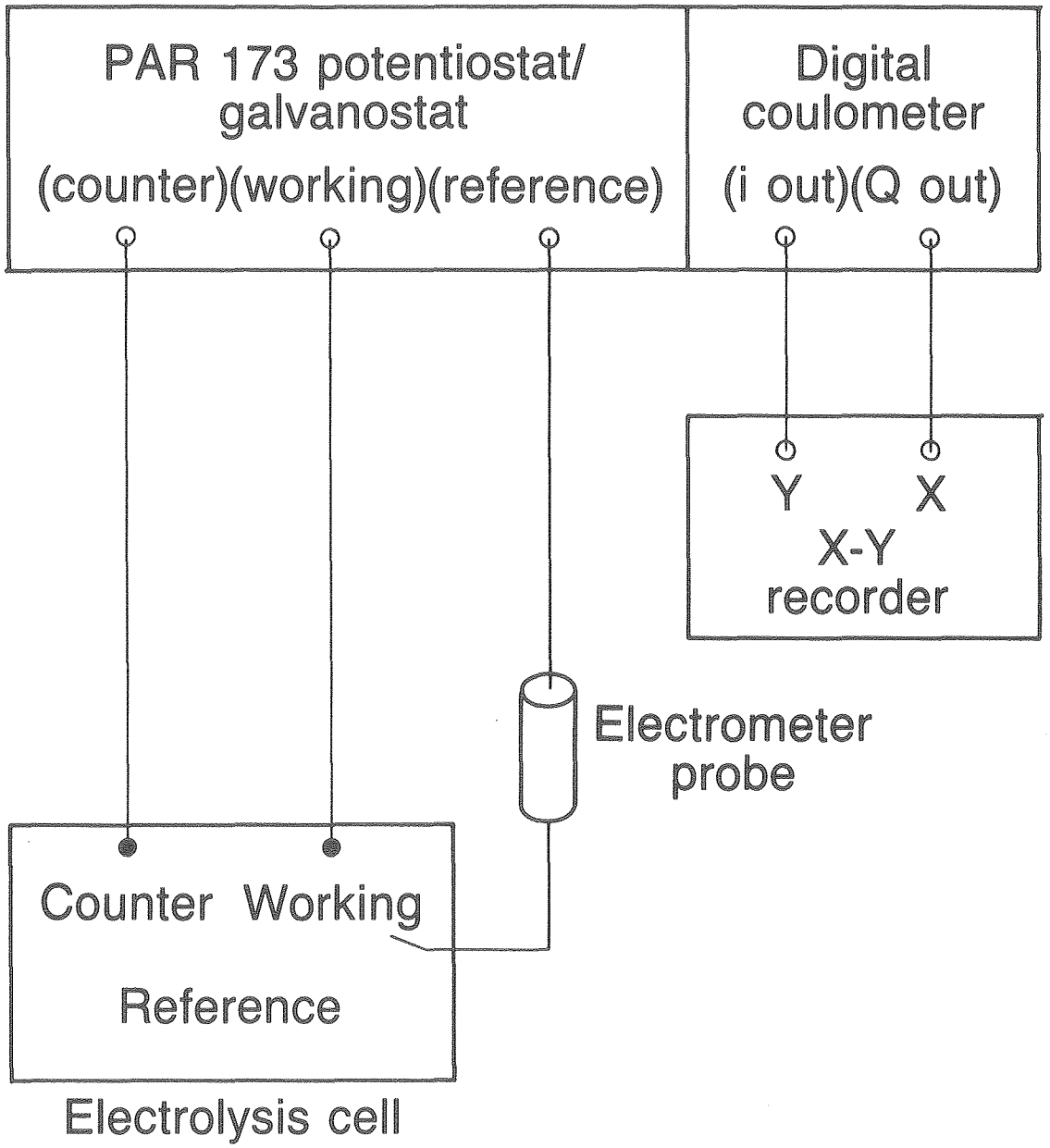

Figure 2.5 Equipment Interconnections for Kinetic Experiments

XBL 849-10778

III. CYCLIC VOLTAMMETRY

III.A. Results

In the first part of this study we wished to assess the general behavior of this system—i.e., zinc electrodeposition on foreign substrates. Potential sweep voltammetry was performed on glassy carbon and Union Carbide pyrolytic graphite in 1.0 M and 3.0 M $ZnCl_2$ electrolyte prepared from the MCB reagent salt. Figures 3.1-3.3 show the resulting voltammograms, at a sweep rate of 50 mv/seconds. Each of the curves in Figures 3.1 and 3.2 were generated from a different limiting cathodic potential; the curve labels refer to these potentials. Figure 3.3 compares the behavior of glassy carbon to that of Union Carbide pyrolytic graphite.

III.B. Comments

The purpose of the cyclic voltammetry experiments was to obtain a qualitative picture of the electrochemical behavior of zinc deposition on various substrates. Two important features were revealed in these experiments. First, only one cathodic peak was evident; this result was substantiated by the multiple sweep experiments shown in Figures 3.1-3.3 where the cathodic end potential was varied.

A general feature borne out in cyclic voltammetry is a current peak for every charge transfer reaction. Although it has been postulated that the hydrogen evolution reaction might play an important role in this system, no separate hydrogen peak or peaks are observed in Figures 3.1-3.3. Admittedly this set of experiments is by no means conclusive. The magnitude of the electrodeposition current could conceivably obscure a

relatively smaller hydrogen current.

Potential sweep voltammetry also provides kinetic information about electrochemical systems. Fletcher et al. give an interesting analysis of the cathodic portion of cyclic voltammograms for electrodepositing systems. If the cathodic current after the potential sweep is reversed is higher than that obtained while sweeping in the cathodic direction nucleation processes are indicated (25). In Figures 3.1-3.3 such cathodic current maxima are observed. McBreen et al. obtained similar voltammograms for deposition on glassy carbon from zinc halide electrolytes; he called this behavior of the cathodic current a nucleation loop (7).

An additional conclusion can be drawn concerning initial deposition on foreign substrates. In Figure 3.3 the cathodic current for deposition on the glassy carbon electrode is significantly larger than that on the Union Carbide pyrolytic graphite substrate. This can be interpreted to mean that zinc electrodeposits more easily on glassy carbon than on pyrolytic graphite.

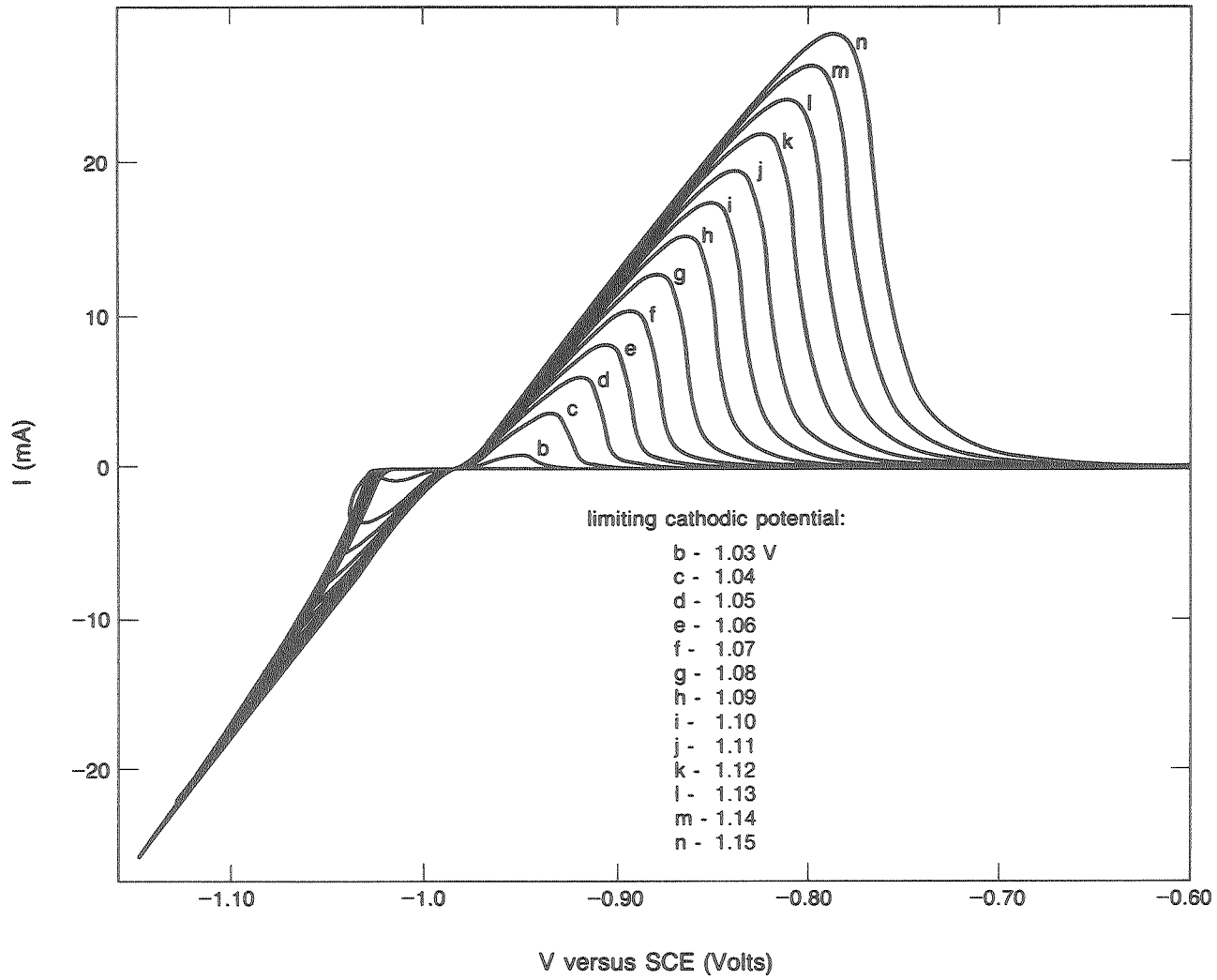

Fig. 3.1 Cyclic voltammograms of zinc deposition on Union Carbide pyrolytic graphite,
3.0 M $ZnCl_2$ (MCB reagent)
sweep rate = 50 mV/second

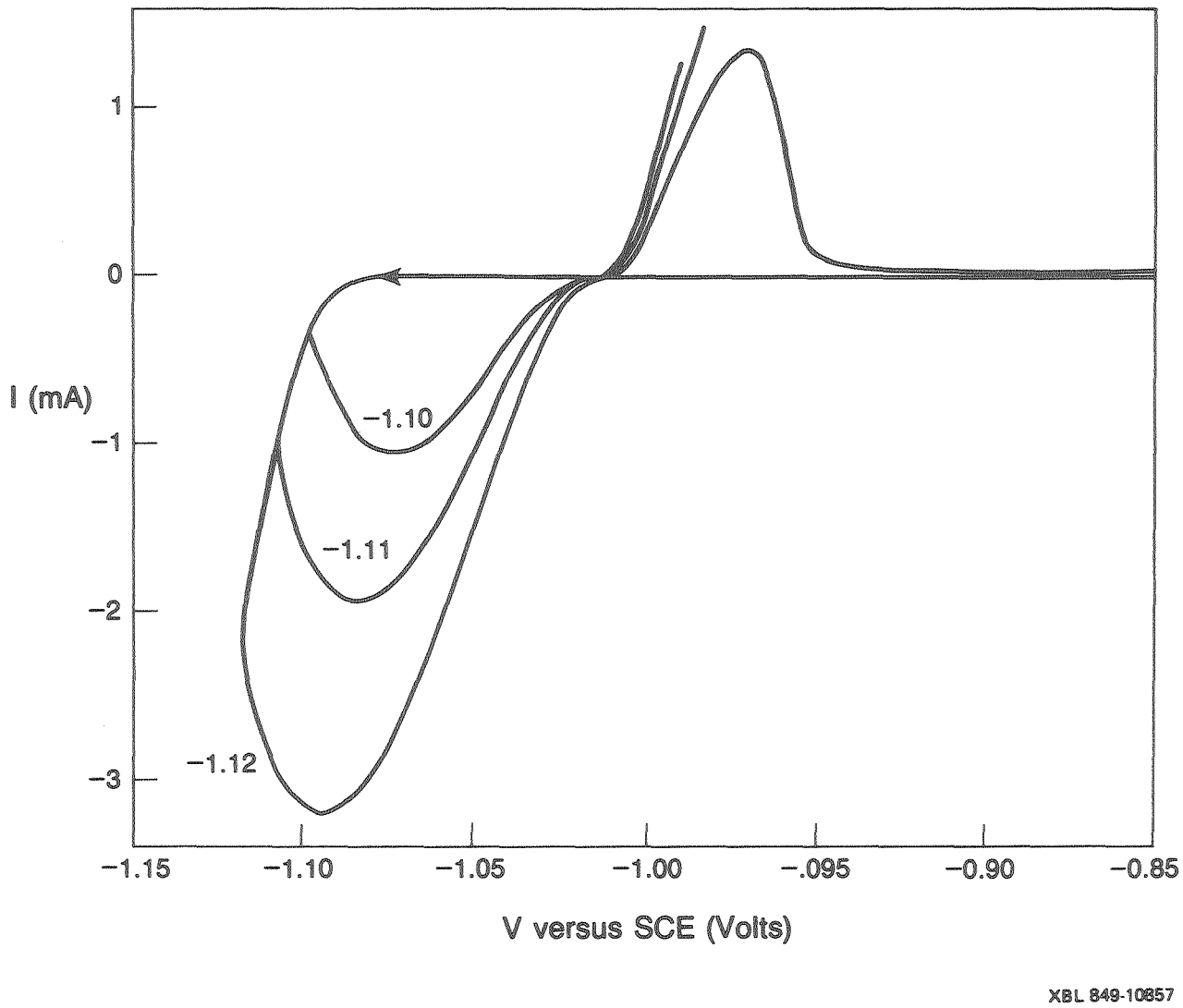

Fig. 3.2 Cyclic voltammograms of zinc deposition on glassy carbon, 1.0 M $ZnCl_2$ (MCB reagent) sweep rate = 50 mV/second

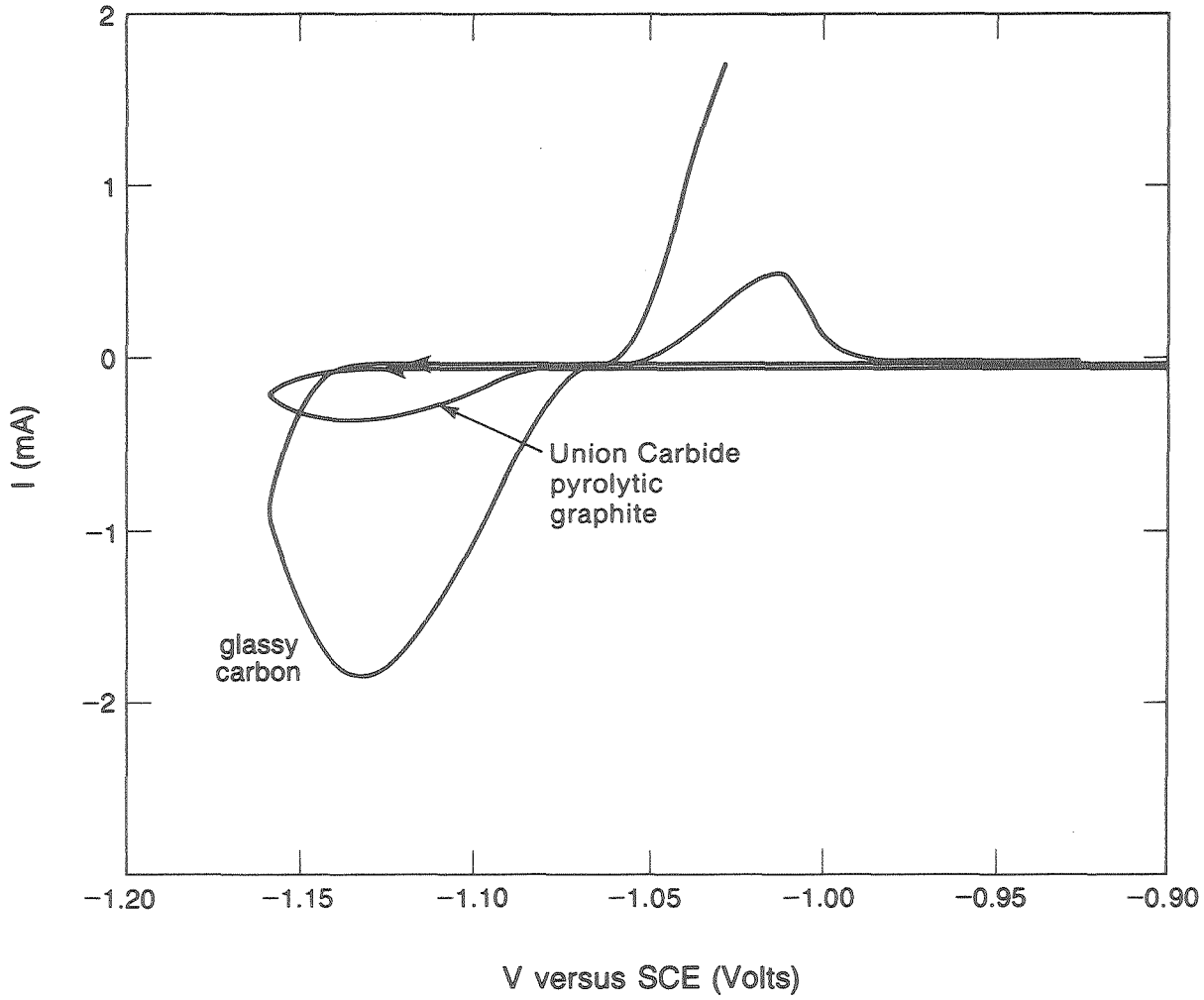

XBL 849-10856

Fig. 3.3 Comparison of cyclic voltammograms of zinc deposition on glassy carbon and on Union Carbide pyrolytic graphite, 1.0 M $ZnCl_2$ (MCB reagent) sweep rate = 50 mV/second

IV. KINETIC MEASUREMENTS

IV.A. Results

Measurements of the Butler Volmer kinetic parameters for zinc deposition from acid electrolytes, as reported in the literature, have yielded inconsistent results (see Table 1.1). Most experiments in the present work deal with small thicknesses of zinc (from 235 to 8600 monolayers) deposited on foreign substrates. It can be argued that under these conditions significant substrate effects might exist. For these reasons kinetic measurements were made on several foreign substrates.

Pseudo-steady state potential step experiments were performed on Union Carbide pyrolytic graphite, pyrolytic graphite used by Gould, and single crystal zinc. Figures 4.1-4.3 are plots of charge versus current in response to various potential steps. For each substrate the average current density at 100 millicoulombs/cm^2 is plotted against the potential in Figures 4.4-4.6. The potential data were adjusted for ohmic drop using resistance values from Table 2.1.

The resulting data, shown in Figures 4.4-4.6 are not linear. However, a pattern is discernable in this non-linearity; the data curve concave downwards, especially in Figure 4.5. There are a few possible reasons for this. Hydrogen evolution can be ruled out because it would cause a curvature in the opposite direction. One explanation is the non-uniform current distribution which changes with current density. From this standpoint, it is not clear what is taking place because we are actually measuring a net current in response to a range of surface overpotentials. A third reason for the curvature of data is that all

the measurements were not made at steady state, particularly at the higher potentials where 100 millicoulombs were passed the most quickly ≈2 seconds). Although these experiments were performed well below the limiting current (Appendix F), the interfacial concentration of zinc might be different than that at steady state. This explanation has the advantage that it qualitatively accounts for the concave downwards curvature of the data.

One is faced with the problem of estimating kinetic parameters from this data. Although this curvature renders the slopes and intercepts of the chosen lines somewhat arbitrary, least square linear fits of points in the Tafel region were made. These are also shown in Figures 4.4-4.6 and yield the kinetic parameters given in Table 4.1.

Again, the non-uniform current distribution inherent to the rotating disc electrode system complicates interpretation of this data. Tiedemann et al. provide scaling factors for the exchange current density evaluated using the primary resistance to a disc (29). For a reference electrode located infinitely far away this correction factor is between that for a reference electrode adjacent to the disc's edge and that for a reference electrode adjacent to the disc's center. According to these authors

$$i_o(\text{actual})/i_o(\text{apparent}) = i(r)/i_{avg} \qquad (4.1)$$

for a reference electrode adjacent to the disc's surface, where i_o is the actual and apparent exchange current density, i(r) is the local current density and i_{avg} is the average current density. This scaling factor varies with current density in the Tafel region. Table 4.2 limits the ranges of the exchange current density correction factor for the

current density range of interest. The parameters given in Table 4.1 may be compared to those in Table 1.1, keeping in mind the correction factors shown on Table 4.2.

IV.B. Comments

The purpose of the kinetic measurements was two-fold. First we wanted to determine the proper kinetic parameters (i_o, α_o) for zinc deposition and compare them to literature values given in Table 1.1. Secondly we wished to assess the extent of possible surface effects due to the small amounts of zinc deposited (from 235 to 8600 monolayers).

From Table 4.2 it is evident that the experimental results here are of low precision; this pitfall is common among systems with non-uniform current distributions. In contrast, Landau et al. (see Introduction/Background) performed kinetic experiments using a specially constructed cell with a uniform current distribution (1). Expression 1.1 in the Introduction gives the range of possible exchange current densities they published; the results of our experiments are consistent with the lower limit of this range (1 ma/cm^2). The exchange current density is assumed equal to 1 ma/cm^2 when assessing the current distribution in the Nodule Studies section.

Two additional conclusions can be drawn from Figure 4.3. The results here indicate that the Gould pyrolytic graphite substrate is more "reactive," more conductive to the electrodeposition of zinc than Union Carbide pyrolytic graphite. Also, lower exchange current densities were observed on the pyrolytic graphite substrates than on the Zinc substrate.

Table 4.1. Measured Kinetic Parameters in 1.0 M $ZnCl_2$ (MCB reagent).

Substrate	i_o (ma/cm^2)	Cathodic Transfer Coefficient α_c	Coefficient of Determination R^2
Union Carbide pyrolytic graphite	0.44	0.77	87%
Gould pyrolytic graphite	1.48	0.52	91%
single crystal zinc	1.68	0.43	88%

Table 4.2. Range of Exchange Current Density Correction Factor From Reference 29.

$i_{avg.}$ (ma/cm^2)	i_o (actual)/i_o (apparent) min	max
20	0.81	1.17
64	0.66	>1.8

*Cathodic transfer coefficient assumed 0.5.

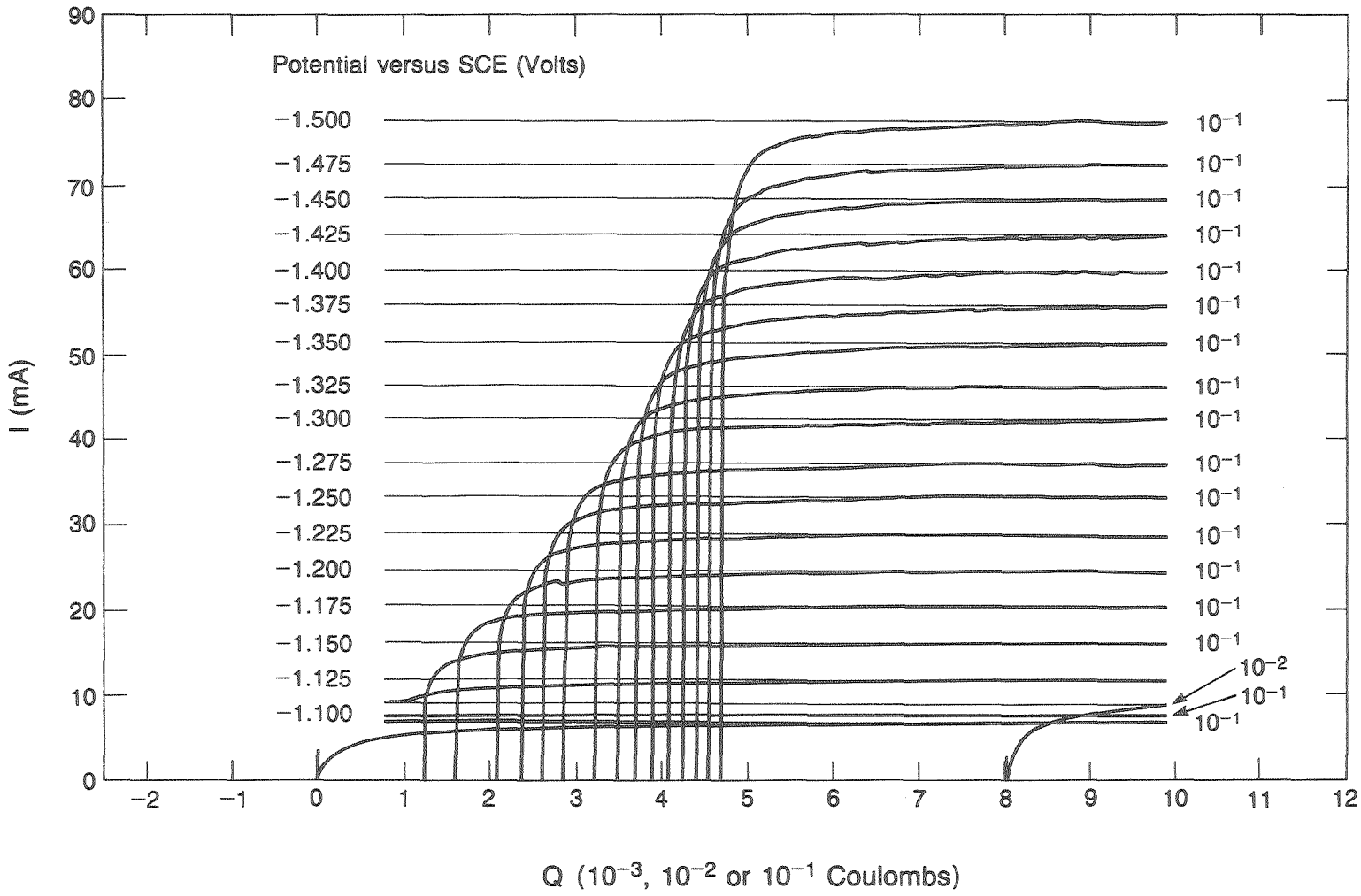

Fig. 4.1 Current versus charge in response to a potential step, Union Carbide pyrolytic graphite 1.0 M $ZnCl_2$ (MCB reagent)

XBL 849-10855

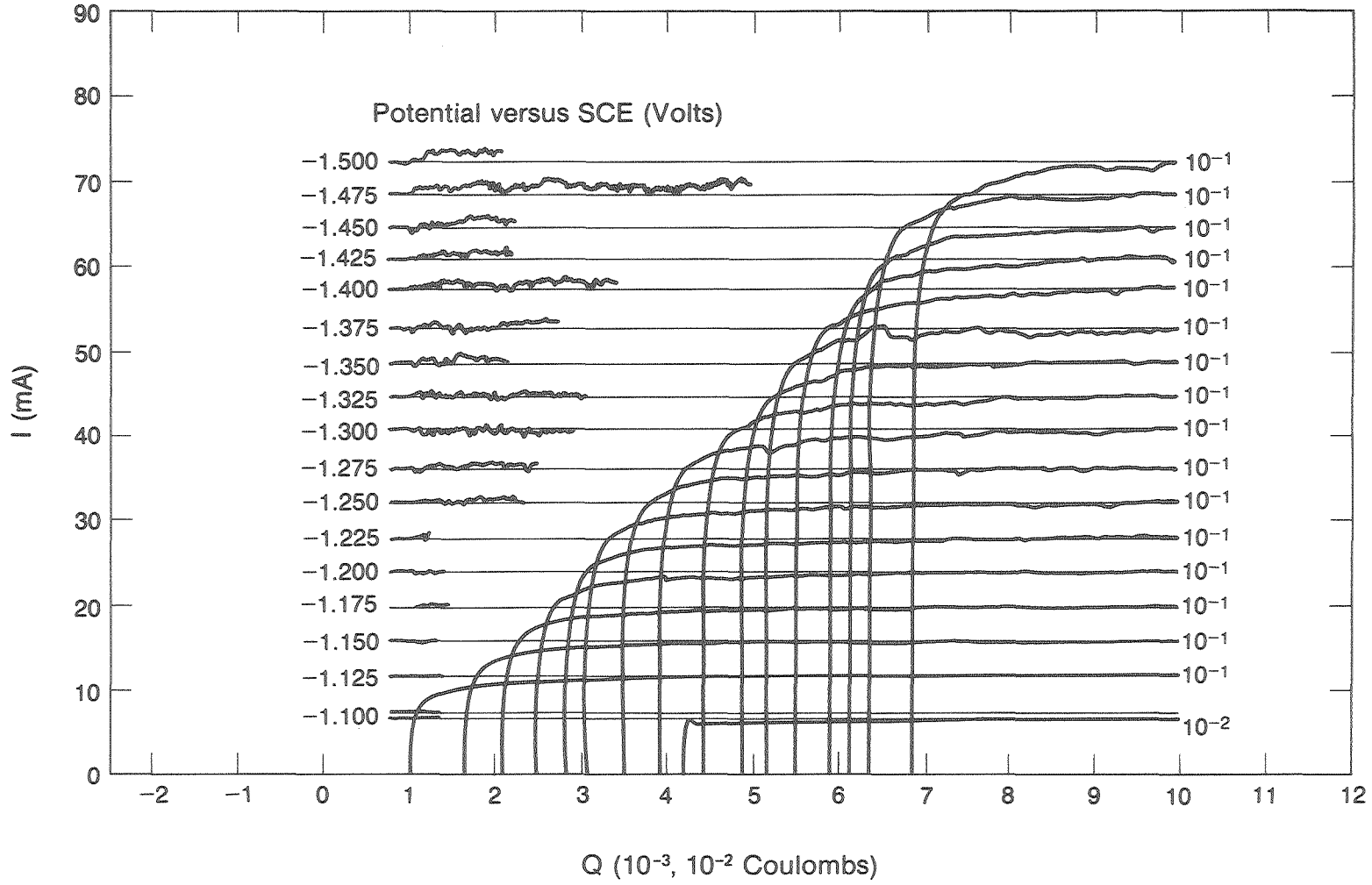

Fig. 4.2 Current versus charge in response to a potential step, Gould pyrolytic graphite 1.0 M $ZnCl_2$ (MCB reagent)

XBL 849-10854

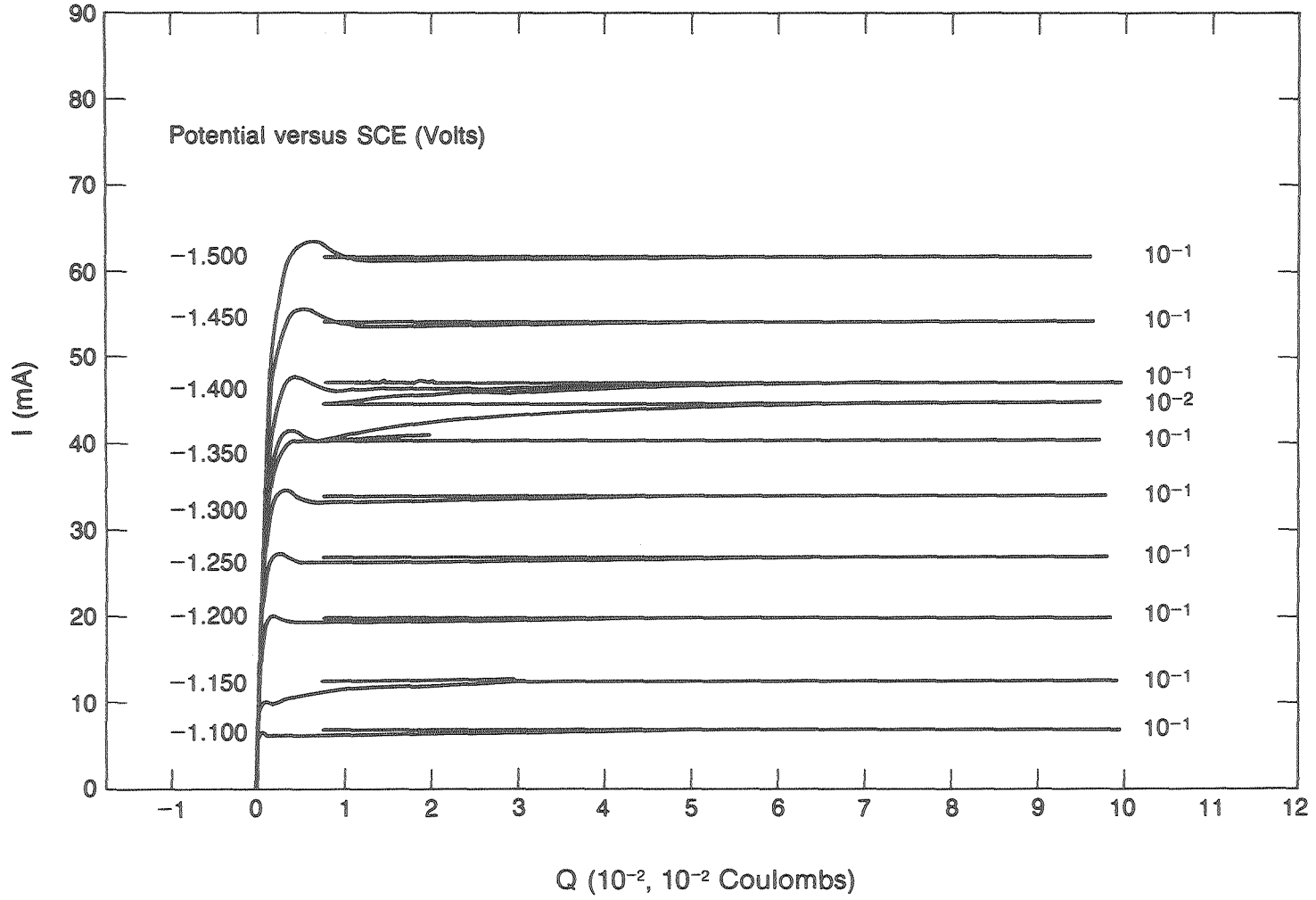

Fig. 4.3 Current versus charge in response to a potential step, Single Crystal Zinc
1.0 M $ZnCl_2$ (MCB reagent)

XBL 849-10853

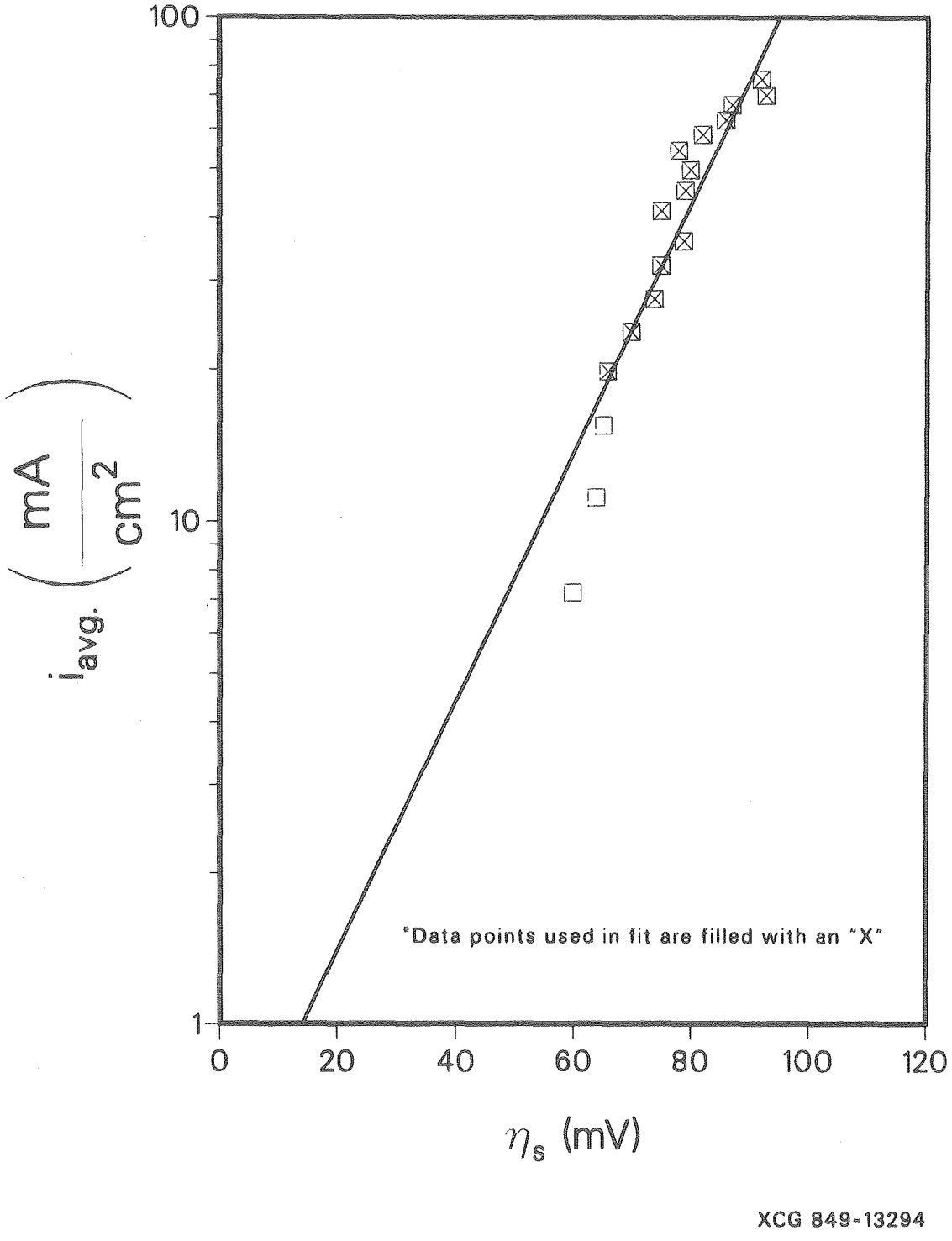

Fig. 4.4 Surface overpotential versus current density
Union Carbide pyrolytic graphite
100 m.Coulombs cm^2 (470 A)

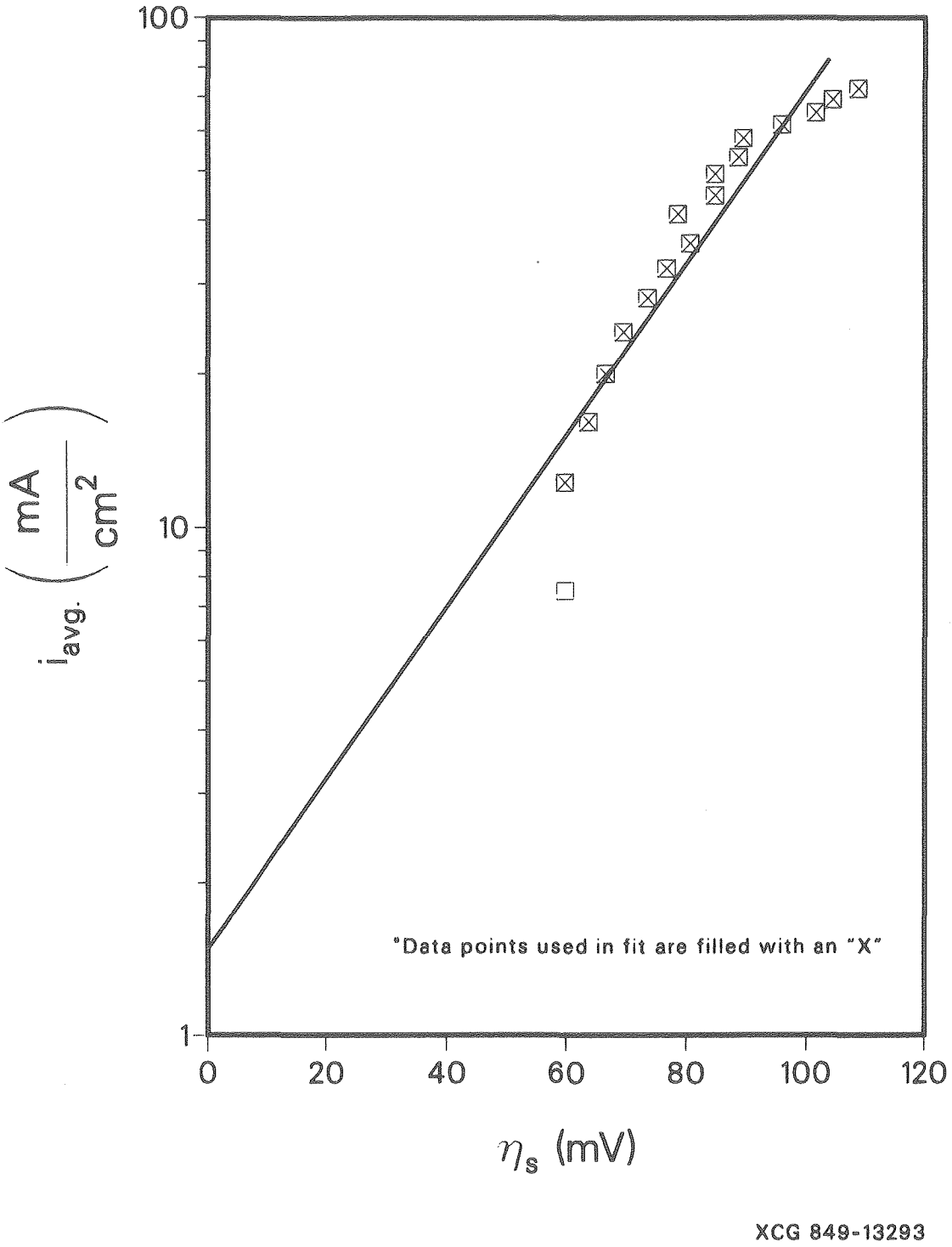

Fig. 4.5 Surface overpotential versus current density
Gould pyrolytic graphite
100 m.Coulombs/cm^2 (470 A)

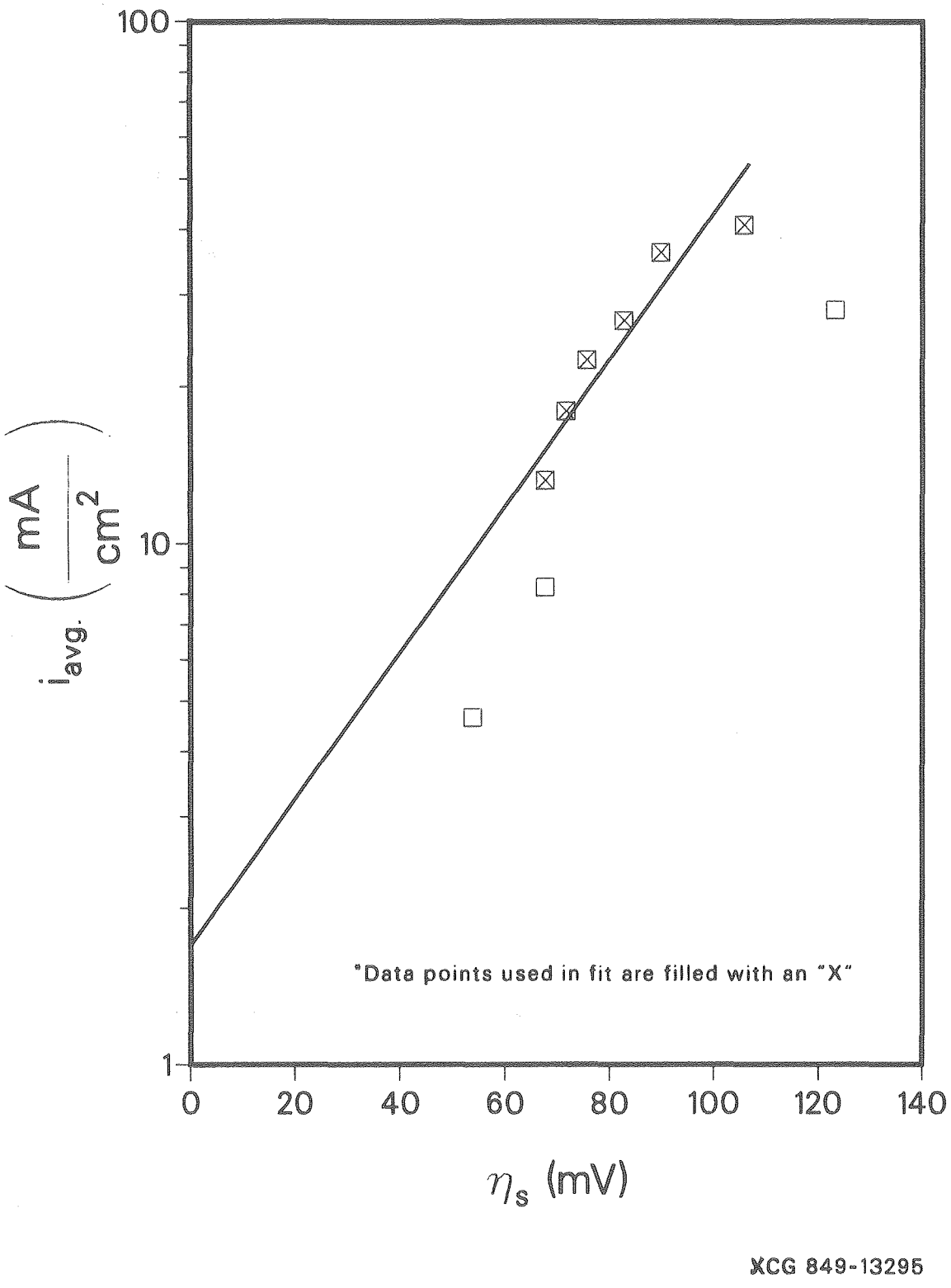

Fig. 4.6 Surface overpotential versus current density
Single Crystal Zinc
100 m. Coulombs/cm^2 (470 A)

V. NODULE STUDIES

V.A. Treatment of Data

Much of the literature on electrodeposition concerns the observation of grown nuclei, or nodules (6,26,30-42). These three dimensional shapes, usually 1 to 10 μm in diameter, have been used as clues to the mechanisms involved in morphological development. Previous workers in this laboratory have referred to similar surface features using the term, "initial protrusions" (step A in Figure 1.1) (2,6).

In this work Scanning Electron Microscopy was used in conjunction with image analysis to provide a quantitative assessment of surface features and thus further insight into the mechanism of morphological development. Photographs taken at nominal magnifications of 300× and 1000× were subsequently examined using an image analyzer. This instrument can indicate the number of features detected and will cut off features below a variable "oversize" setting; through subsequent processing of this data one can determine the size distribution. Figures 5.1-5.7 show typical distributions for zinc nodules on various substrates and photographs of corresponding surface features. It is interesting to compare the size distributions obtained from the low magnification photographs with those from the higher magnification photos. Image analyses performed on photographs of the lower magnification (nominally 300×) were confined to the areas seen on the higher magnification photographs (nominally 1000×). This was to allow for better comparison of the detected size distributions by virtually eliminating differences due to local variations in nodule densities. A large discrepancy is apparent between the measurements of nodule densities from 0 to 1 μm on

the low and high magnification photographs, on all substrates but the glassy carbon (Figure 5.7). The reason for this is clear upon examining the higher magnification photographs. Between the nodular growths on the high magnification SEM photos in Figures 5.1-5.6 fine, needle-like growth structures are apparent. Although undoubtably an important facet of the zinc's developing morphological structure, these needle-like crystals are difficult to quantify using an image analyzer. This is because these crystalline structures overlap and vary in darkness. When defining, and so counting a "feature," the image analyzer assumes an object with a closed outline. A detection level seting must be selected to give a measurement which accurately describes the surface morphology. At one setting parts of a crystal might be measured as several features, while at a higher detection level setting a large region of zinc crystals might be detected as one large feature. When analyzing the fine structures resolved in the higher magnification photographs the detection level, and consequently the measurement become arbitrary. This study accordingly addresses only features, or nodules, with diameters greater than 1 μm. For this reason, low magnification (300×) photos are used for nodule number density measurements.

In the following treatment of the data, knowledge of two electrochemical parameters during the experiments is required: the current density at the center of the disc and the surface overpotential at the same position. Evaluation of the secondary current distribution requires knowledge of kinetic parameters which, for this system (Table 1.1 and Kinetic Section IV.) are not known with adequate precision. Because the range of i_o determined in this work (Table 4.1: ≈0.4-1.7) falls close

to the lower limit given by Selman et al. (1-5 ma/cm^2) the following approximate values will be used to calculate current distributions:

$$i_o = 1\ ma/cm^2 \quad ; \quad \alpha_c = 0.5 \tag{5.1}$$

The sensitivity of i/i_{avg} at the center to the choice of different exchange current densities is assessed in Appendix G.

Each data point in Figures 5.20 through 5.50 represent a single electrodeposition experiment. Nodule formation experiments in the electrolyte prepared using the Mallinckrodt reagent salt on a given substrate were carried out on the same day in the same electrolyte. The time between experiments performed at a specific current density was kept to a minimum. Experiments in the electrolyte prepared using the MCB reagent salt were performed on various days and in electrolytes prepared at different times. Figures 5.11-5.13 may be used to assess the reproducibility of the experiments in the former electrolyte. The scatter of these experiments was as high as 50%.

The measured surface overpotentials in the nodule formation experiments exhibited anomalous behavior. Therefore, the data in Section V.C. are presented using surface overpotentials which are calculated from the kinetic parameters shown in Expression 5.1.

V.B. Effect of Current Density

SEM photographs of nodules formed at different current densities on various substrates are shown in Figures 5.20-5.29.

Figures 5.14 and 5.15 show measured nodule density as a function of current density for deposition from electrolytes prepared from MCB and Mallinckrodt reagent salts, respectively. Both the average current density and the estimated current density at the center are indicated.

For each particular substrate a general increase in nodule density with current density is apparent. In both electrolytes the nodule density is higher on the Union Carbide pyrolytic graphite than on the Gould pyrolytic graphite. The graphite loaded polymer clearly produces lower nodule densities than either type of pyrolytic graphite in the Mallinckrodt electrolyte.

V.C. Effect of Surface Overpotential

The surface overpotential at steady state was calculated using the Butler-Volmer equation and kinetic parameters given in Expression 5.1. An additional assumption was that $\alpha_a = 0.5$. Measured nodule densities are plotted against this calculated surface overpotential in Figures 5.30-5.36.

Each substrate exhibits a sharp increase in nodule density between 50 and 100 mv. The first derivatives of the nodule density versus surface overpotential at selected overpotentials are estimated in Section VII.B.

Nodule densities on the glassy carbon substrate exhibited significant scatter, as evident in Figure 5.36. This may be due to the highly non-porous nature of this substrate (see Appendix E).

V.D. Effect of Charge

As explained in Section VI.C., there is reason to believe that additional passage of current after the potential maxima has been reached (within the first few seconds) will result in no new nucleation—and therefore would have no effect on the nodule densities. Perhaps over longer periods of time nodules might even meld together and as a consequence a drop in the nodule density might be expected.

Investigation of this effect was limited to the two pyrolytic graphite substrates in the Mallinckrodt reagent. Figures 5.40 and 5.41 present SEM photographs of nodules formed on Union Carbide and Gould pyrolytic graphites, while Figure 5.42 shows nodule density as a function of charge density for both substrates.

The nodule density did not vary appreciably with charge density (Coulombs/cm^2) on the Gould pyrolytic graphite. At higher charge densities on the Union Carbide pyrolytic graphite the nodule density increased. These changes were small however compared to the scatter found when experiments were repeated.

V.E. Effect of pH

Since hydrogen codeposition is suspected of playing an important role in zinc electrodeposition kinetics and nucleation in particular, an investigation was carried out in which zinc was deposited from electrolytes in the pH range of 0.7 to 2.1. Figure 5.50 and 5.51 show zinc nodules deposited on Union Carbide and Gould pyrolytic graphites, respectively, at three different values of pH under otherwise identical conditions; the measured nodule densities are plotted against ionic

hydrogen concentration in Figure 5.52.

Changes in pH had virtually no effect on the formation of nodules on the Gould pyrolytic graphite. However, the area density of nodules formed on the Union Carbide pyrolytic graphite first decreased and later increased with increasing hydrogen ion concentration. These results are inconclusive as to the effect of pH in the 0.7 to 2.1 range on the formation of nodules.

V.F. Theory and Comments

The primary goal of this study was the quantitative determination of nucleation rates in response to different current densities and surface overpotentials. The theoretical aspects of electrochemical nucleation are well developed in the literature. Classical expressions for rates of nucleation were developed by Erdey-Gruz and Volmer (43). The relationships between nucleation rate and overpotential are different for two dimensional and three dimensional nucleation.

$$\text{2-d:} \quad J = k_1 \times \exp(-k_2/\eta)$$

$$\text{3-d:} \quad J = k_1 \times \exp(-k_3/(\eta)^2) \qquad (5.2)$$

where k_1 is a constant and k_2 and k_3 are functions of the work of nucleation. A major drawback of these formulae is the assumption of a single valued activity of nucleation sites; in reality a distribution of nucleation sites with various activities would be operative (35).

Experimentally we observe nodules which are the net result of nucleation and growth over time. Coalescence of nodules, growth of smaller shapes mentioned in part A of this section, and nucleation onto

grown nodules could all complicate the relationship between nucleation and observed nodule shapes. Furthermore, both the surface overpotential and the nucleation rate vary with time. Strictly speaking, equations 5.2 cannot be applied to the data from this study.

It would be desirable to evaluate the first derivative of the nodule density with respect to the surface overpotential for use in the Discussion Section. Unfortunately the nodule density data had significant scatter. This issue is pursued further in the Application of Results Section of the Discussion.

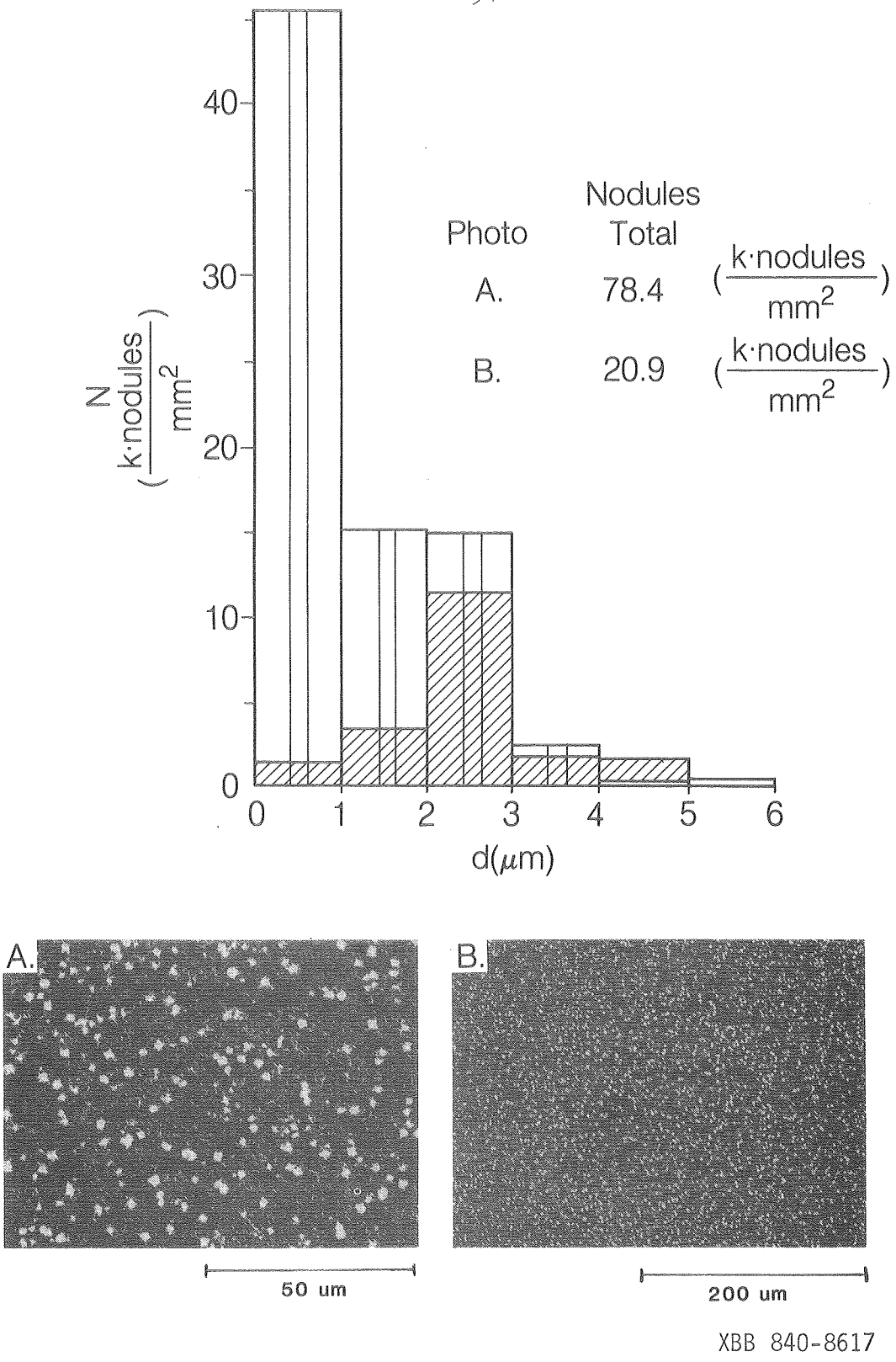

Fig. 5.1 Size distribution of zinc nodules on Union Carbide pyrolytic graphite substrate,
10 mA/cm^2 x 10 seconds
1.0 M $ZnCl_2$ (Mallinckrodt reagent)

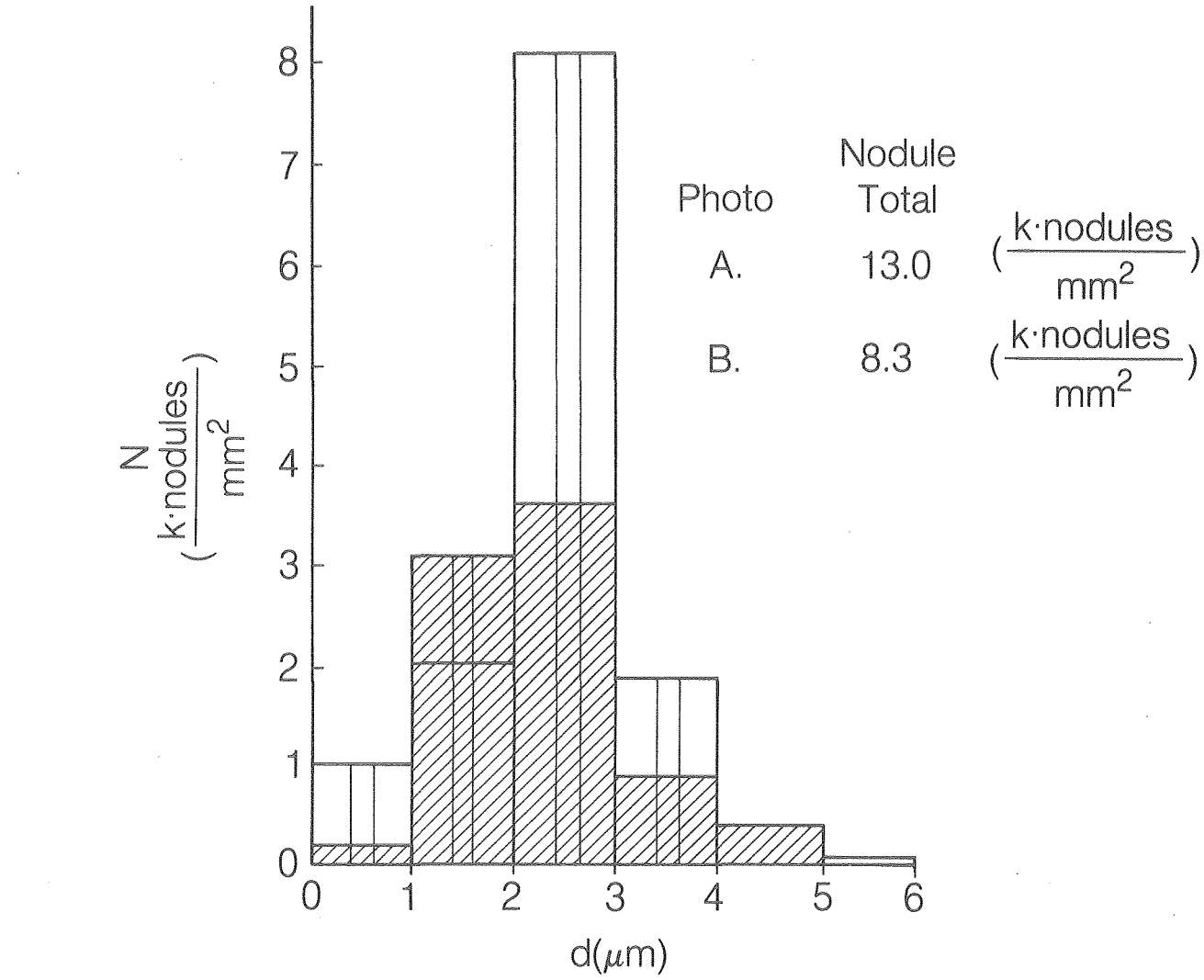

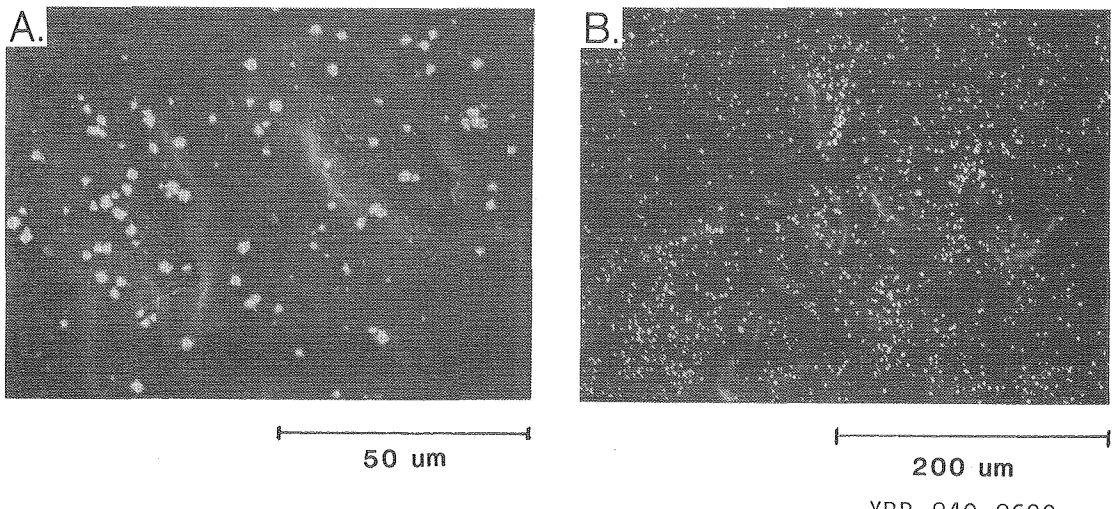

XBB 840-8620

Fig. 5.2 Size distribution of zinc nodules on Gould pyrolytic graphite substrate,
10 mA/cm^2 x 10 sec
1.0 M $ZnCl_2$ (Mallinckrodt reagent)

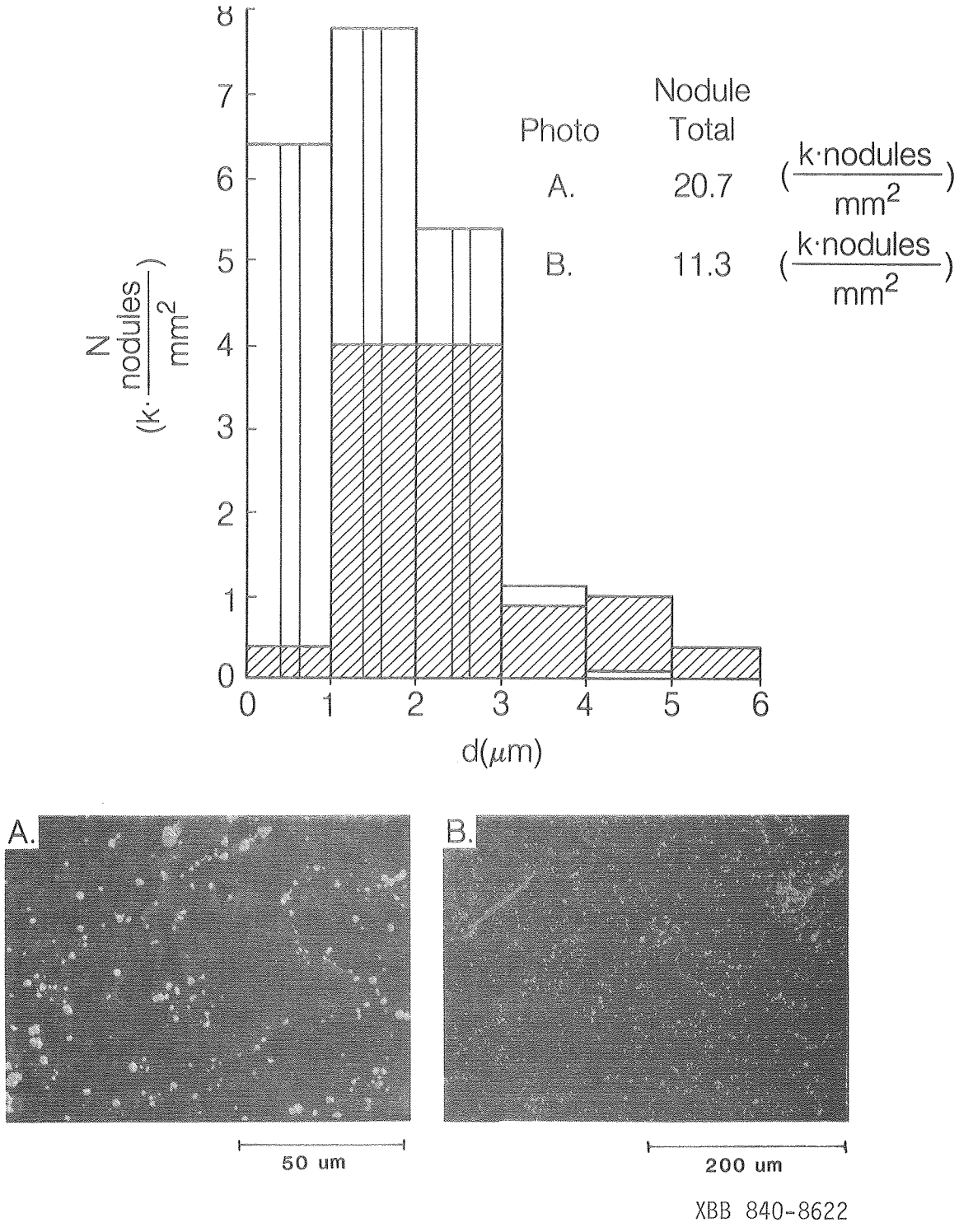

Fig. 5.3 Size distribution of zinc nodules on Exxon graphite loaded polymer substrate,
15 mA/cm^3 x 3.3 sec
1.0 M $ZnCl_2$ (Mallinckrodt reagent)

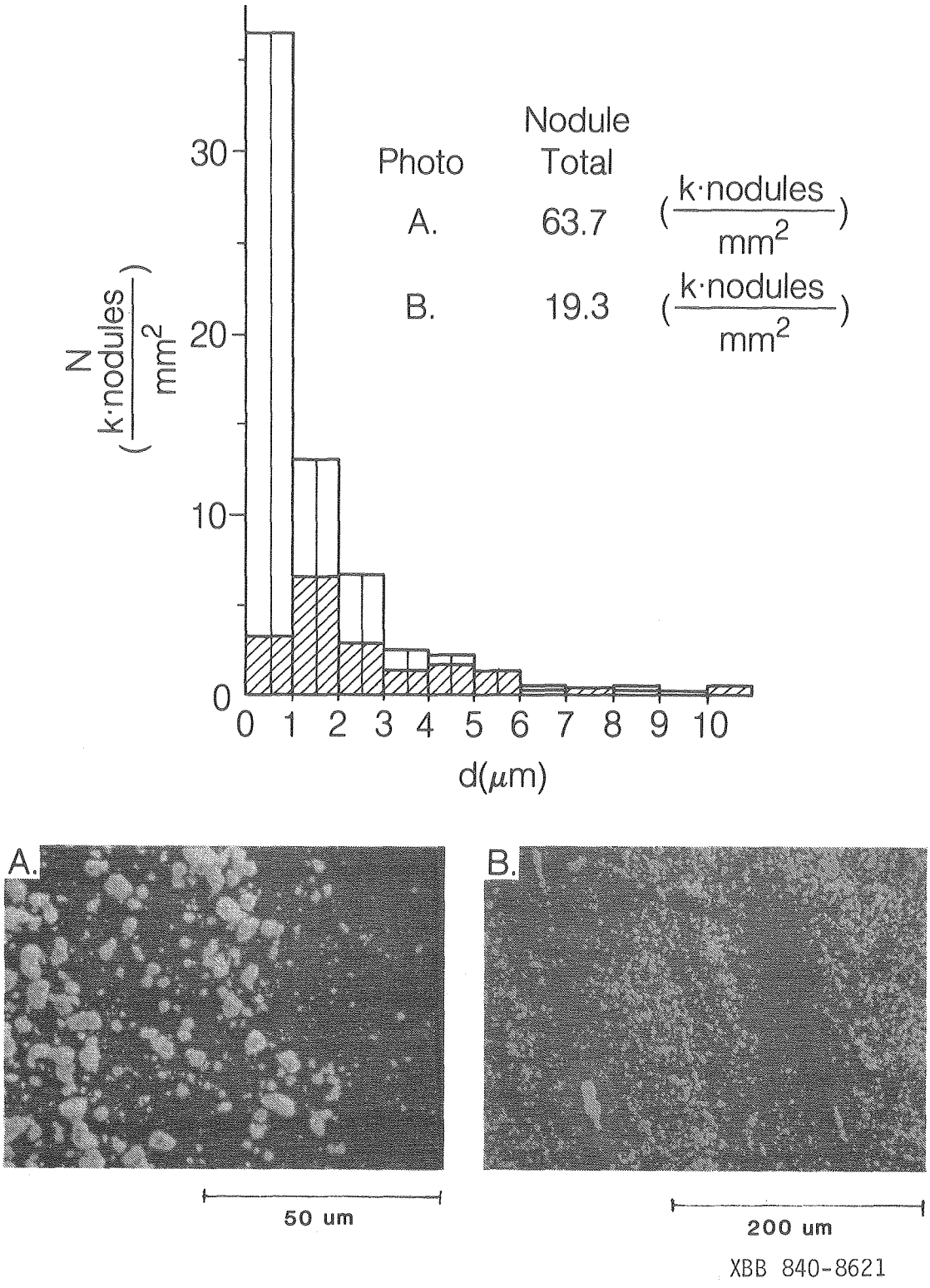

Fig. 5.4 Size distribution of zinc nodules on Union Carbide pyrolytic graphite substrate,
30 mA/cm^2 x 60 sec
1.0 M $ZnCl_2$ (MCB reagent)

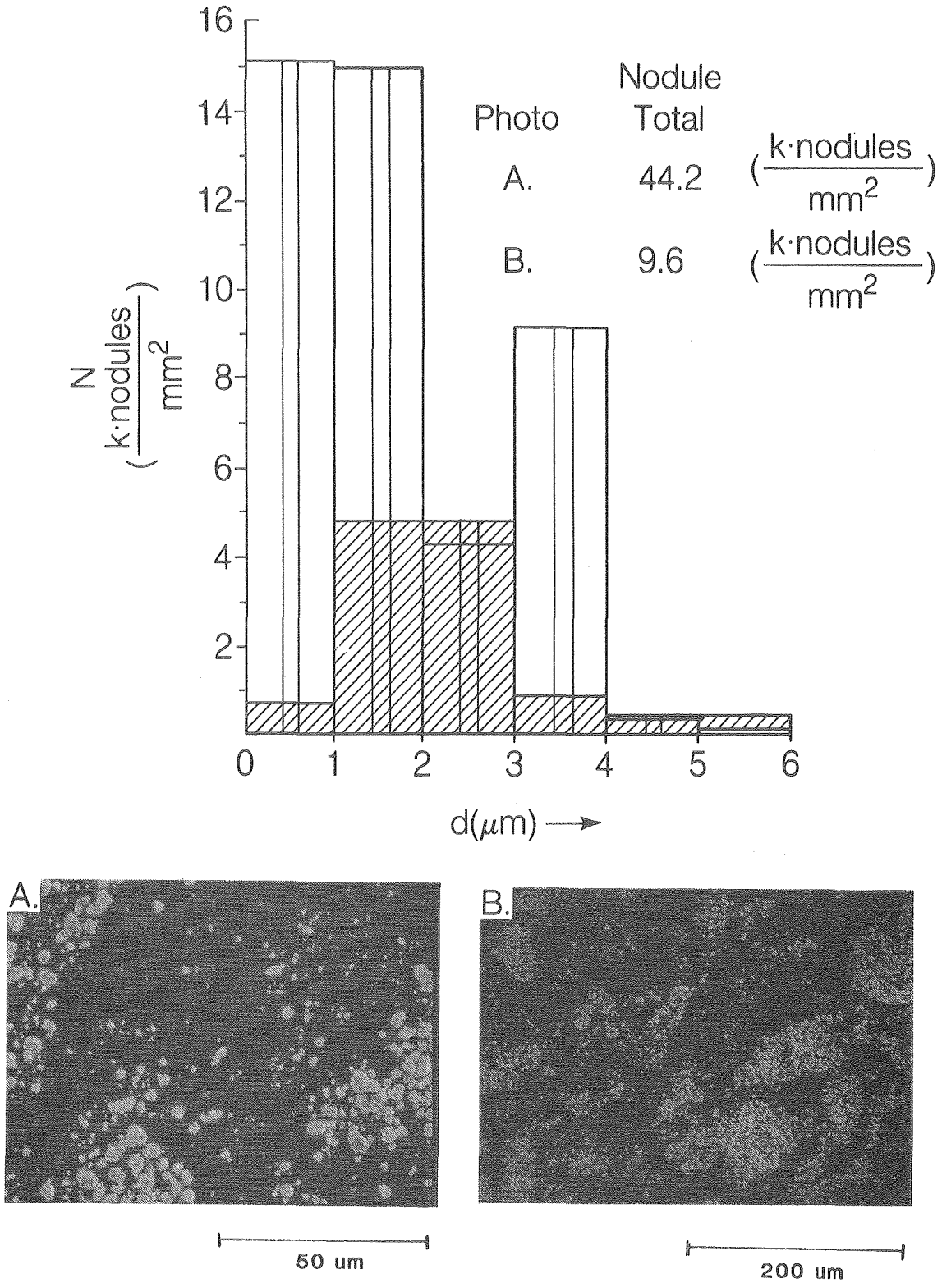

Fig. 5.5 Size distribution of zinc nodules on Gould pyrolytic graphite substrate,
30 mA/cm^2 x 30 sec
1.0 M $ZnCl_2$ (MCB reagent)

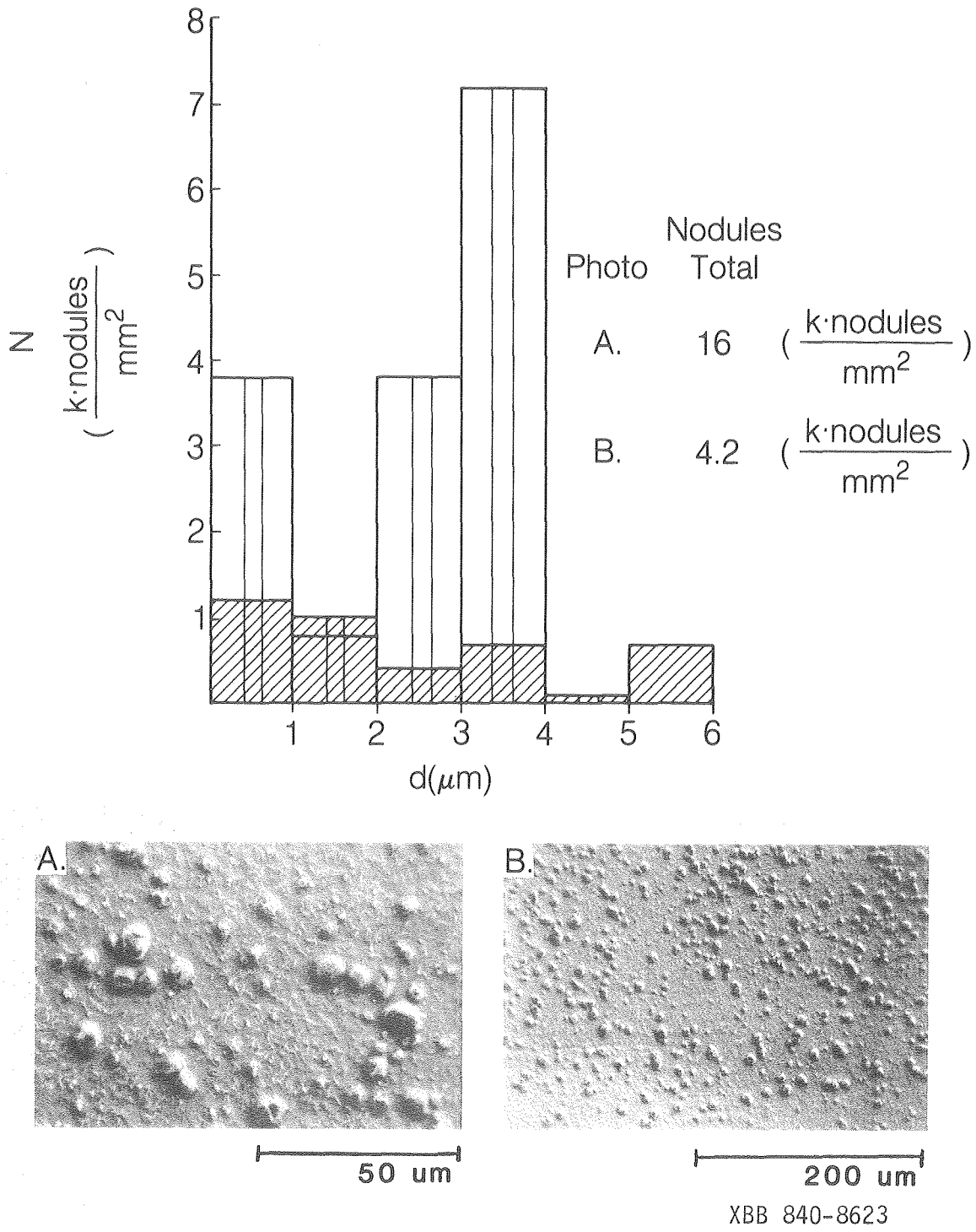

Fig. 5.6 Size distribution of zinc nodules on platinum substrate, 16.5 mA/cm^2 x 90 sec
1.0 M $ZnCl_2$ (MCB reagent)

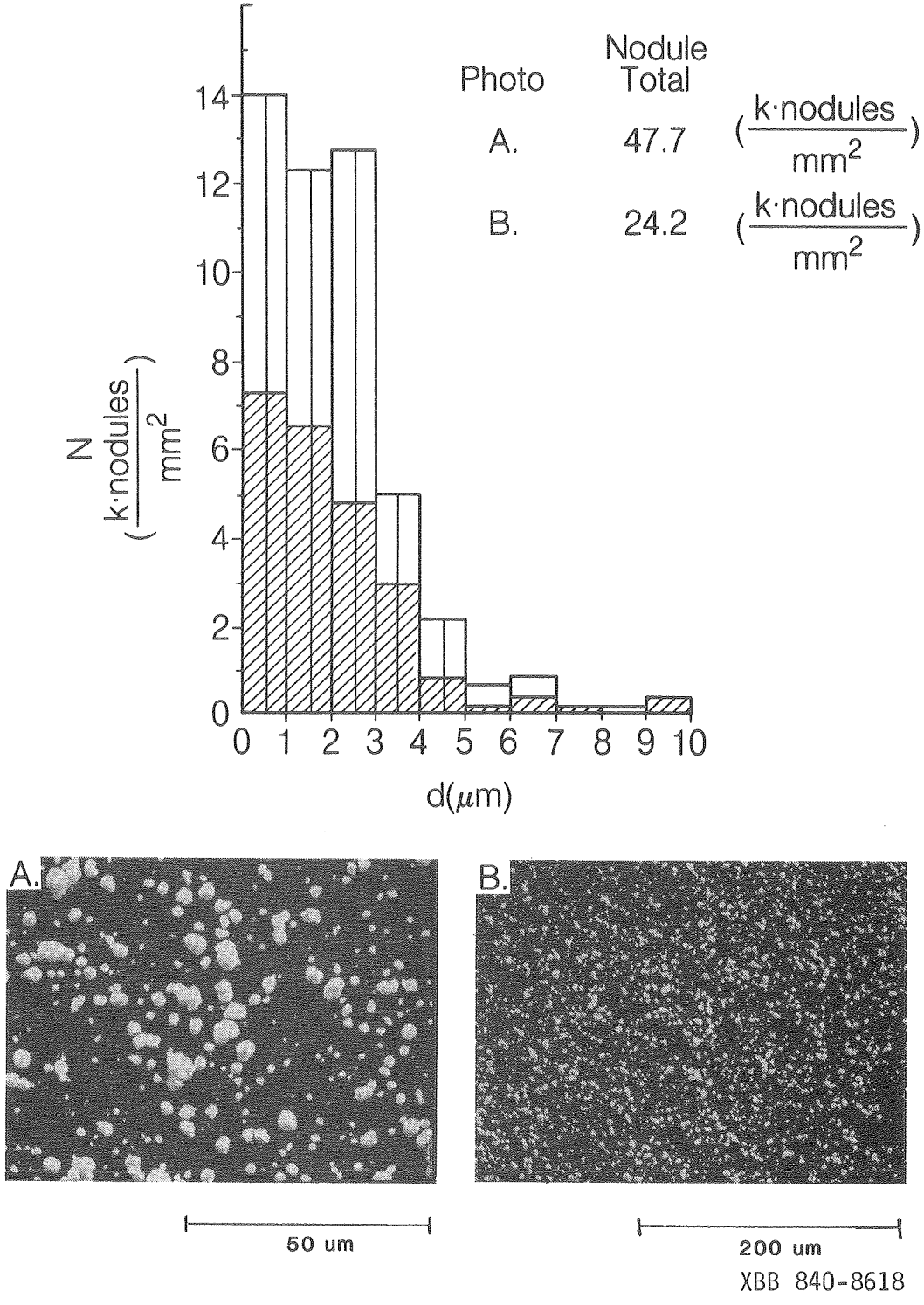

Fig. 5.7 Size distribution of zinc nodules on glassy carbon substrate,
42 mA/cm^2 x 22.5 sec
1.0 M $ZnCl_2$ (MCB reagent)

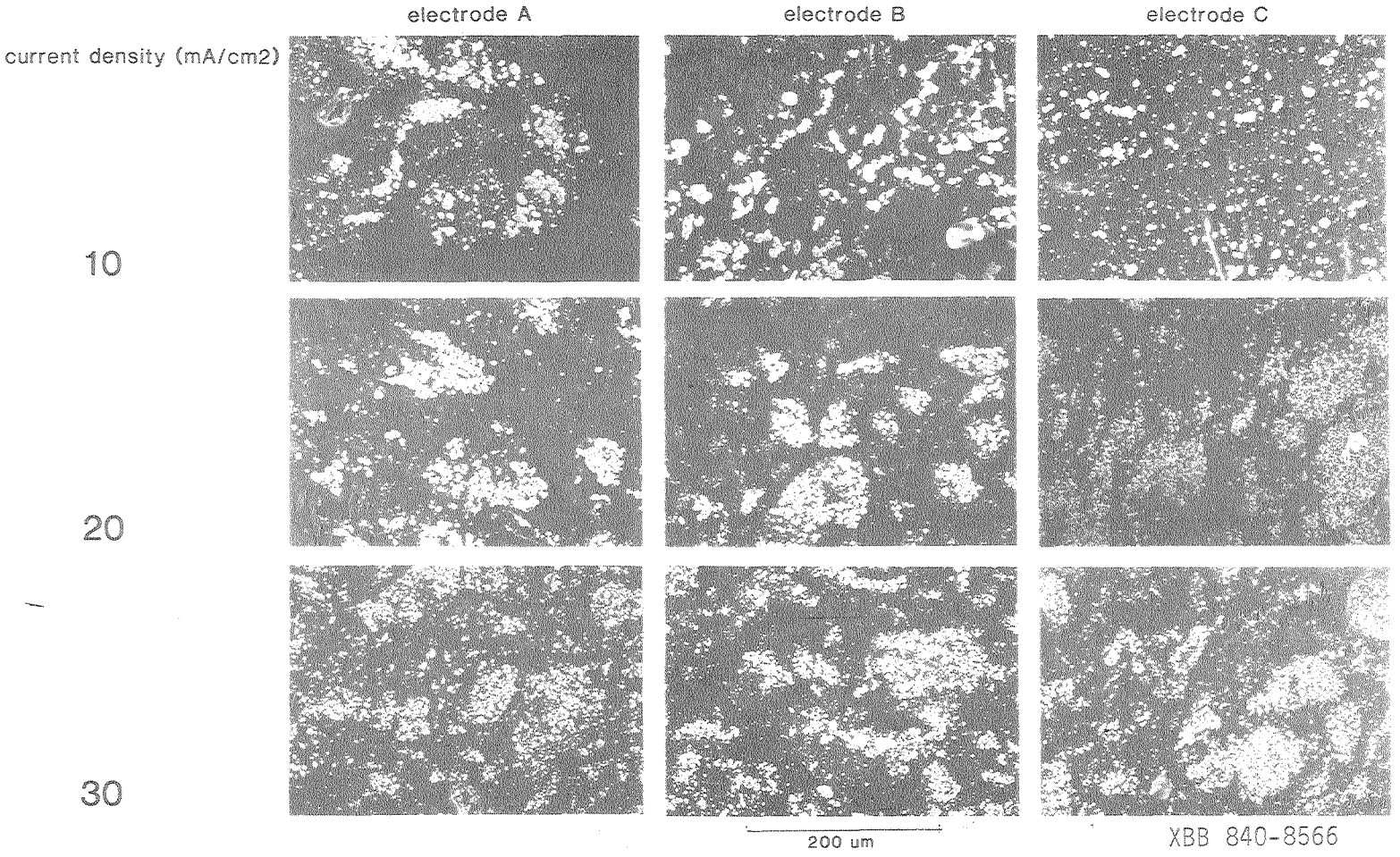

Fig. 5.10A Zinc nodules on Gould pyrolytic graphite substrate,
900 mC/cm^2 (4300 A)
1.0 M $ZnCl_2$ (MCB reagent)

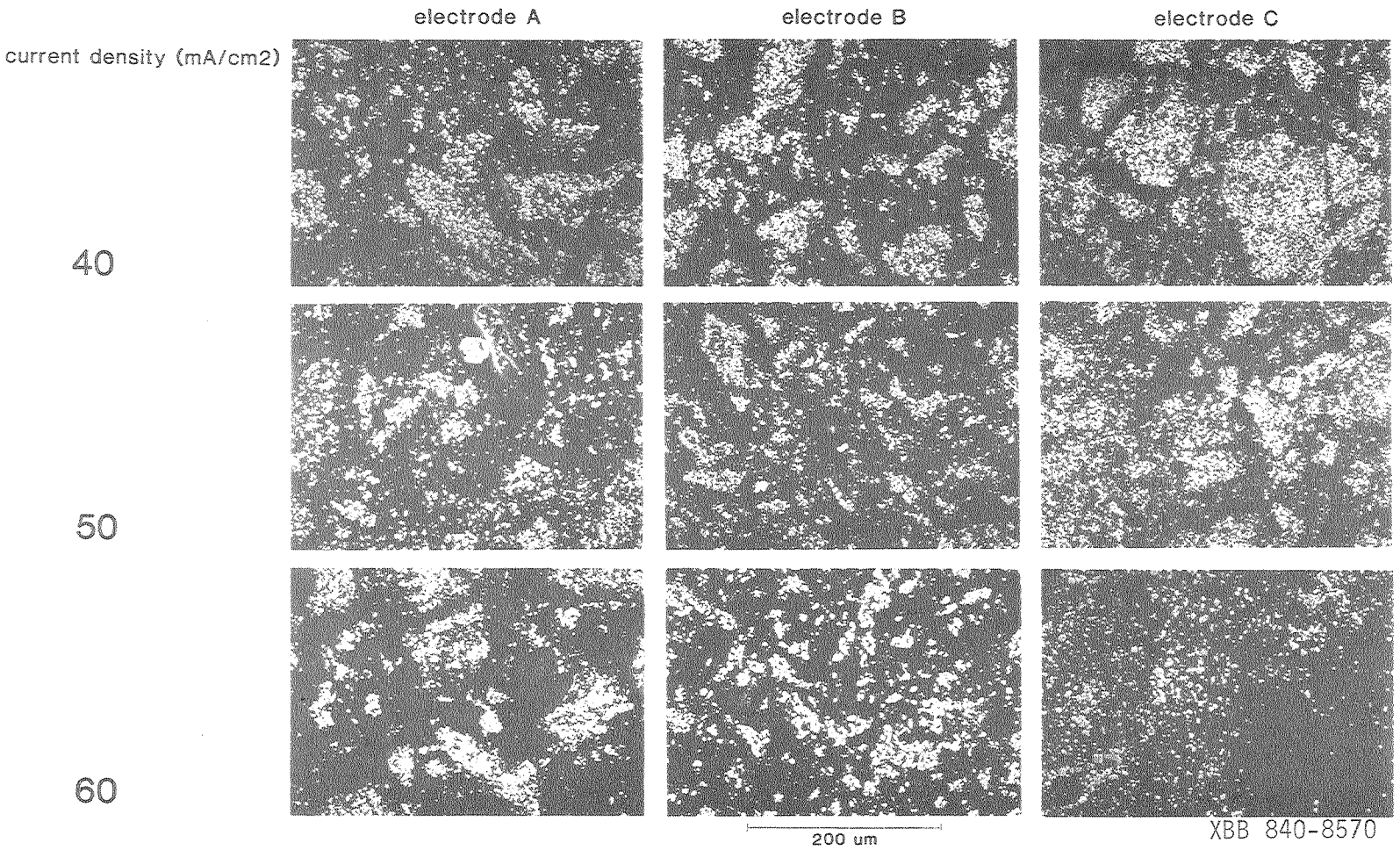

Fig. 5.10B Zinc nodules on Gould pyrolytic graphite substrate,
900 mC/cm^2 (4300 A)
1.0 M $ZnCl_2$ (MCB reagent)

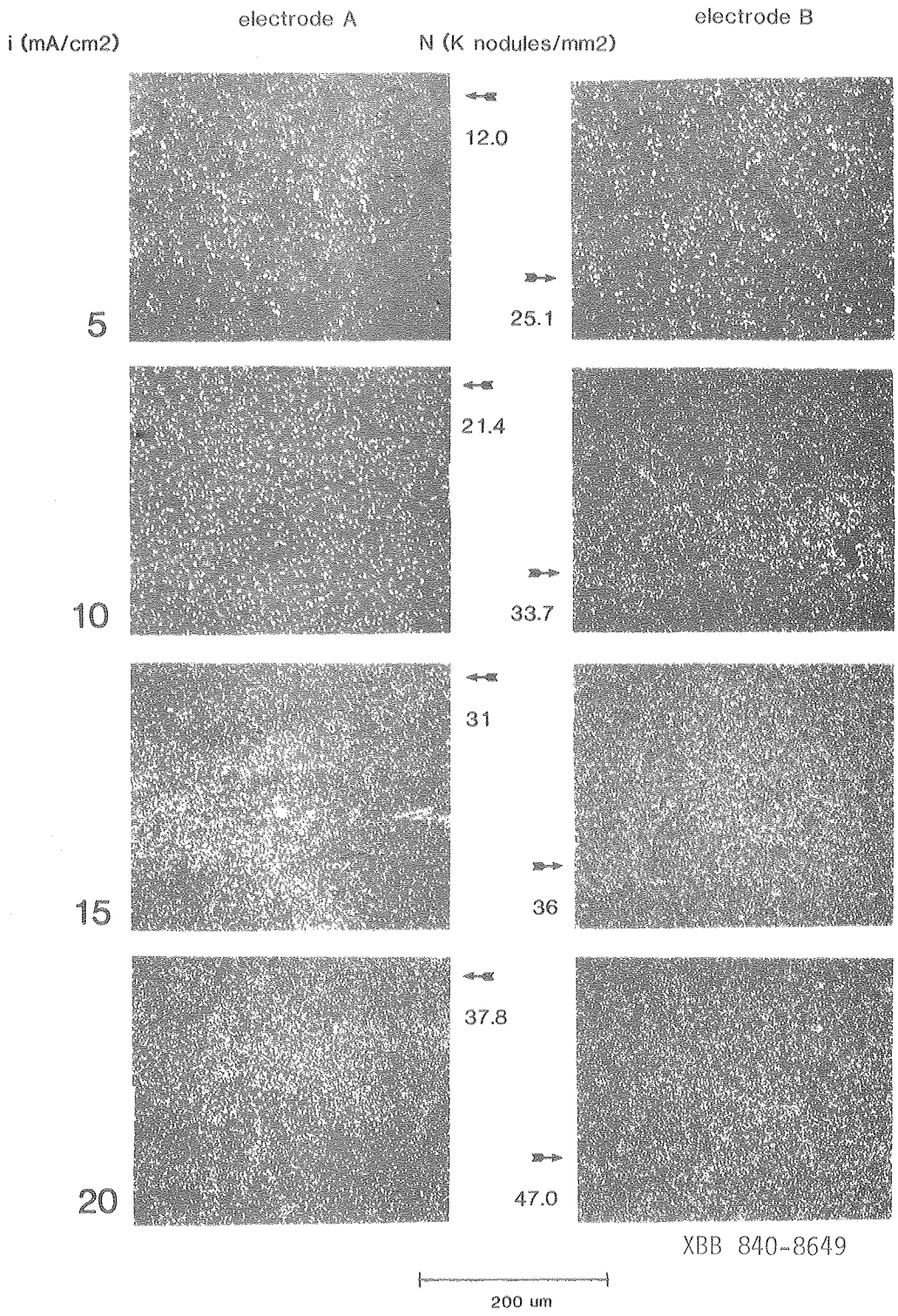

Fig. 5.11 Zinc nodules on Union Carbide pyrolytic graphite substrate,
100 mC/cm^2 (470 A)
1.0 M $ZnCl_2$ (Mallinckrodt reagent)

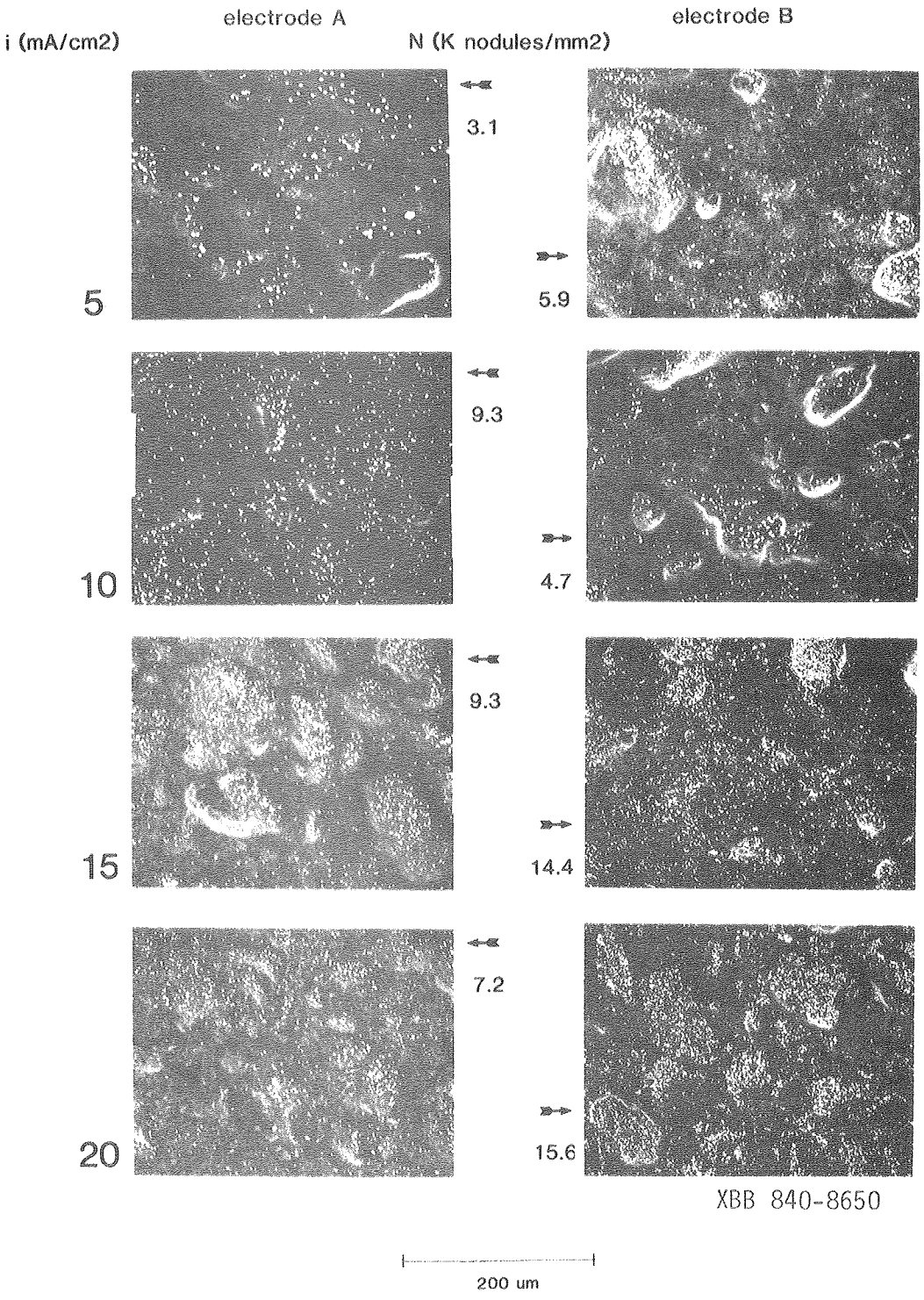

Fig. 5.12 Zinc nodules on Gould pyrolytic graphite substrate
100 mC/cm^2 (470 A)
1.0 M $ZnCl_2$ (Mallinckrodt reagent)

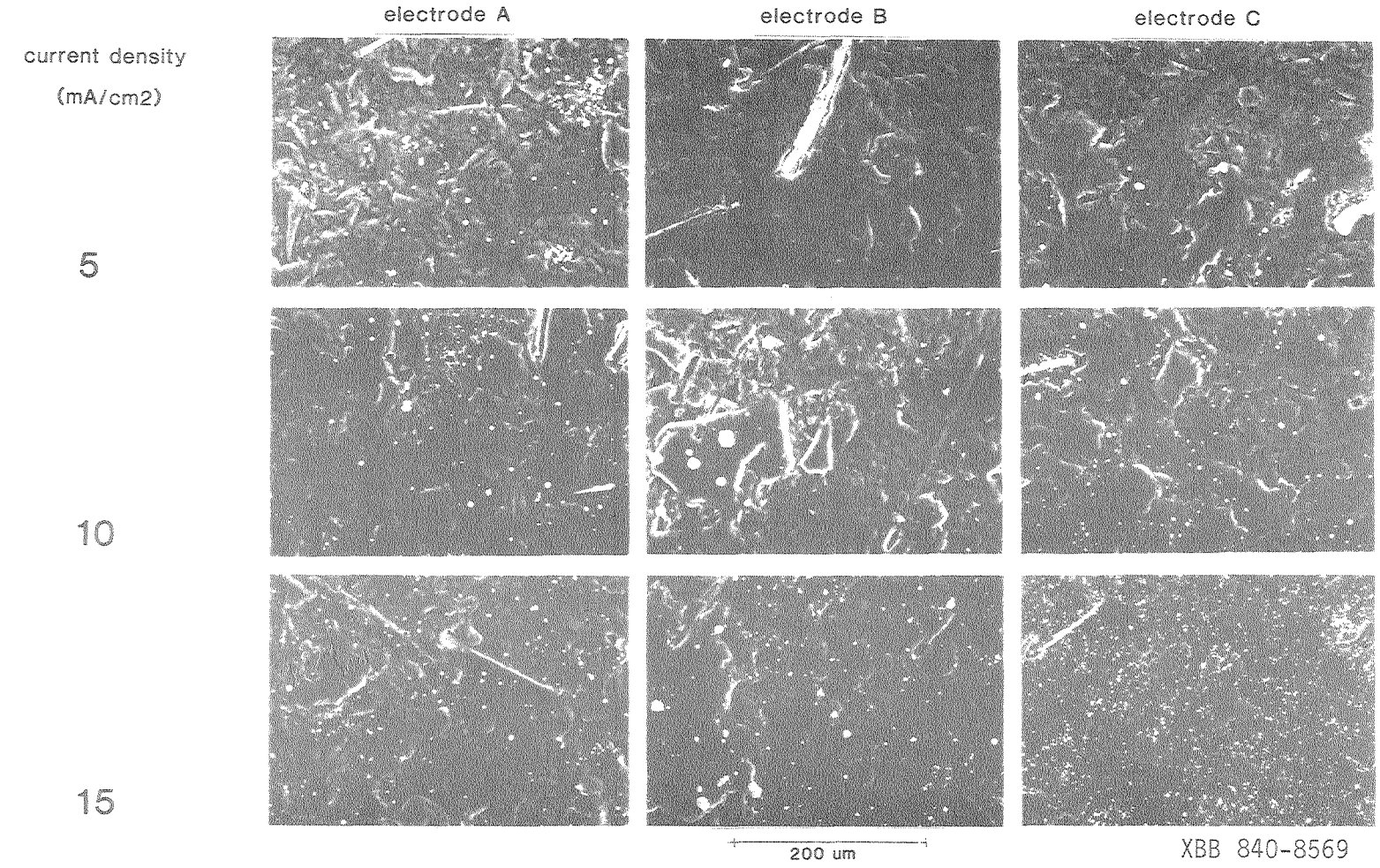

Fig. 5.13A Zinc nodules on graphite loaded polymer substrate,
50 mC/cm^2 (240 A)
1.0 M $ZnCl_2$ (Mallinckrodt reagent)

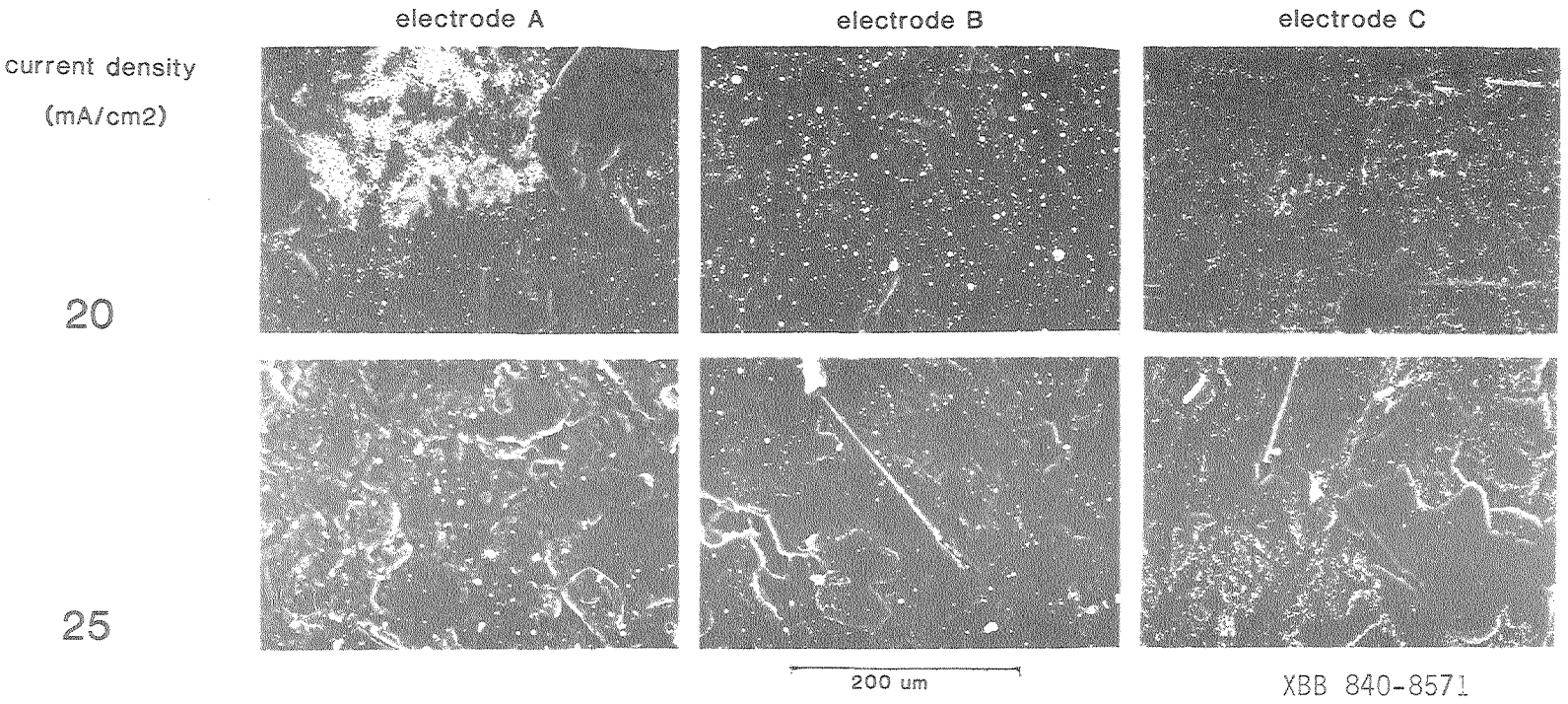

Fig. 5.13B Zinc nodules on graphite loaded polymer substrate.
50 mC/cm^2 (240 A)
1.0 M $ZnCl_2$ (Mallinckrodt reagent)

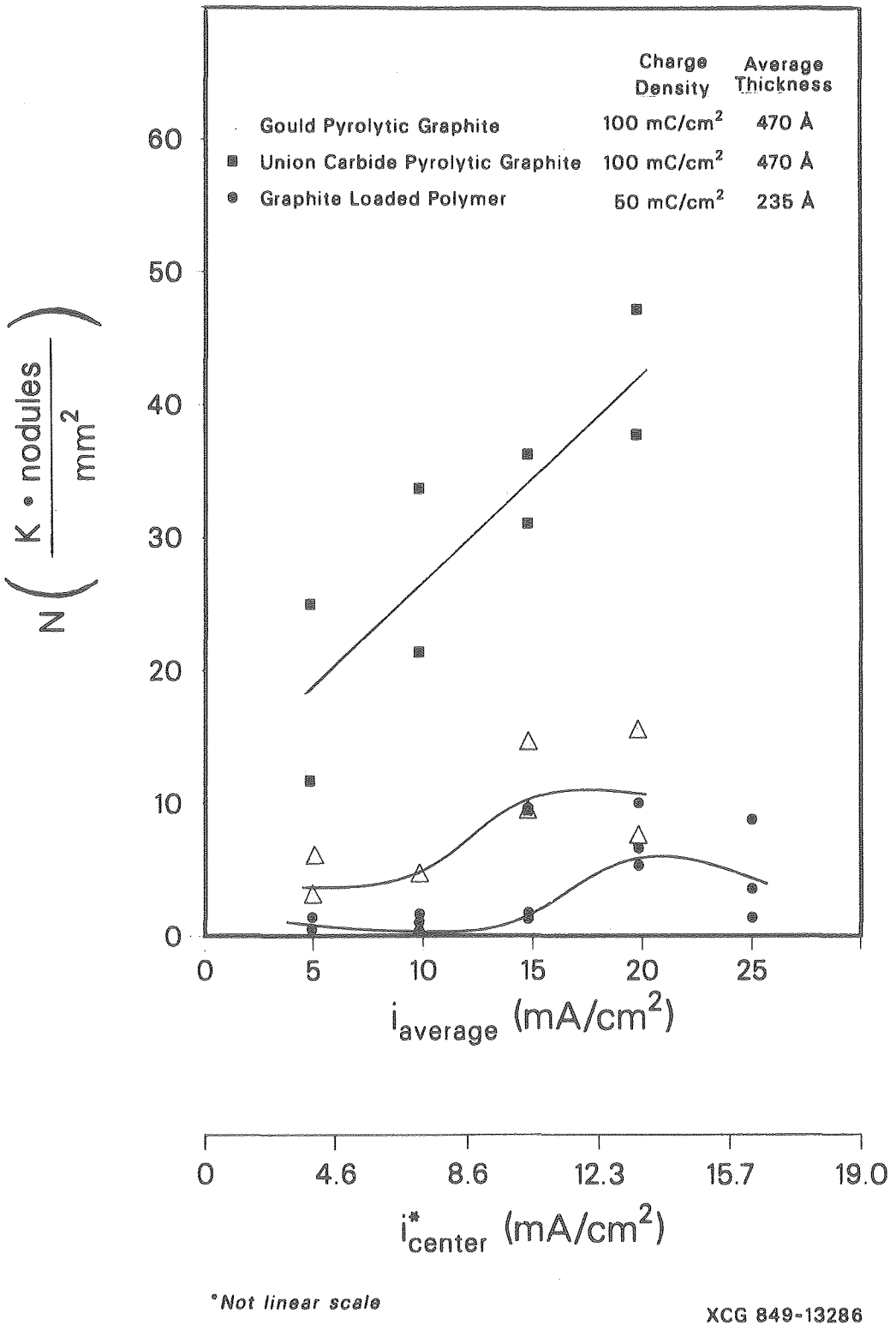

Fig. 5.14 Zinc nodule number density as a function of current density
1.0 M $ZnCl_2$ (MCB reagent)

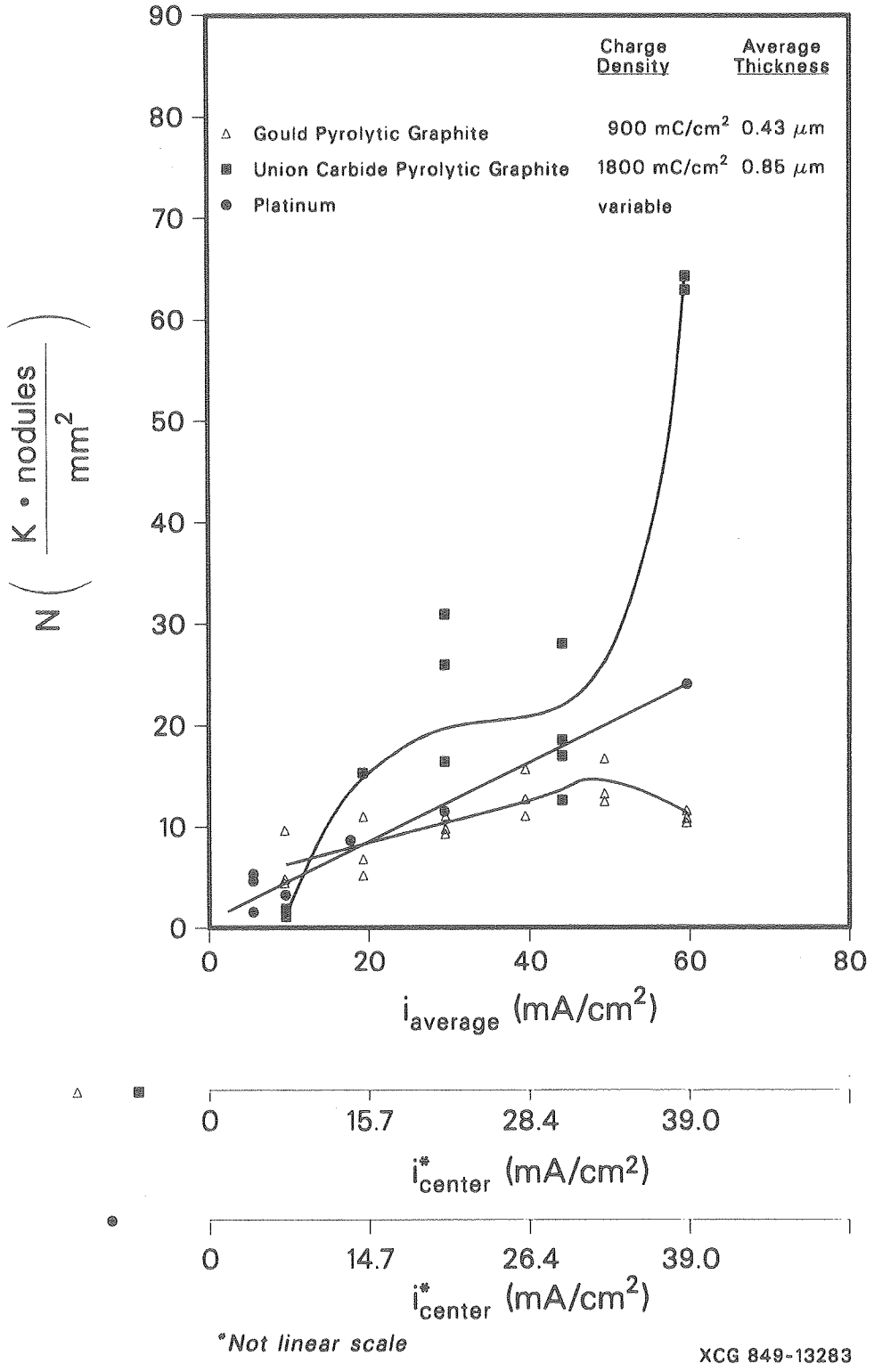

Fig. 5.15 Zinc nodule number density as a function of current density
1.0 M $ZnCl_2$ (Mallinckrodt reagent)

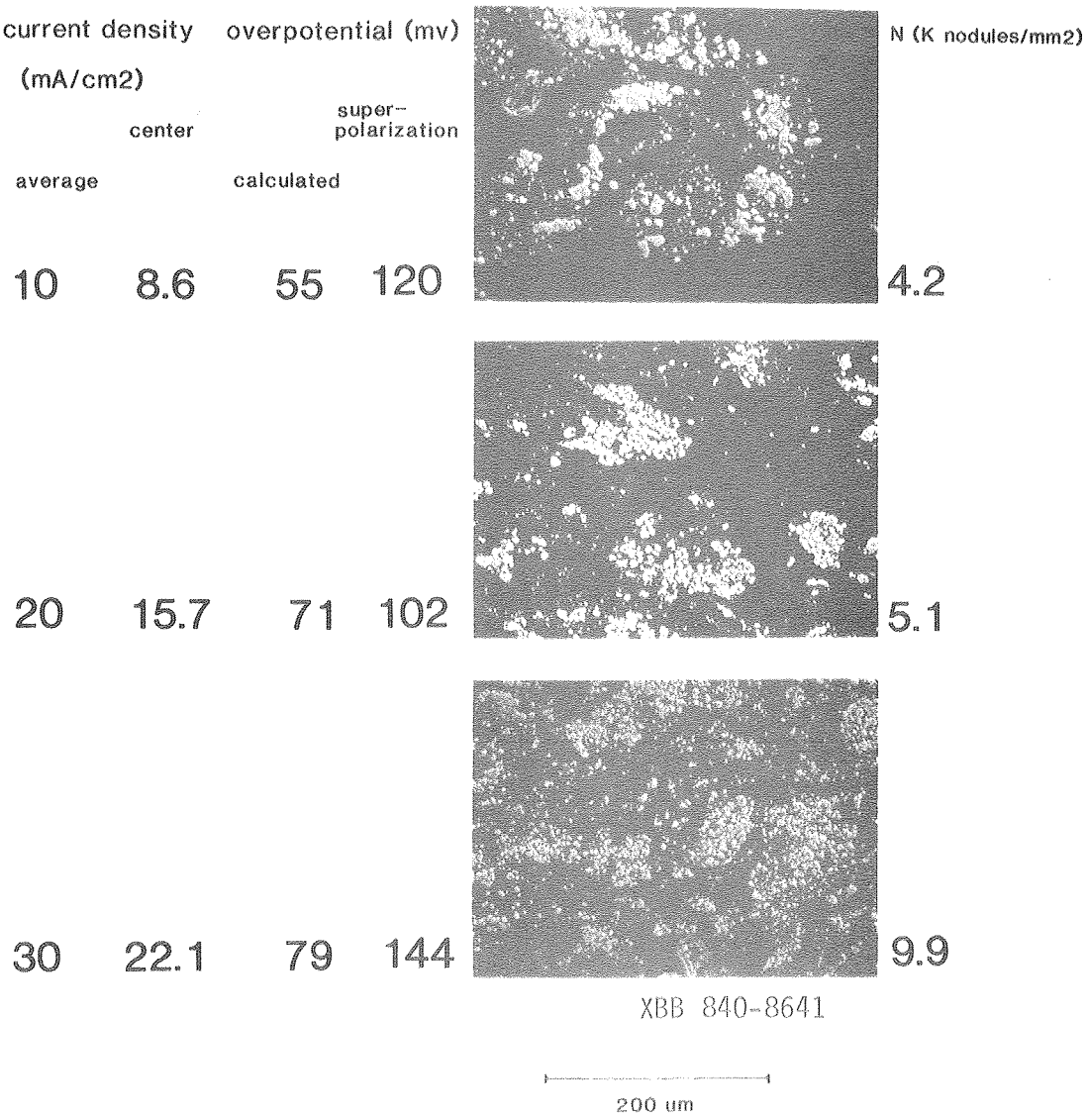

Fig. 5.20A Zinc nodules on Gould pyrolytic graphite substrate, electrode A
900 mC/cm^2 (4300 A)
1.0 M $ZnCl_2$ (MCB reagent)

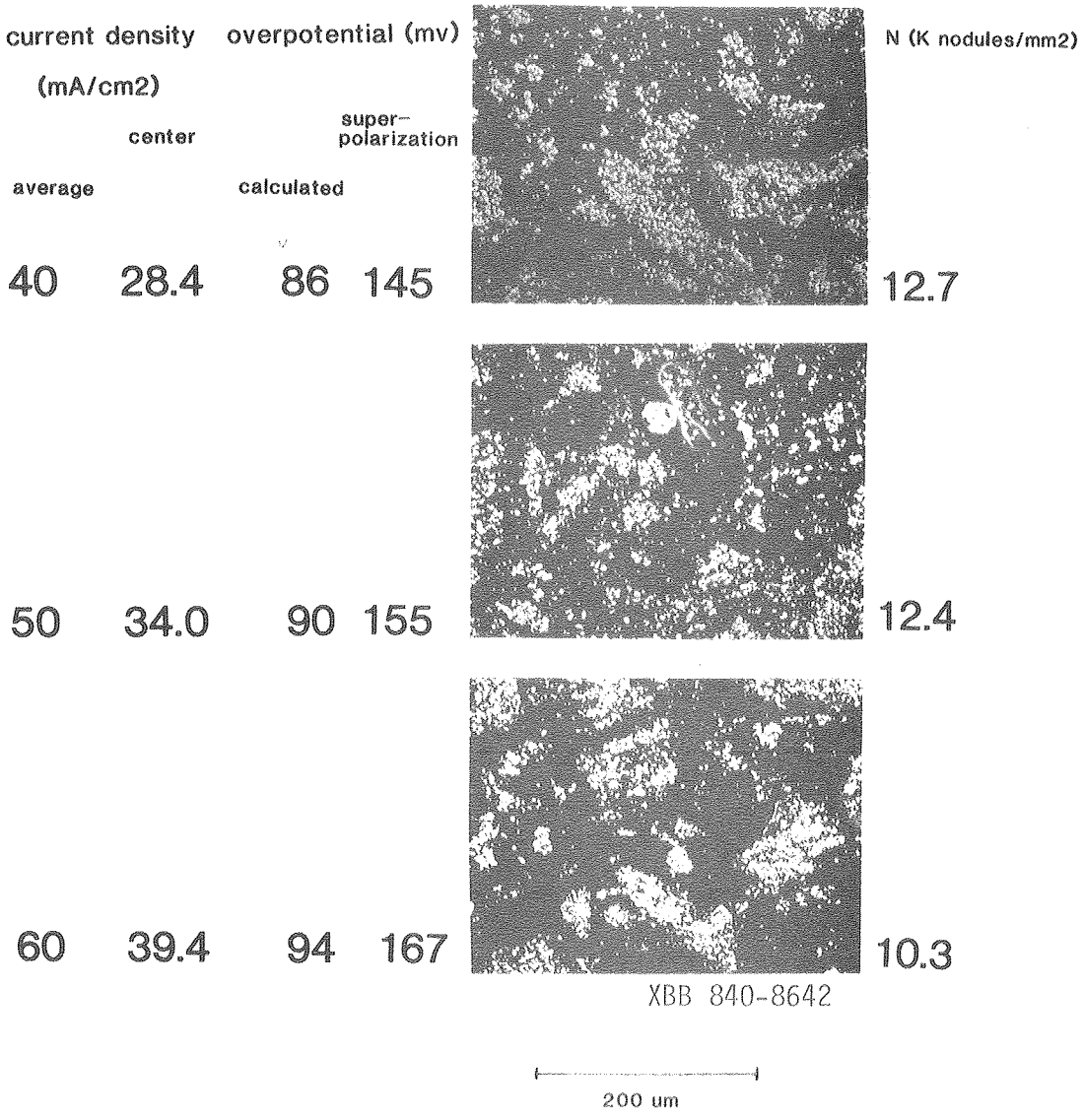

Fig. 5.20B Zinc nodules on Gould pyrolytic graphite substrate, electrode A
900 mC/cm^2 (4300 A)
1.0 M $ZnCl_2$ (MCB reagent)

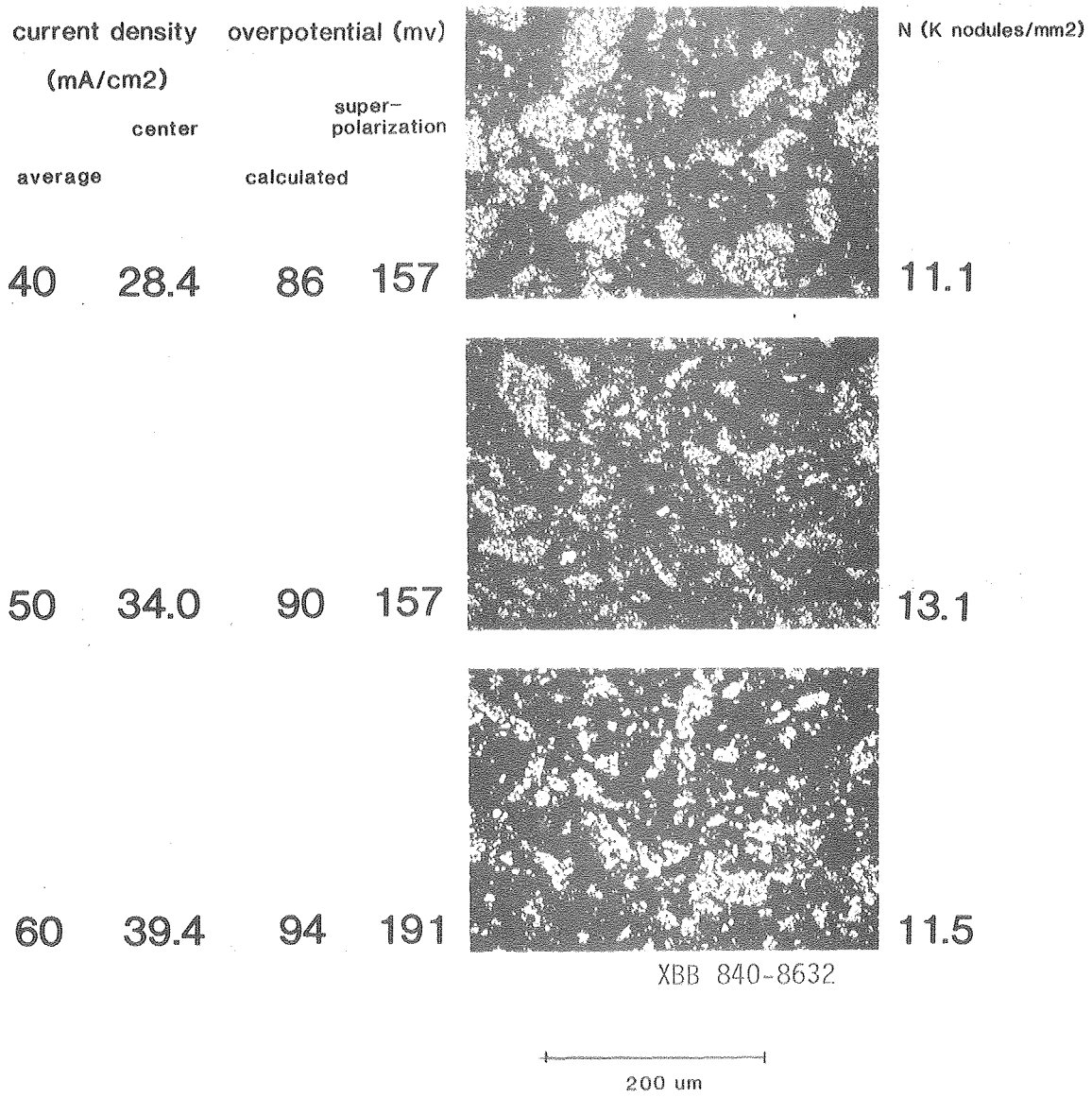

Fig. 5.21A Zinc nodules on Gould pyrolytic graphite substrate, electrode B
900 mC/cm^2 (4300 A)
1.0 M $ZnCl_2$ (MCB reagent)

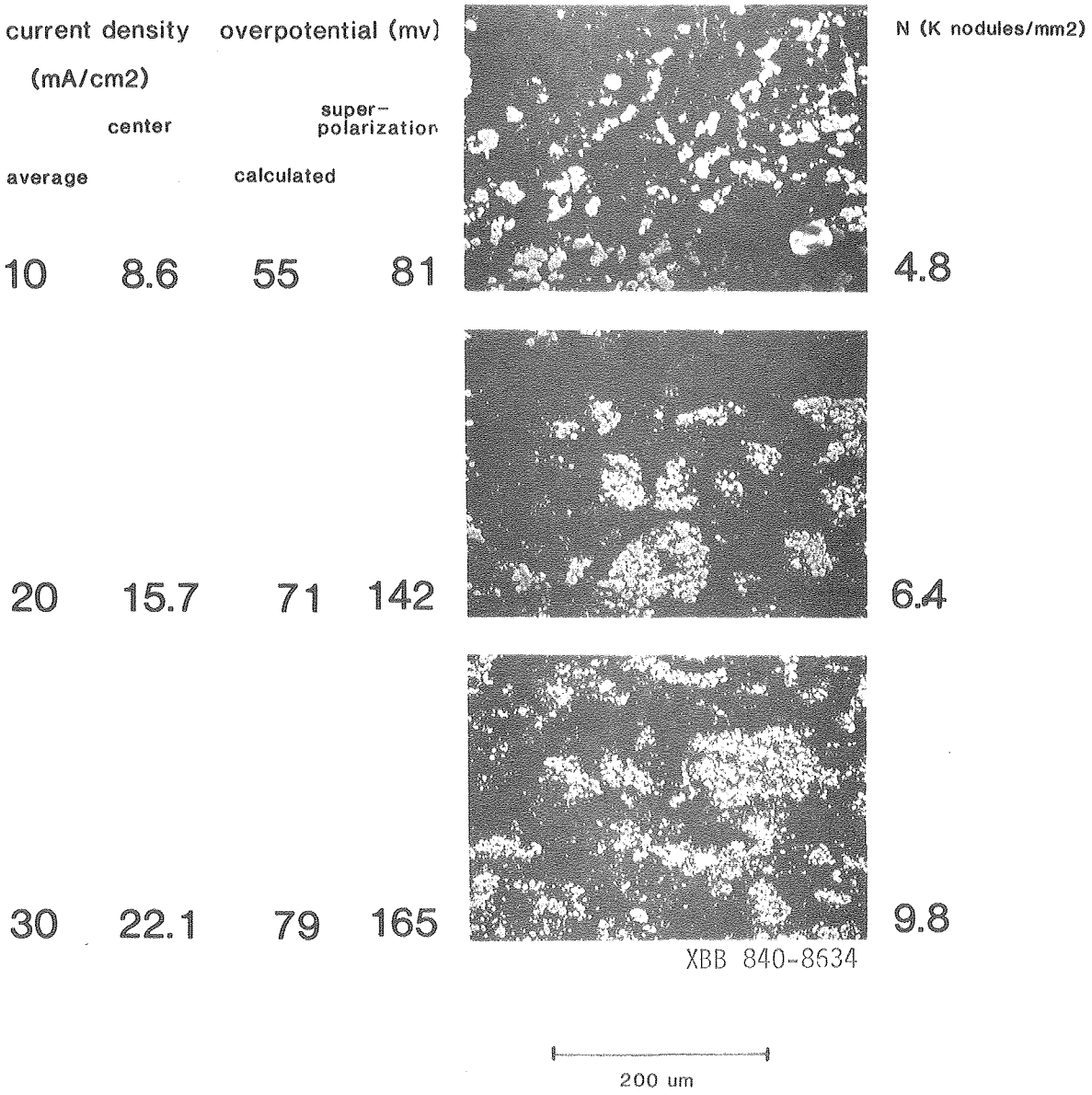

Fig. 5.21B Zinc nodules on Gould pyrolytic graphite substrate, electrode B
900 mC/cm^2 (4300 A)
1.0 M $ZnCl_2$ (MCB reagent)

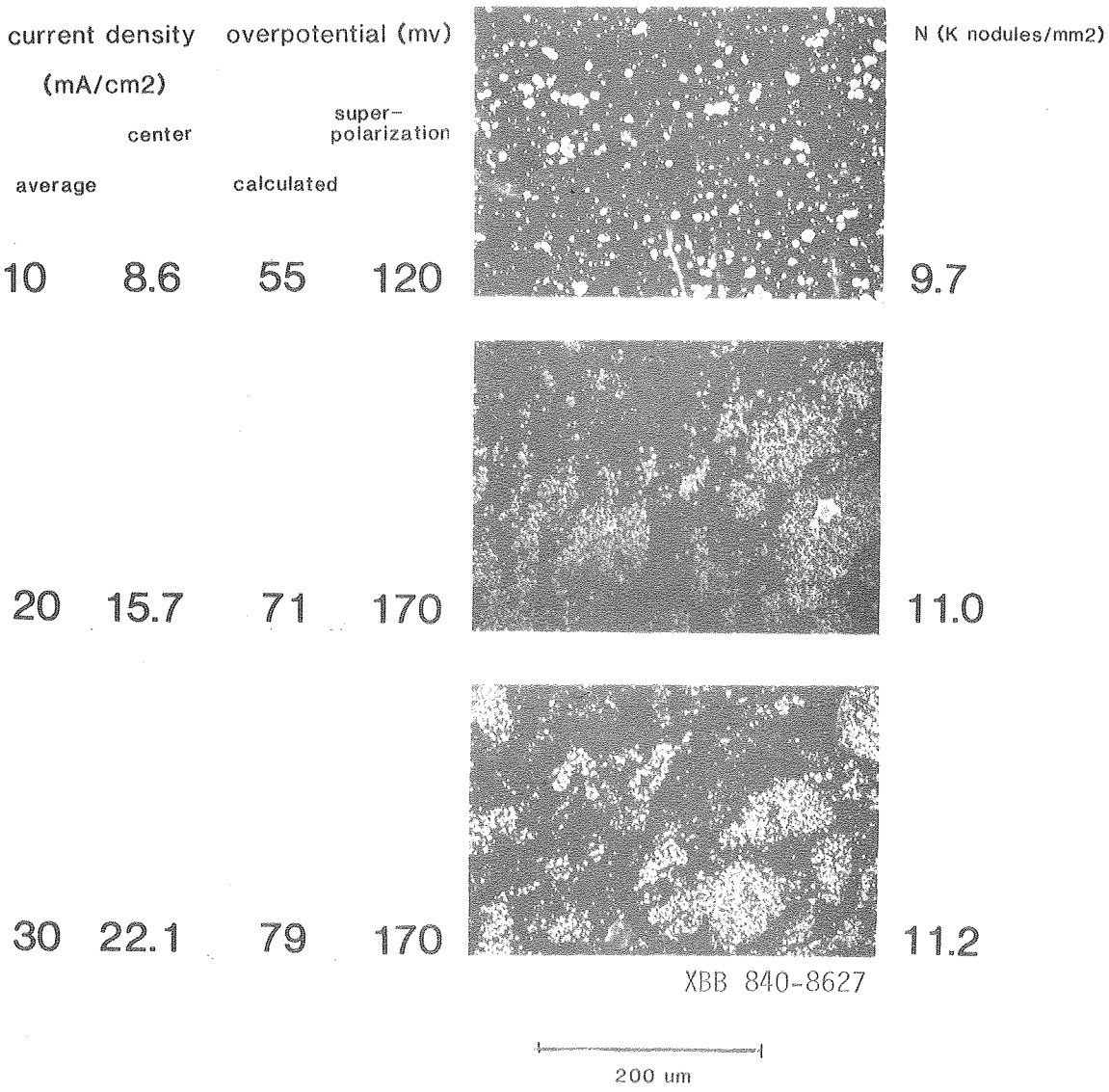

Fig. 5.22A Zinc nodules on Gould pyrolytic graphite substrate, electrode C
900 mC/cm^2 (4300 A)
1.0 M $ZnCl_2$ (MCB reagent)

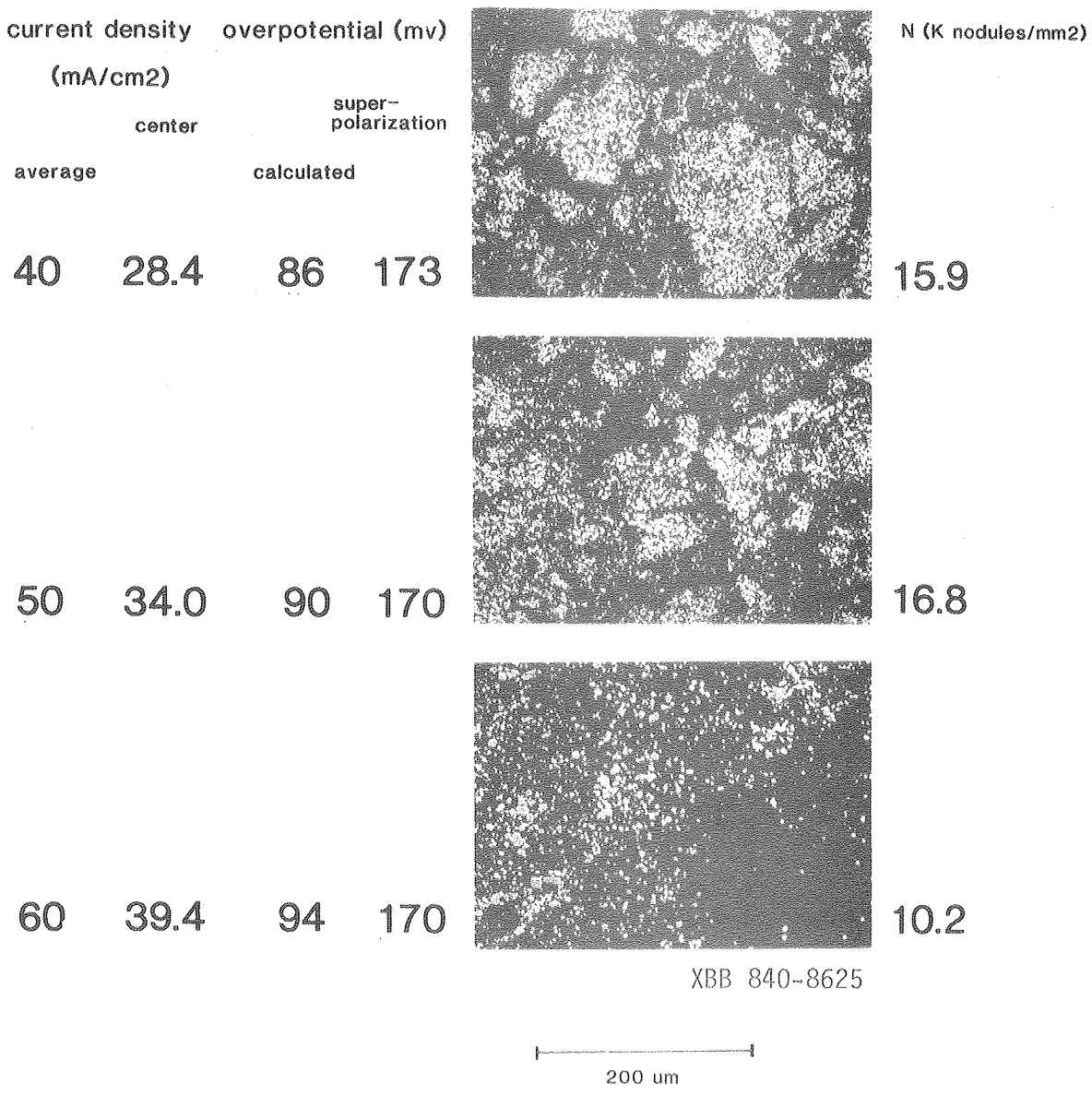

Fig. 5.22B Zinc nodules on Gould pyrolytic graphite substrate.
electrode C
900 mC/cm^2 (4300 A)
1.0 M $ZnCl_2$ (MCB reagent)

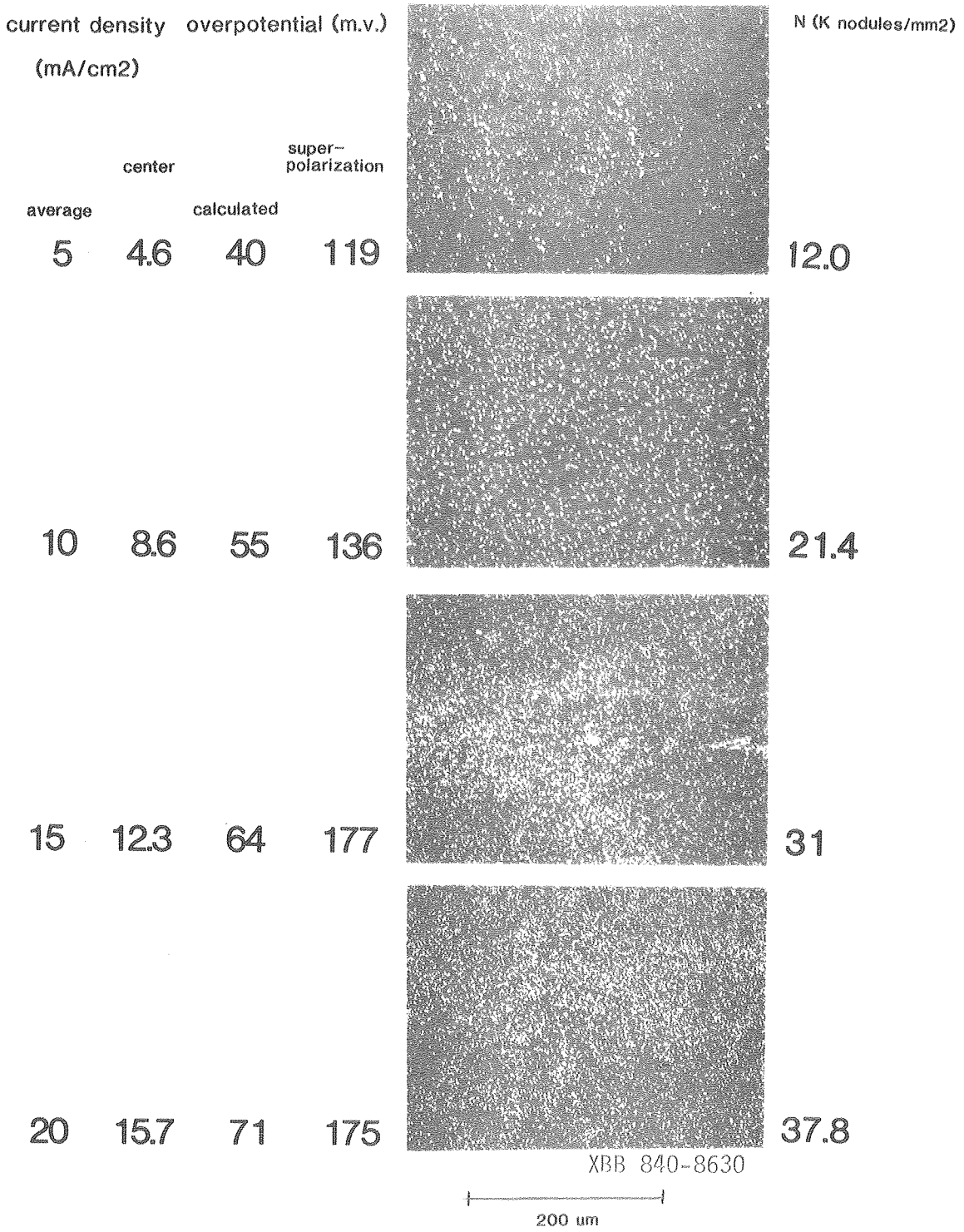

Fig. 5.23 Zinc nodules on Union Carbide pyrolytic graphite substrate, electrode A
100 mC/cm^2 (430 A)
1.0 M $ZnCl_2$ (Mallinckrodt reagent)

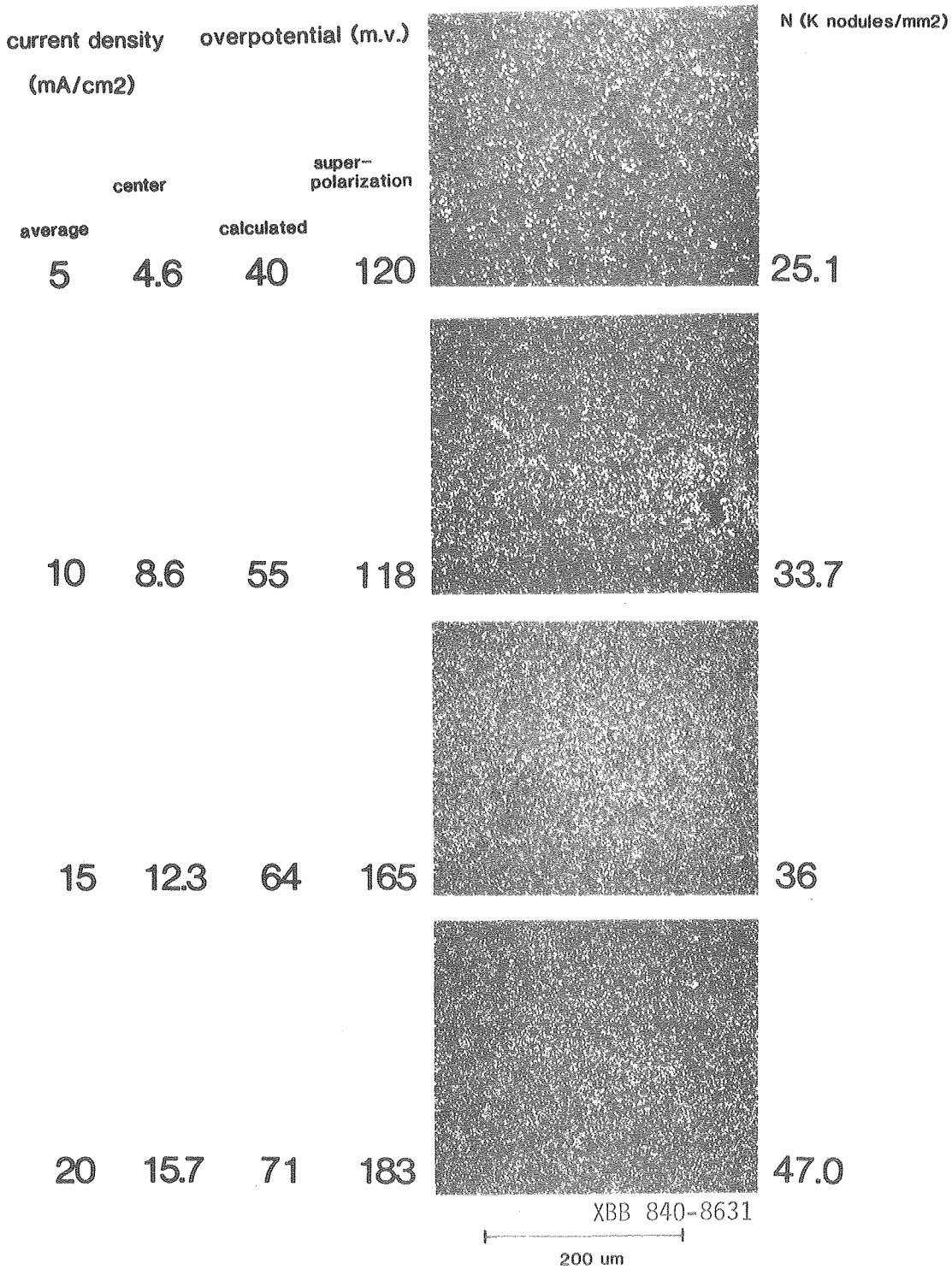

Fig. 5.24 Zinc nodules on Union Carbide pyrolytic graphite substrate, electrode B
100 mC/cm^2 (470 A)
1.0 M $ZnCl_2$ (Mallinckrodt reagent)

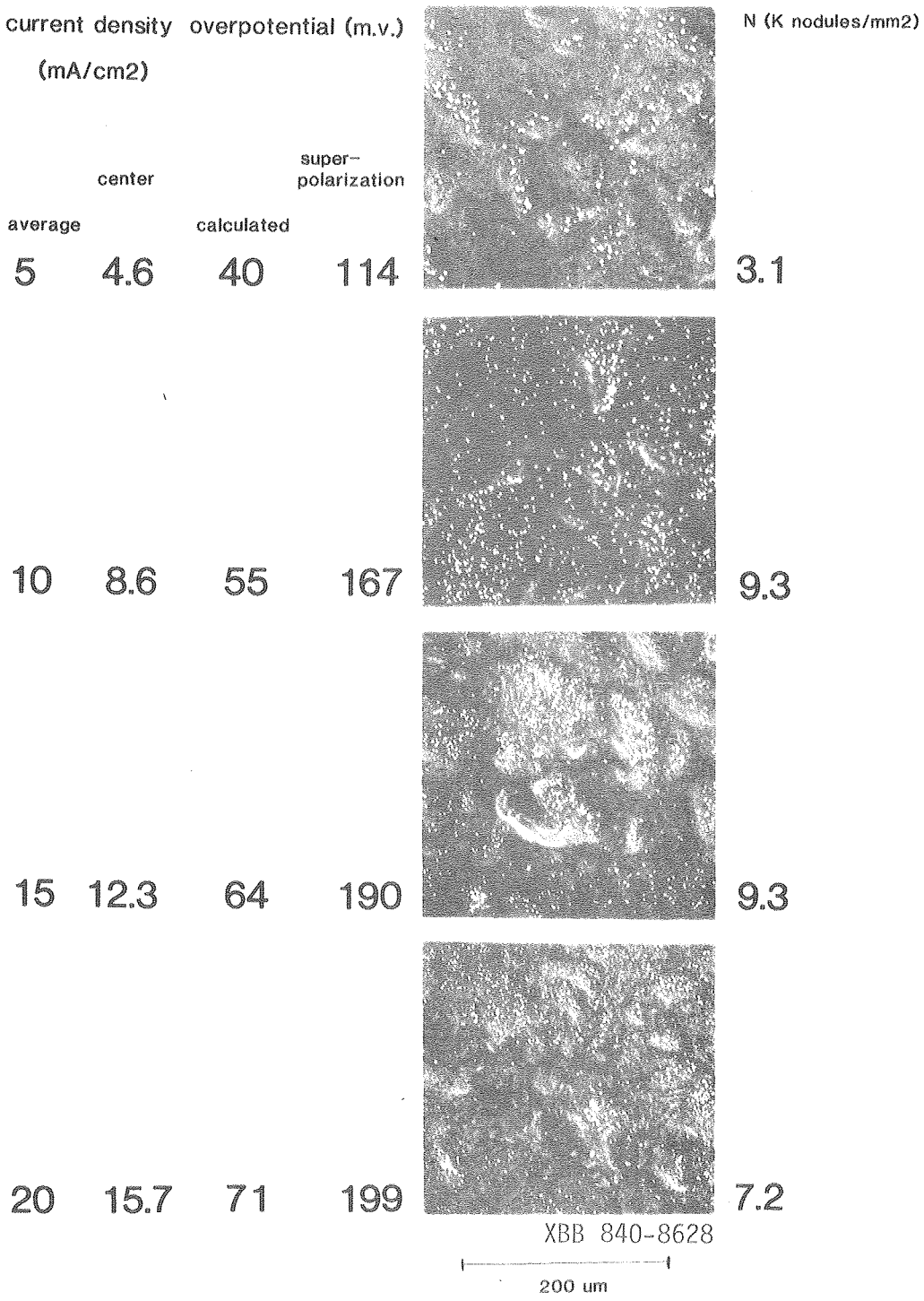

Fig. 5.25 Zinc nodules on Gould pyrolytic graphite substrate, electrode A
100 mC/cm^2 (470 A)
1.0 M $ZnCl_2$ (Mallinckrodt reagent)

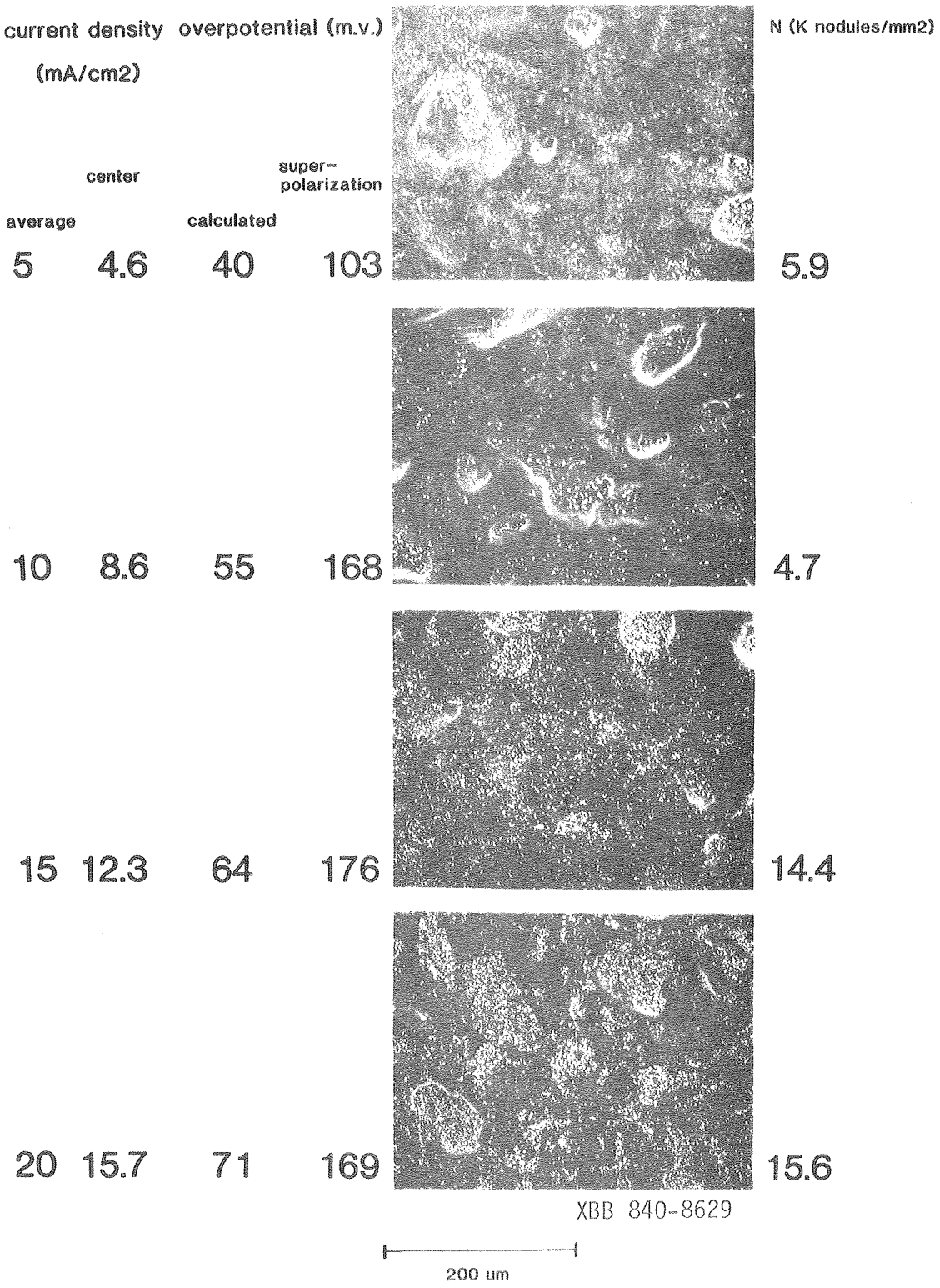

Fig. 5.26 Zinc nodules on Gould pyrolytic graphite substrate, electrode B
100 mC/cm^2 (470 A)
1.0 M $ZnCl_2$ (Mallinckrodt reagent)

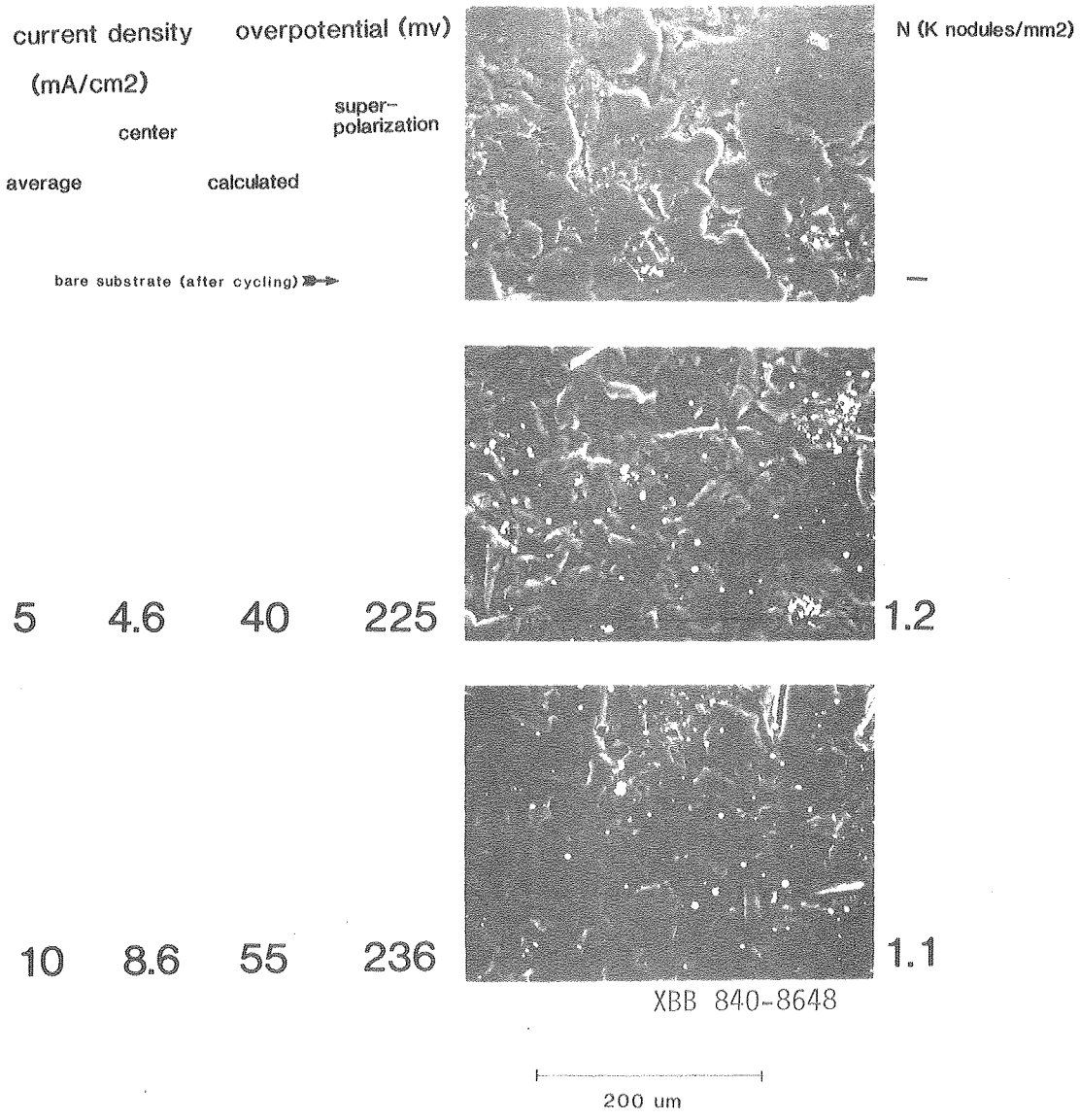

Fig. 5.27A Zinc nodules on graphite loaded polymer substrate, electrode A
50 mC/cm^2 (240 A)
1.0 M $ZnCl_2$ (Mallinckrodt reagent)

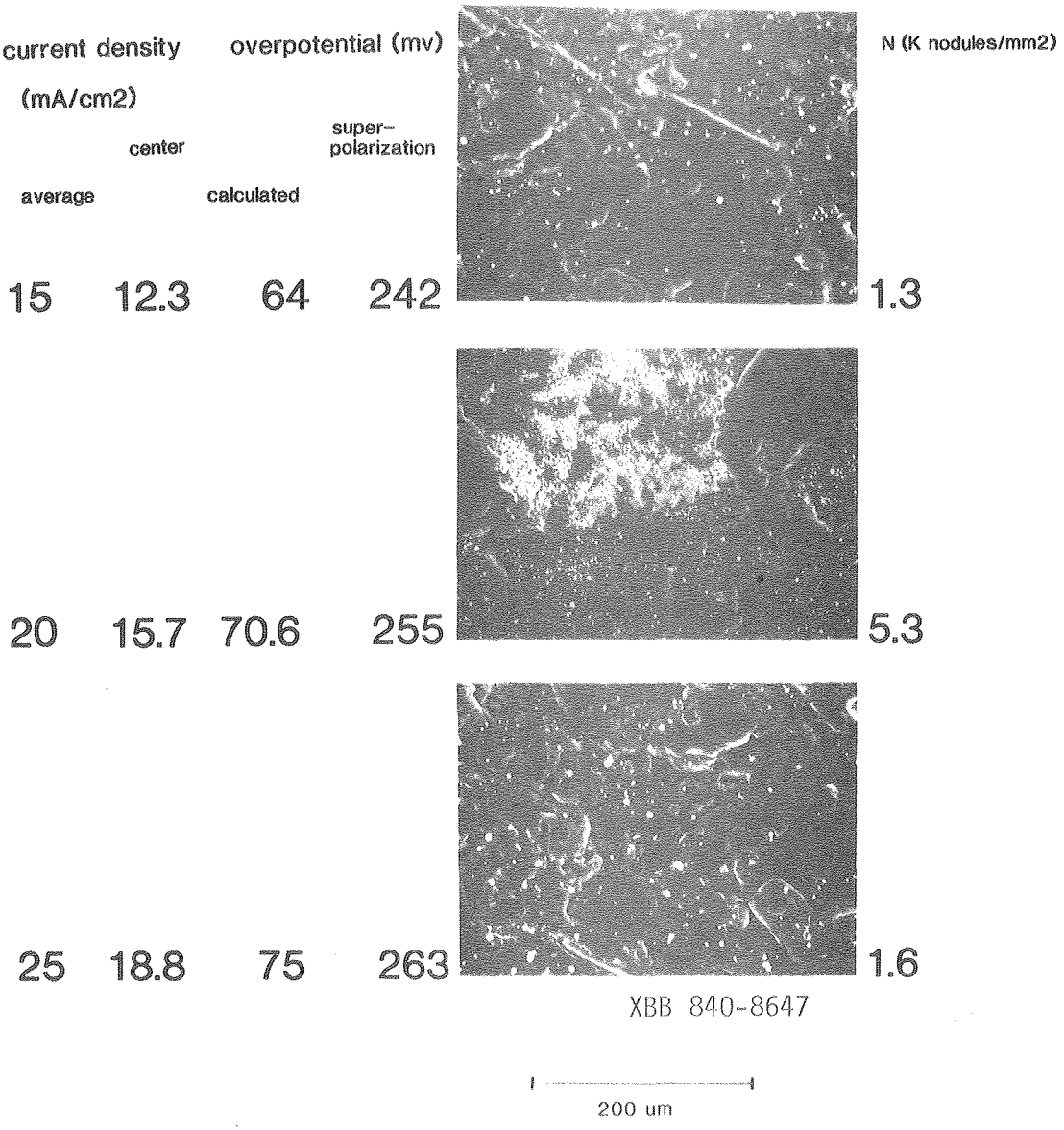

Fig. 5.27B Zinc nodules on graphite loaded polymer substrate, electrode A
50 mC/cm^2 (240 A)
1.0 M $ZnCl_2$ (Mallinckrodt reagent)

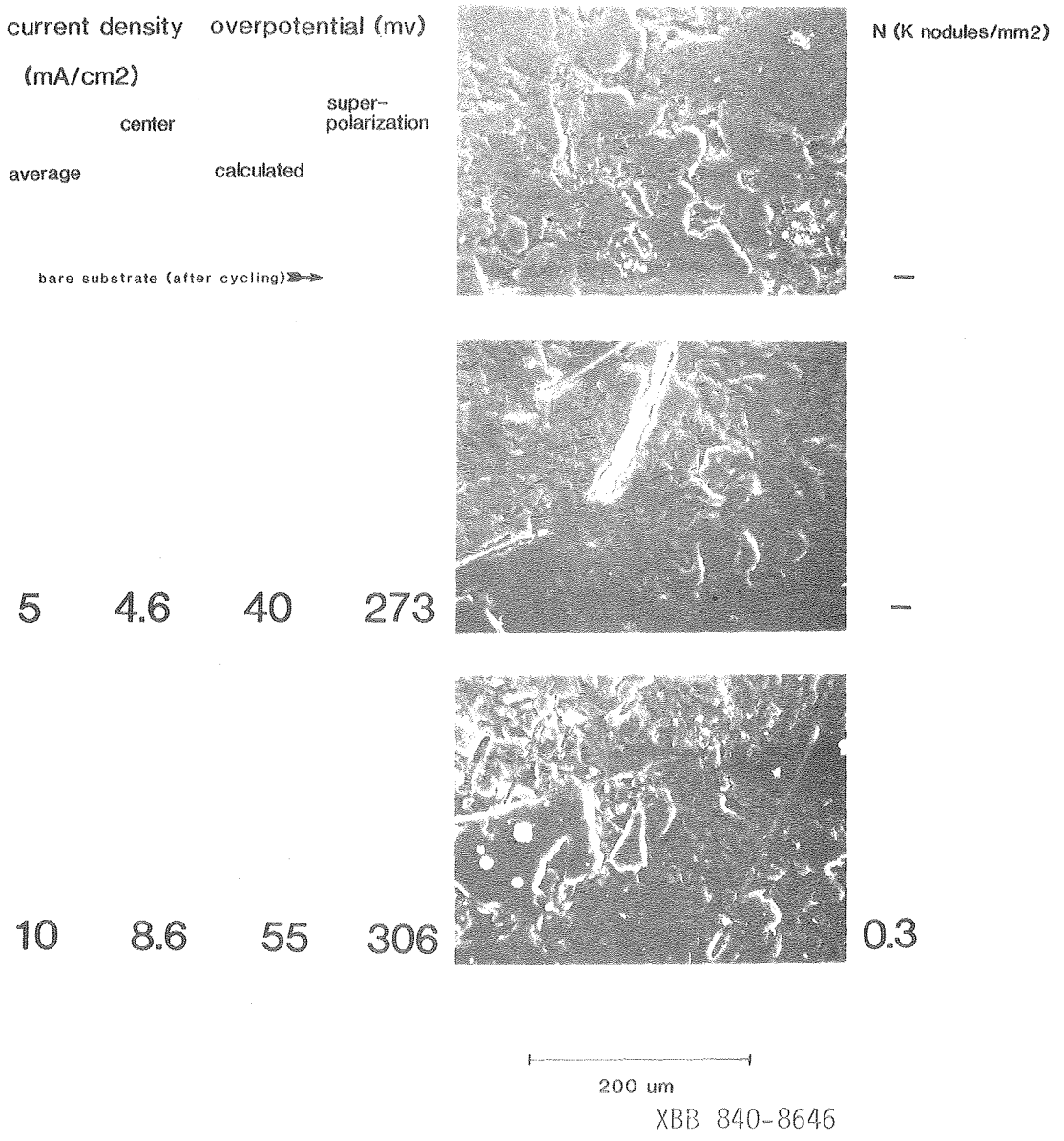

Fig. 5.28A Zinc nodules on graphite loaded polymer substrate, electrode B
50 mC/cm^2 (240 A)
1.0 M $ZnCl_2$ (Mallinckrodt reagent)

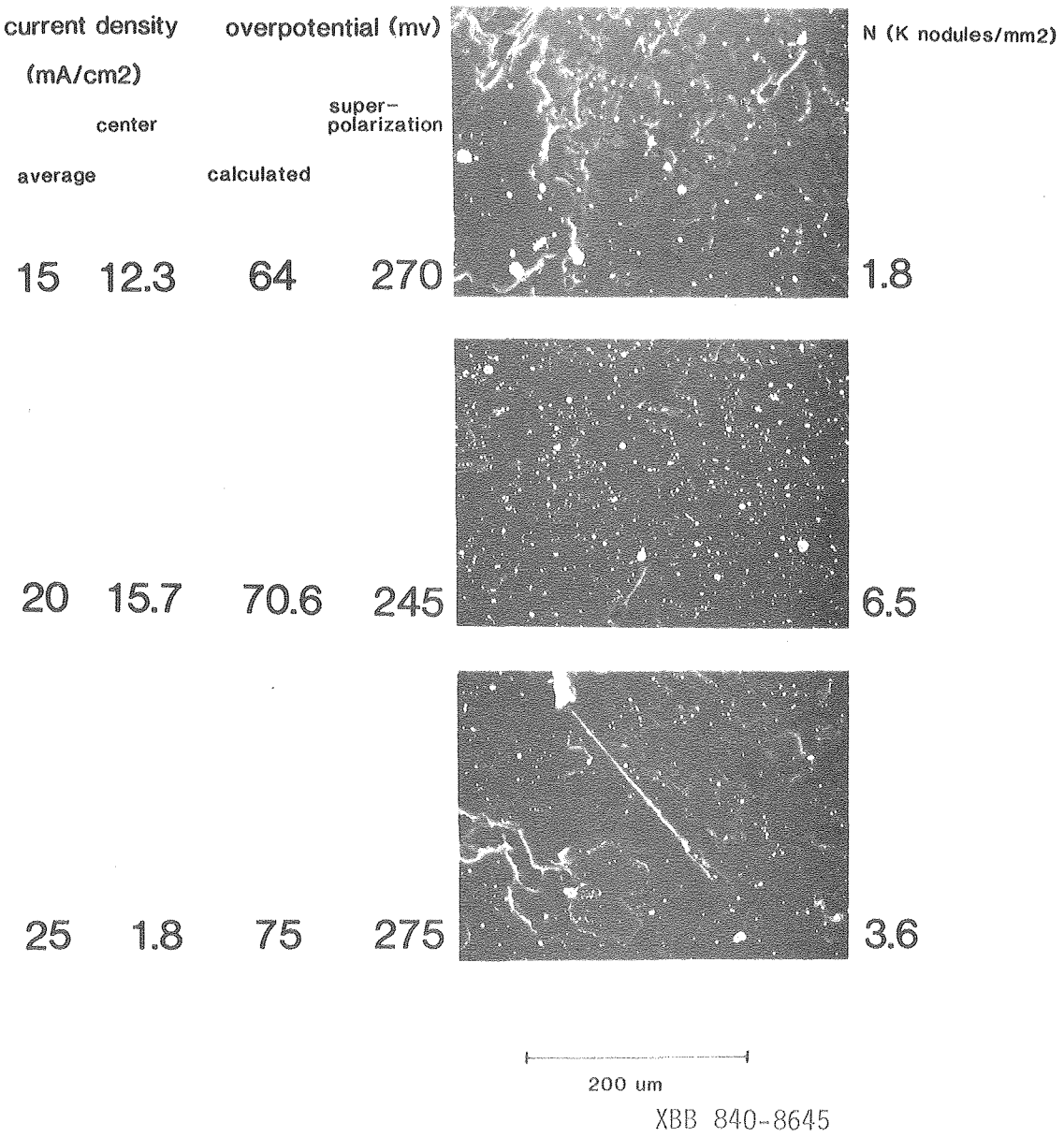

XBB 840-8645

Fig. 5.28B Zinc nodules on graphite loaded polymer substrate, electrode B
50 mC/cm^2 (240 A)
1.0 M $ZnCl_2$ (Mallinckrodt reagent)

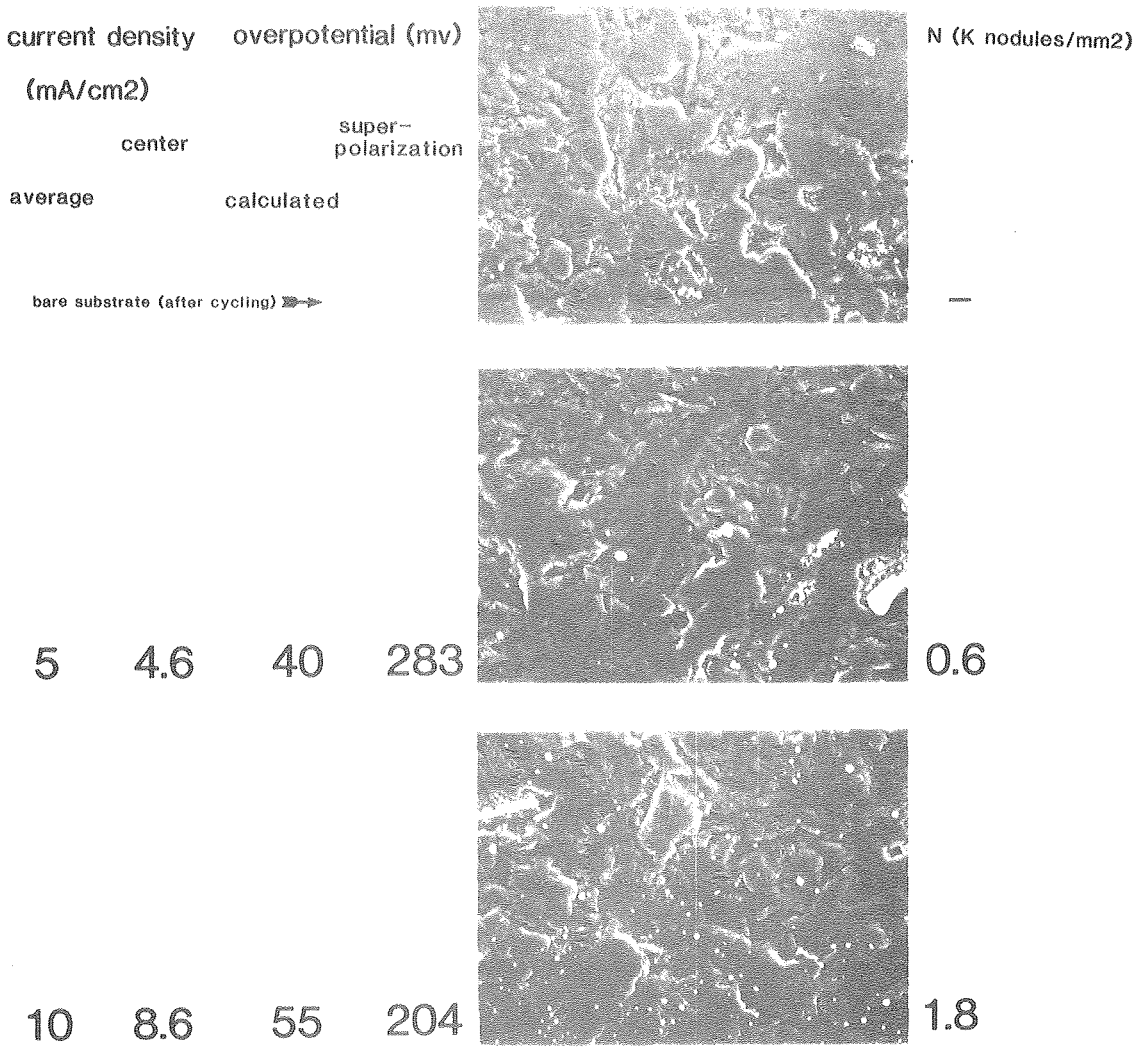

XBB 840-8644

Fig. 5.29A Zinc nodules on graphite loaded polymer substrate, electrode C
50 mC/cm^2 (240 A)
1.0 M $ZnCl_2$ (Mallinckrodt reagent)

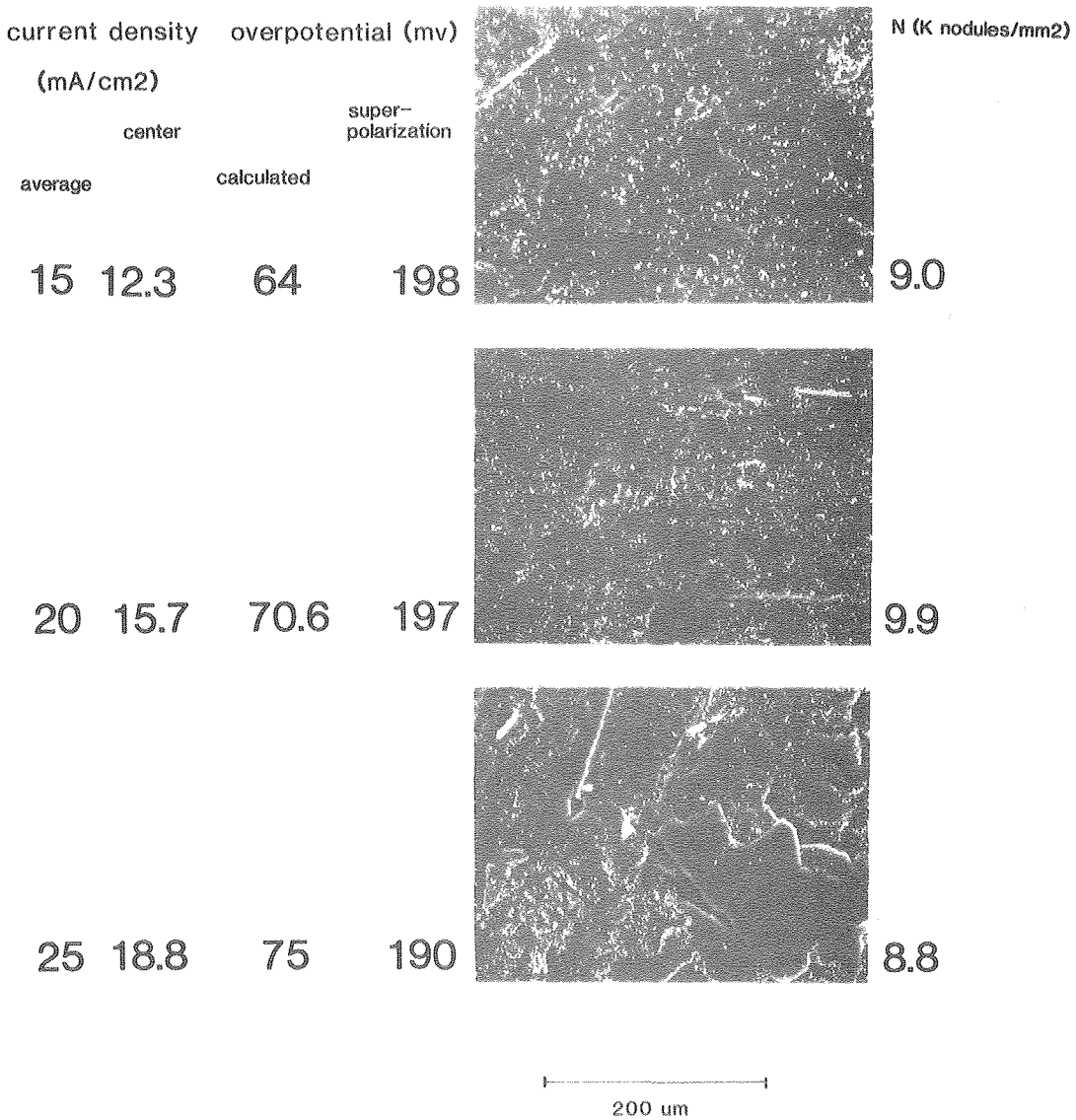

Fig. 29B Zinc nodules on graphite loaded polymer substrate, electrode C
50 mC/cm^2 (240 A)
1.0 M $ZnCl_2$ (Mallinckrodt reagent)

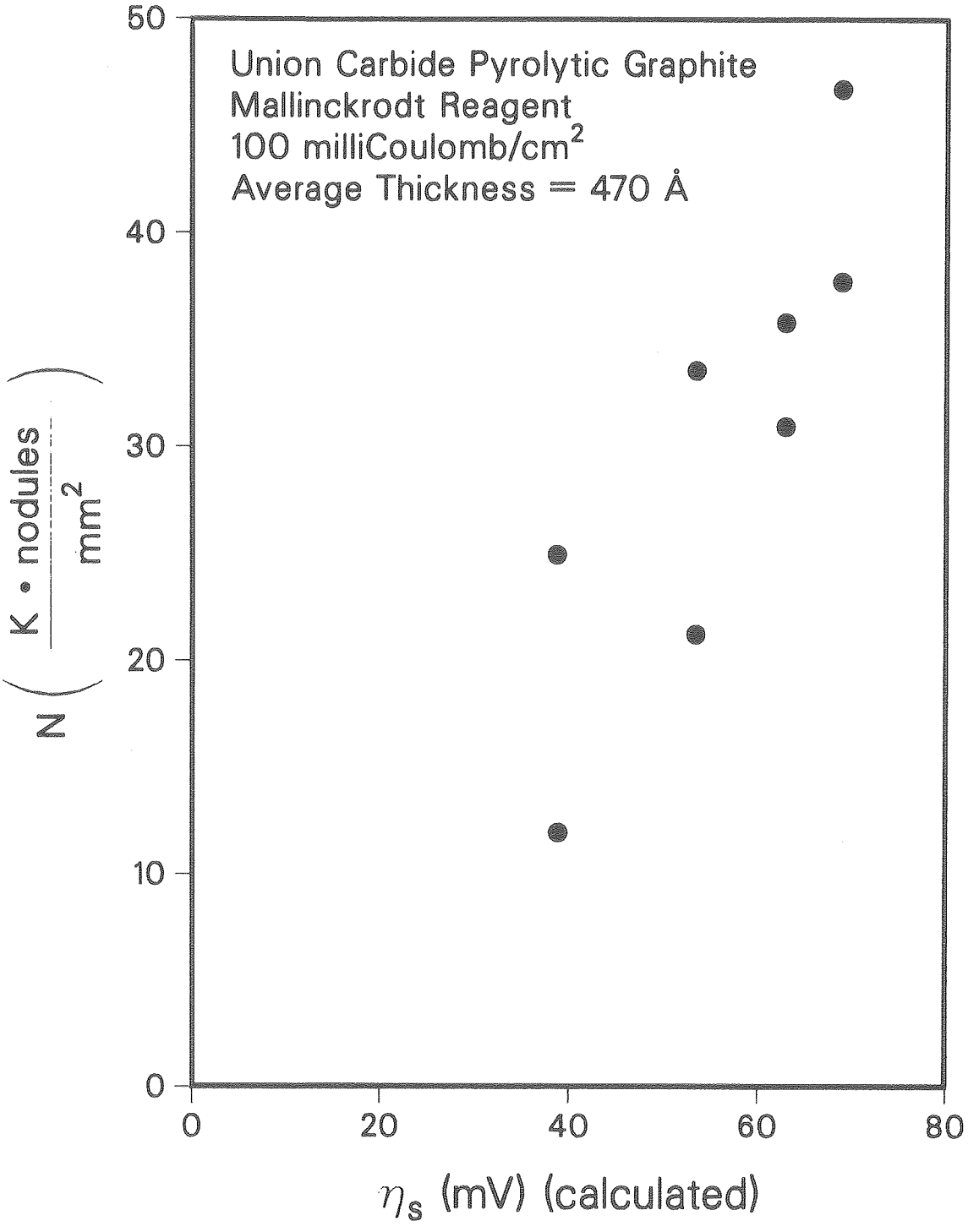

Fig. 5.30 Zinc nodule number density versus calculated surface overpotential

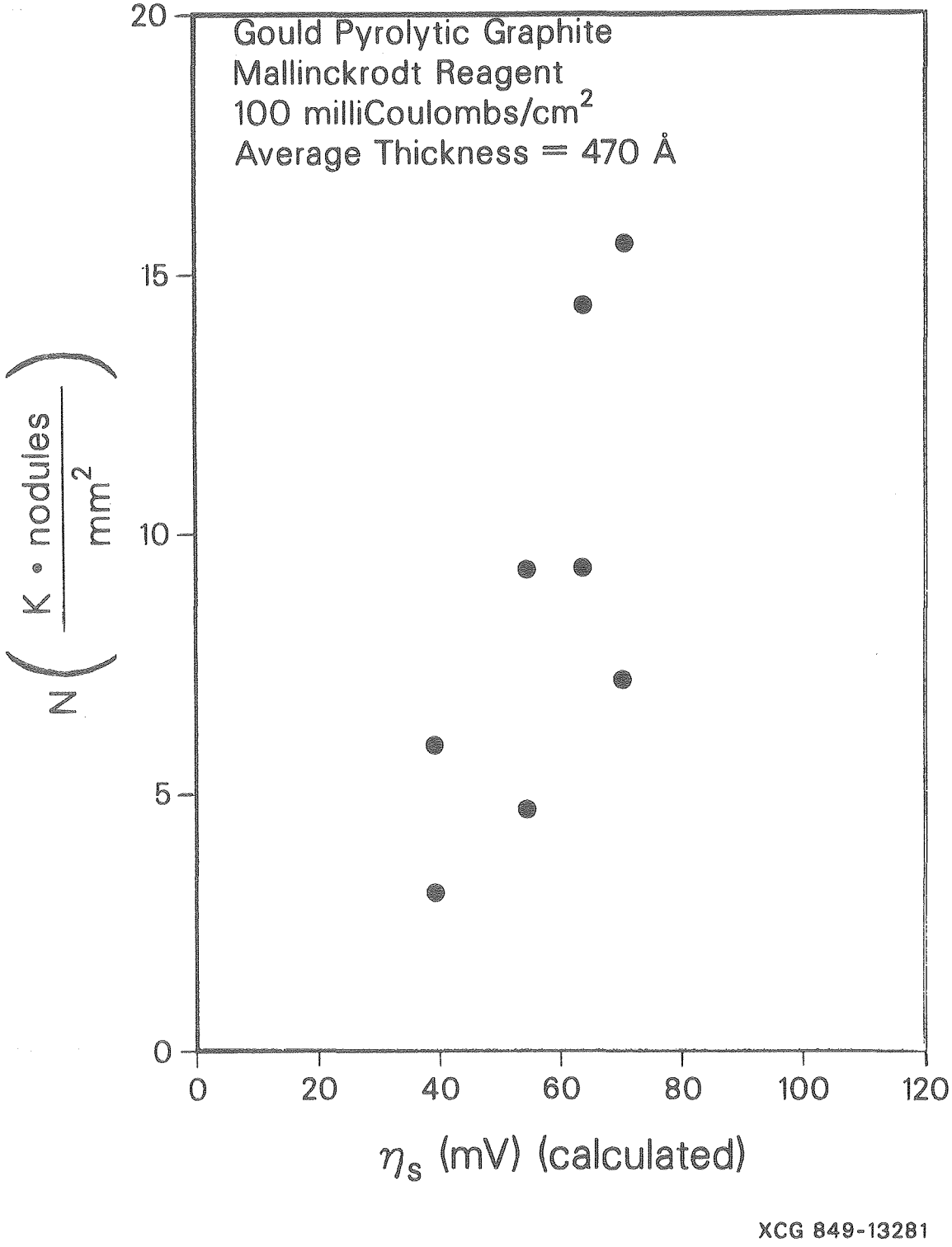

Fig. 5.31 Zinc nodule number density versus calculated surface overpotential

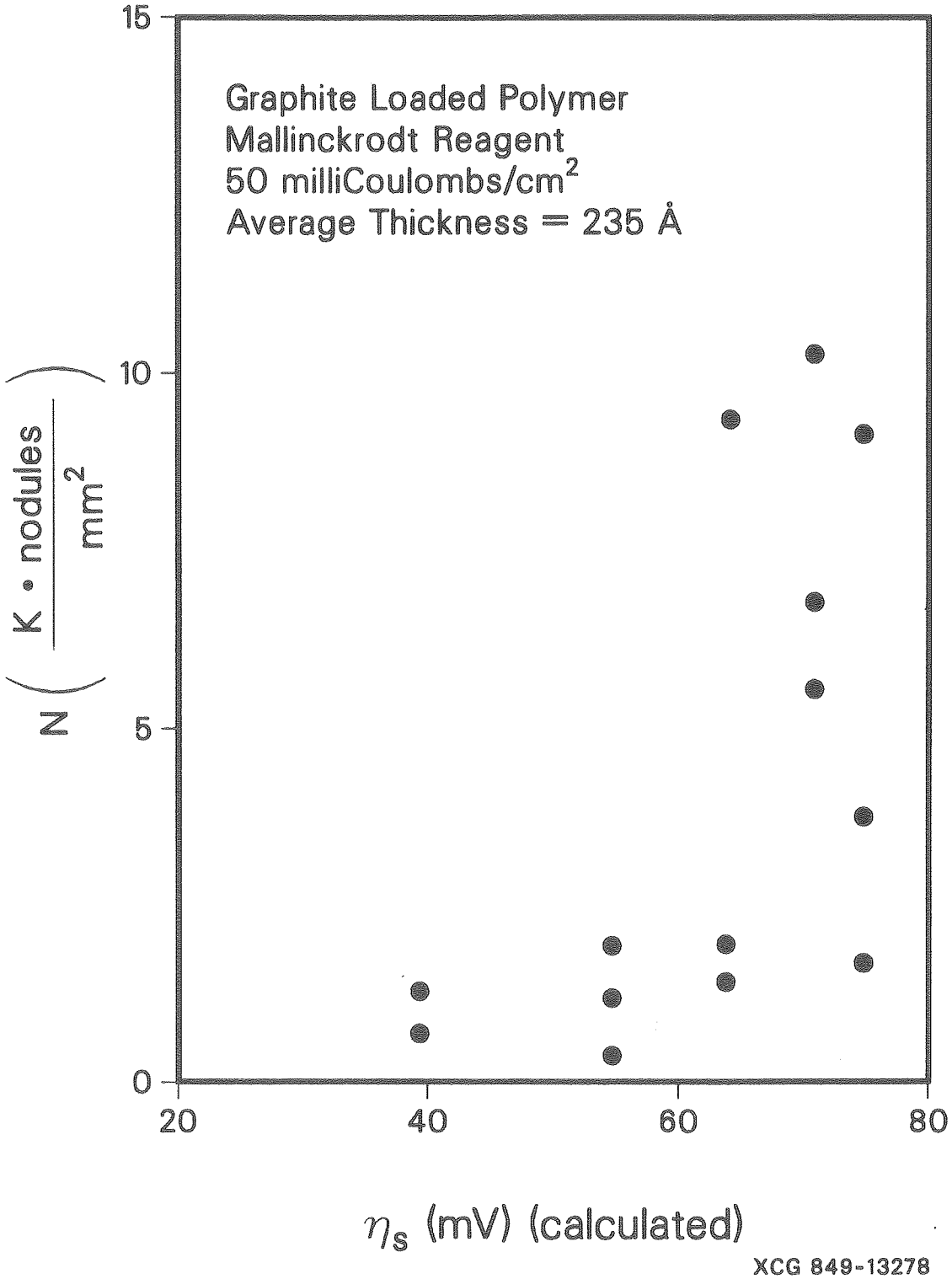

Fig. 5.32 Zinc nodule number density versus calculated surface overpotential

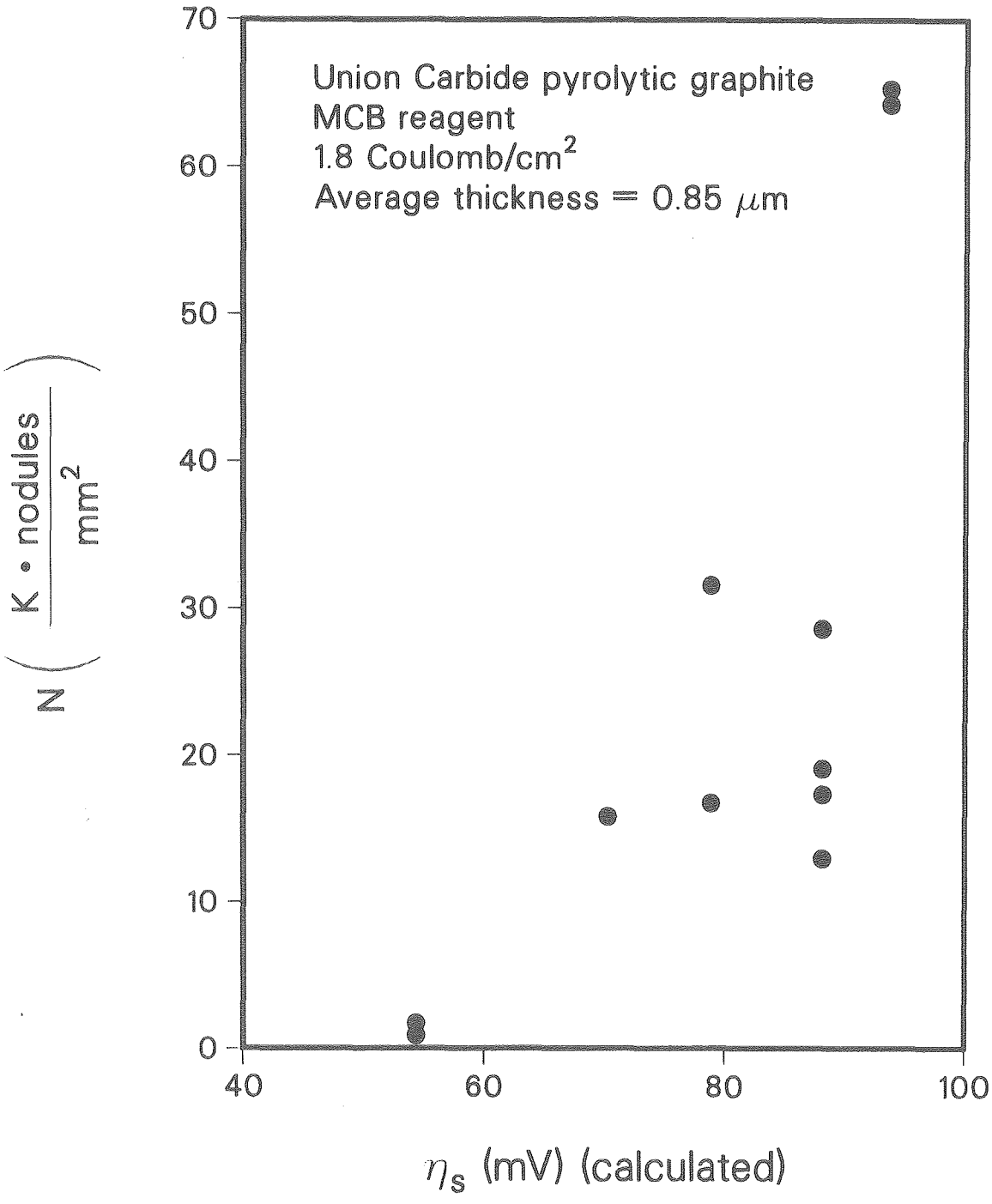

XCG 849-13276

Fig. 5.33 Zinc nodule number density versus calculated surface overpotential

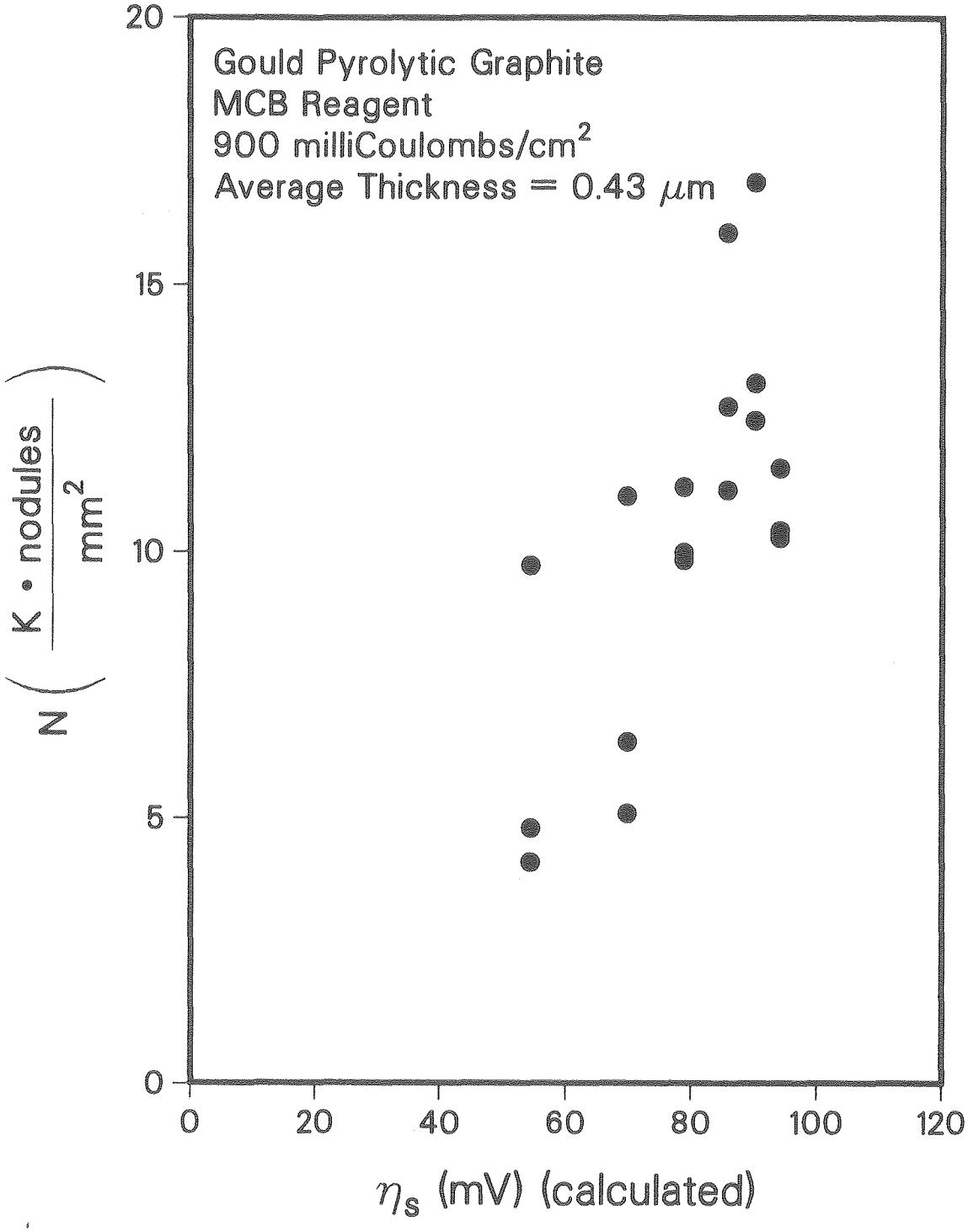

XCG 849-13277

Fig. 5.34 Zinc nodule number density versus calculated surface overpotential

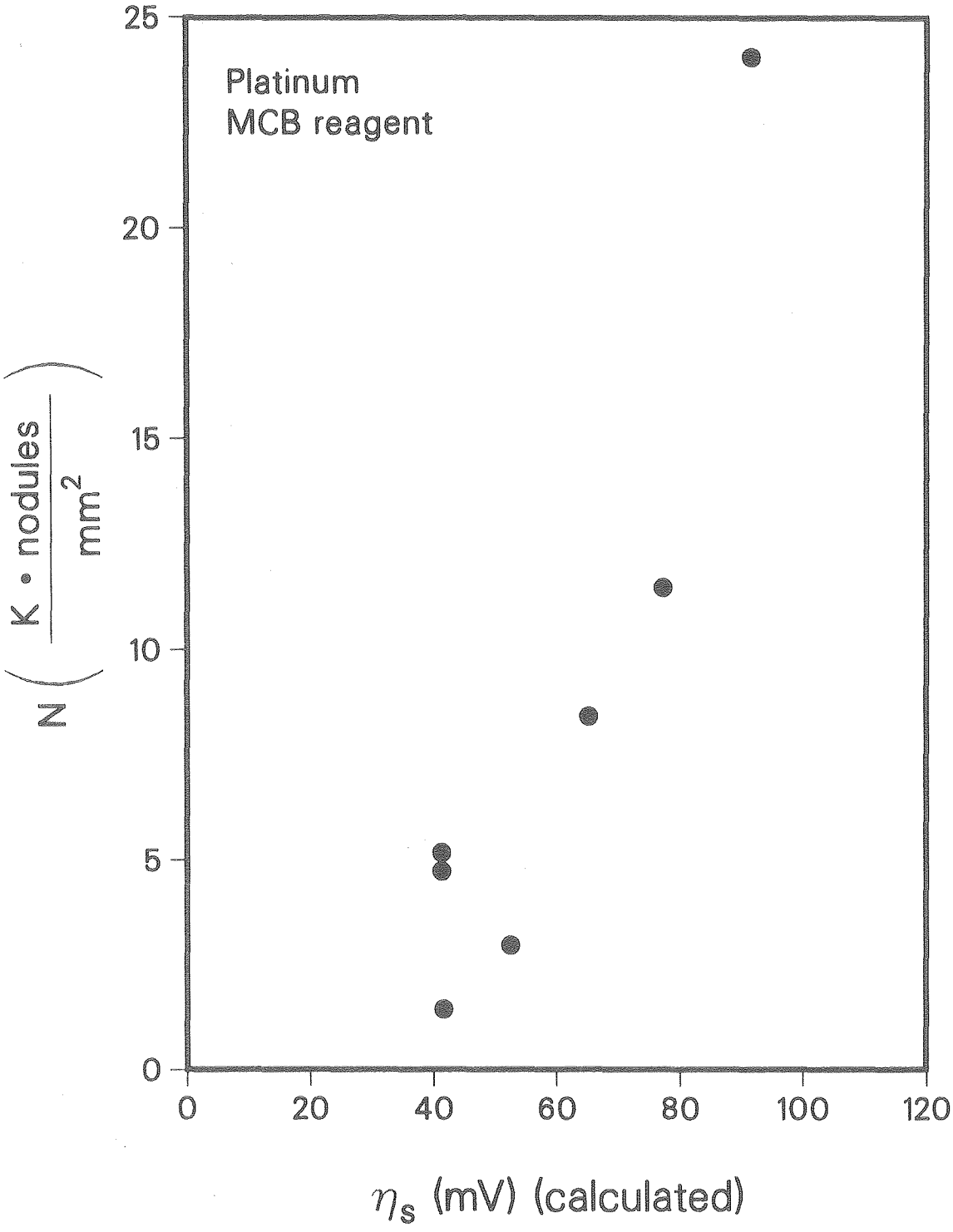

Fig. 5.35 Zinc nodule number density versus calculated surface overpotential

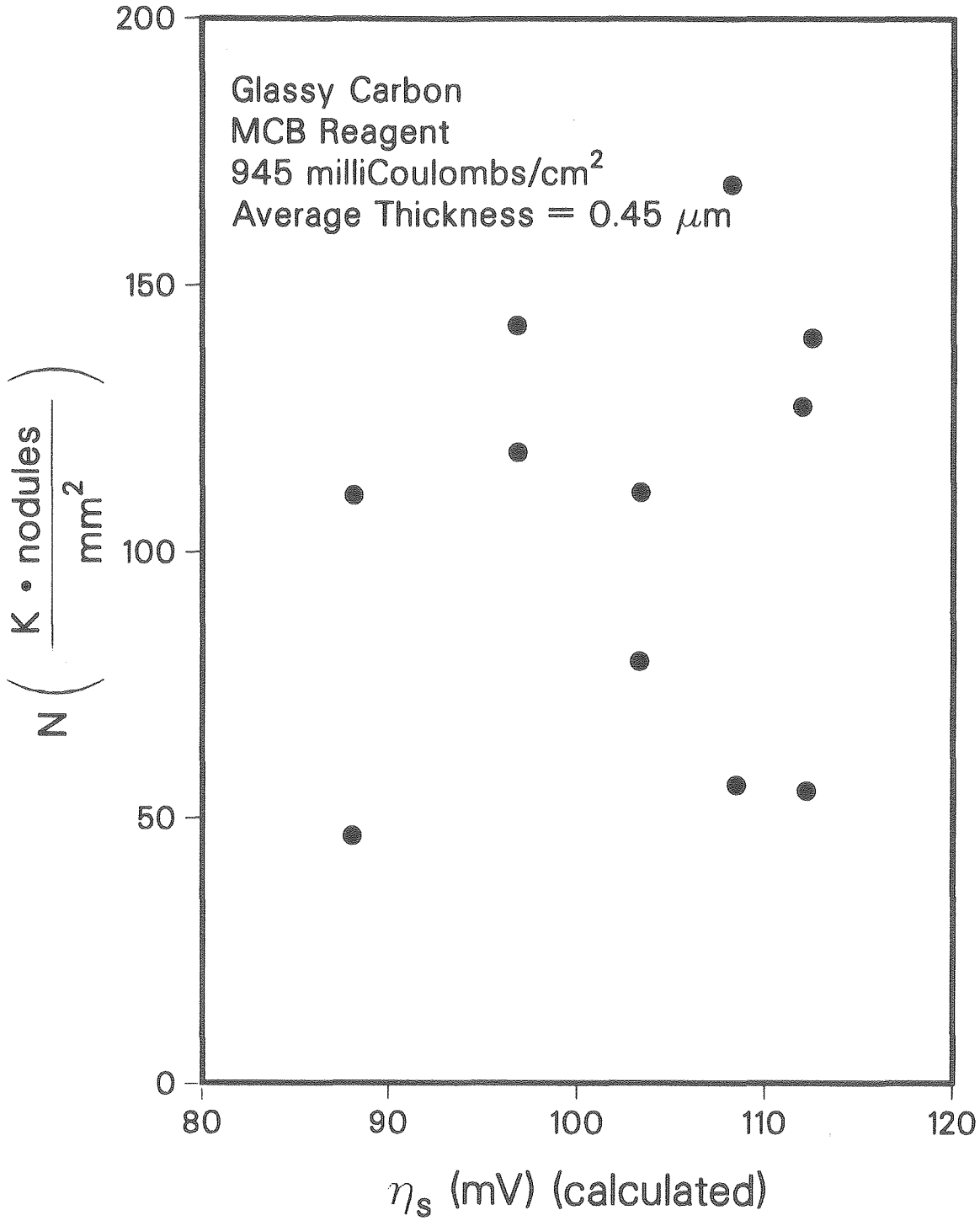

XCG 849-13282

Fig. 5.36 Zinc nodule number density versus calculated surface overpotential

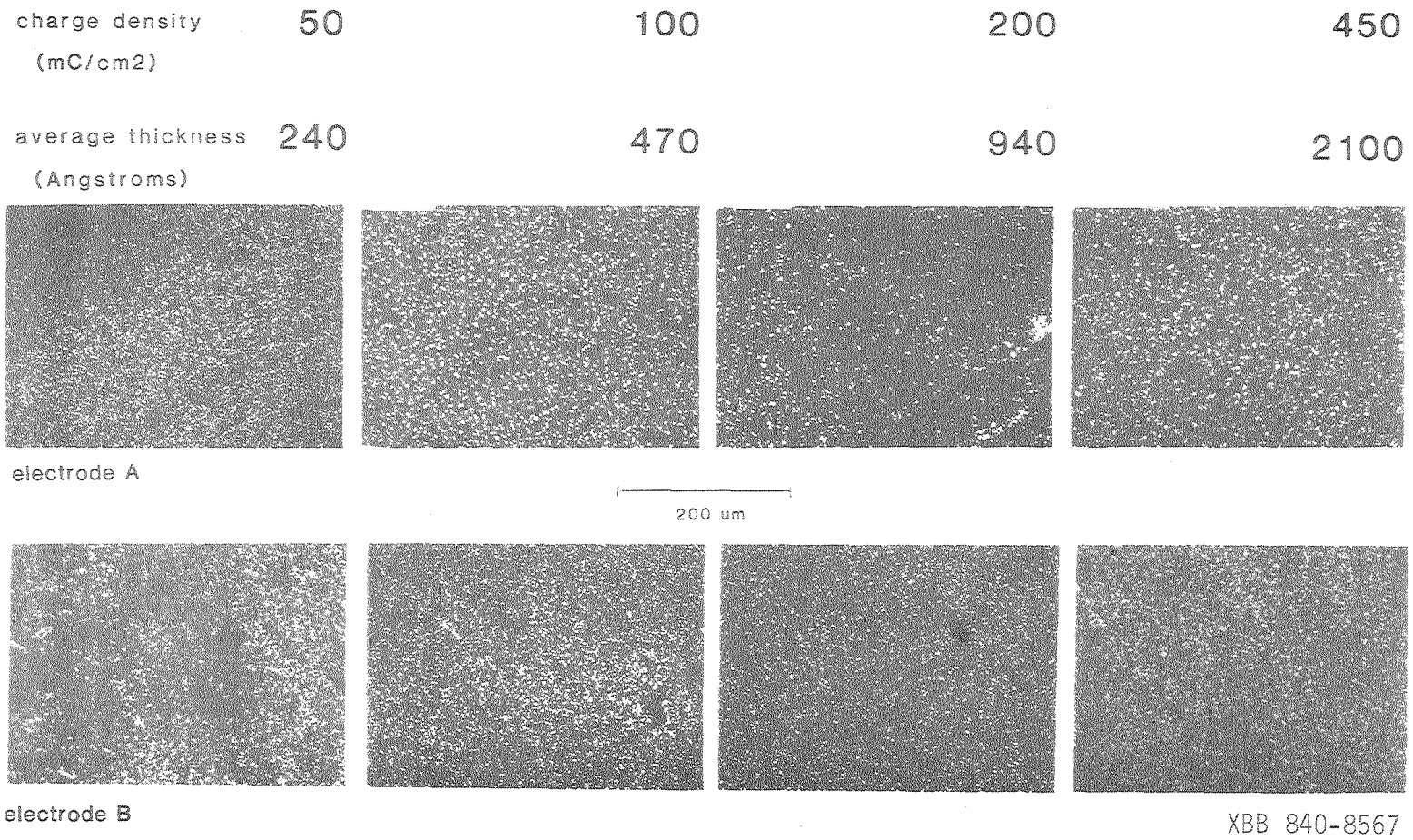

Fig. 5.40 Effect of charge density on the morphology of electrodeposited zinc,
Union Carbide Pyrolytic graphite substrate
10 mA/cm^2
1.0 M $ZnCl_2$ (Mallinckrodt reagent)

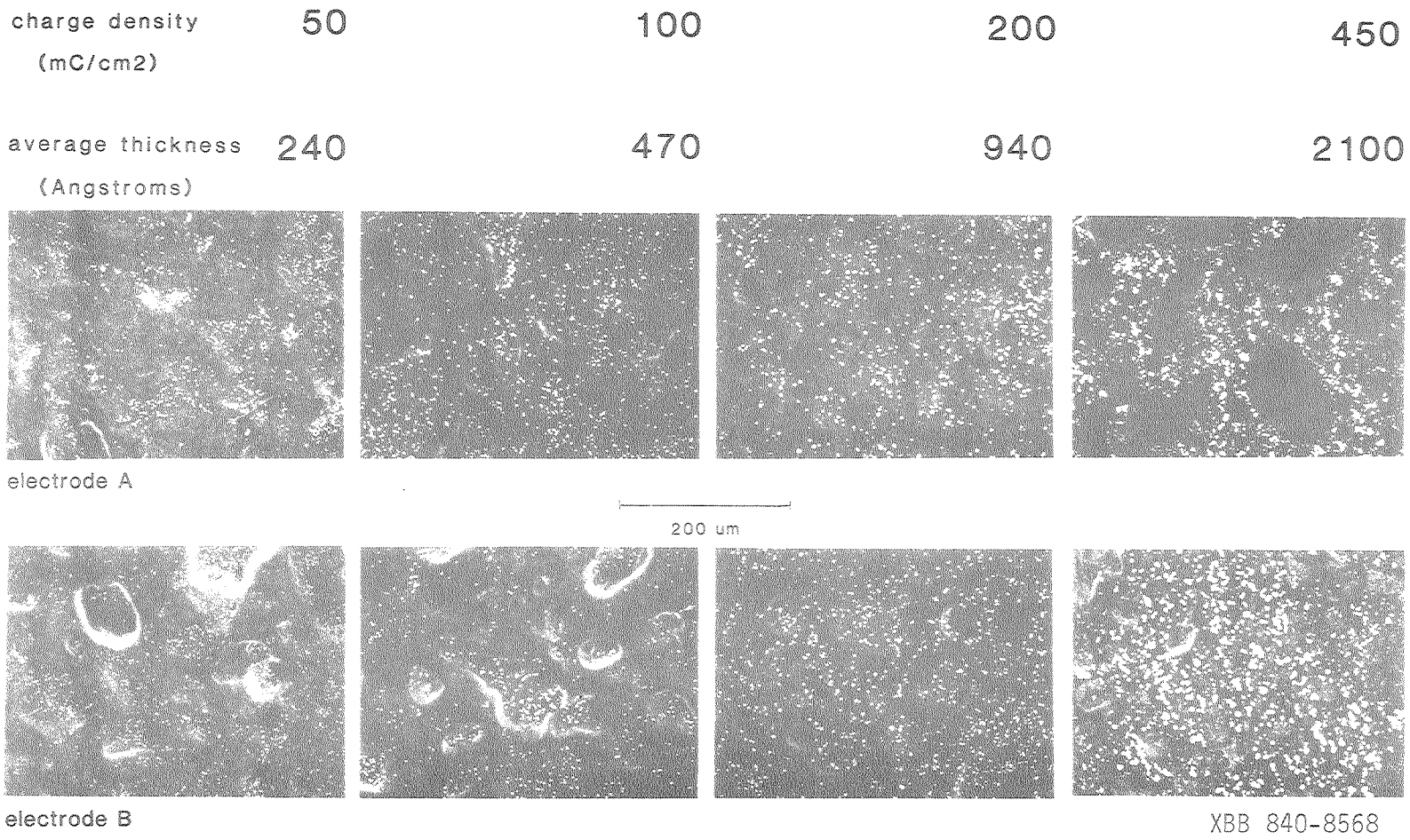

Fig. 5.41 Effect of charge density on the morphology of electrodeposited zinc,
Gould Pyrolytic graphite substrate
10 mA/cm^2
1.0 M $ZnCl_2$ (Mallinckrodt reagent)

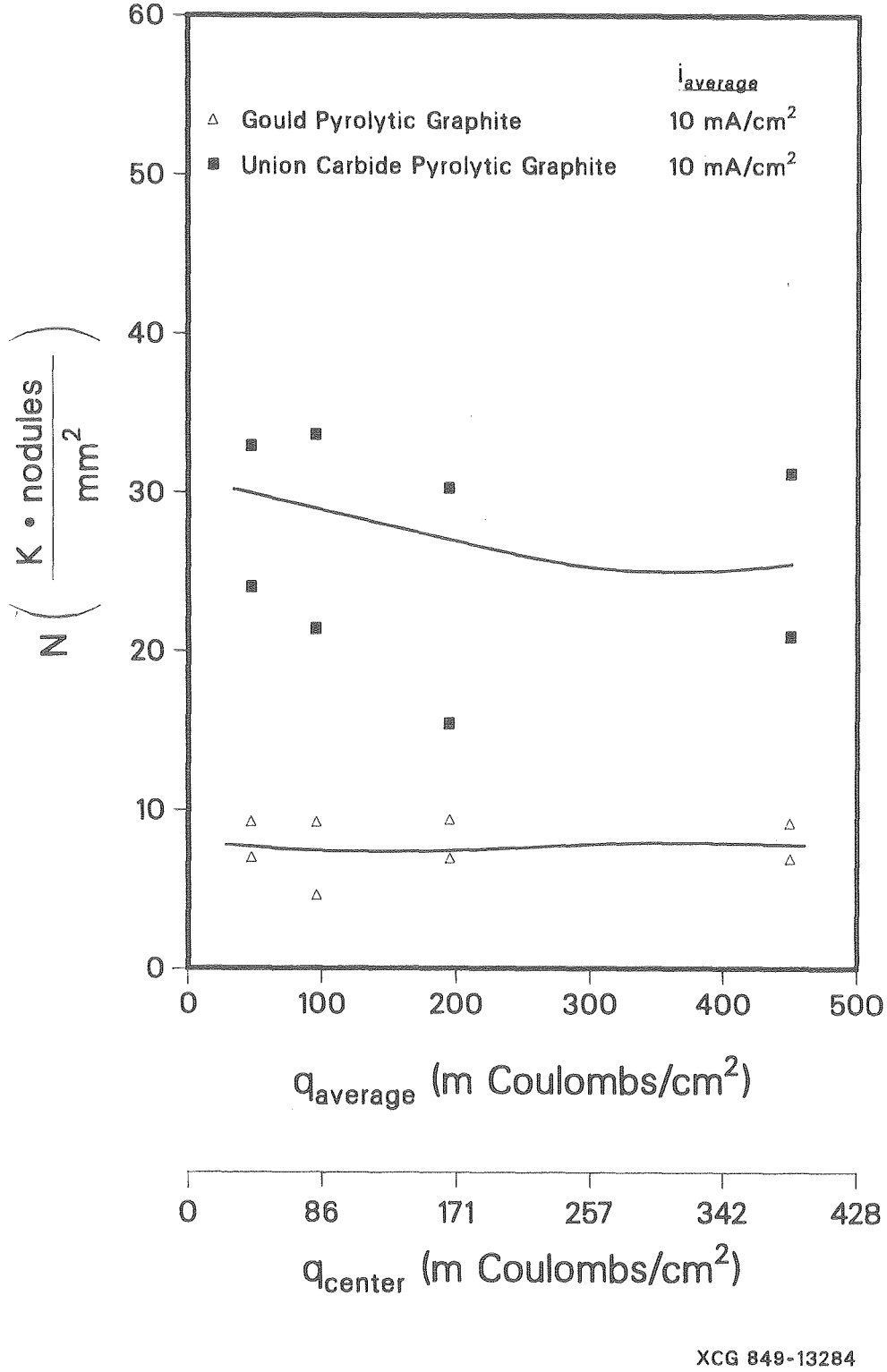

XCG 849-13284

Fig. 5.42 Effect of charge density on nodule number density,
1.0 M $ZnCl_2$ (Mallinckrodt reagent)

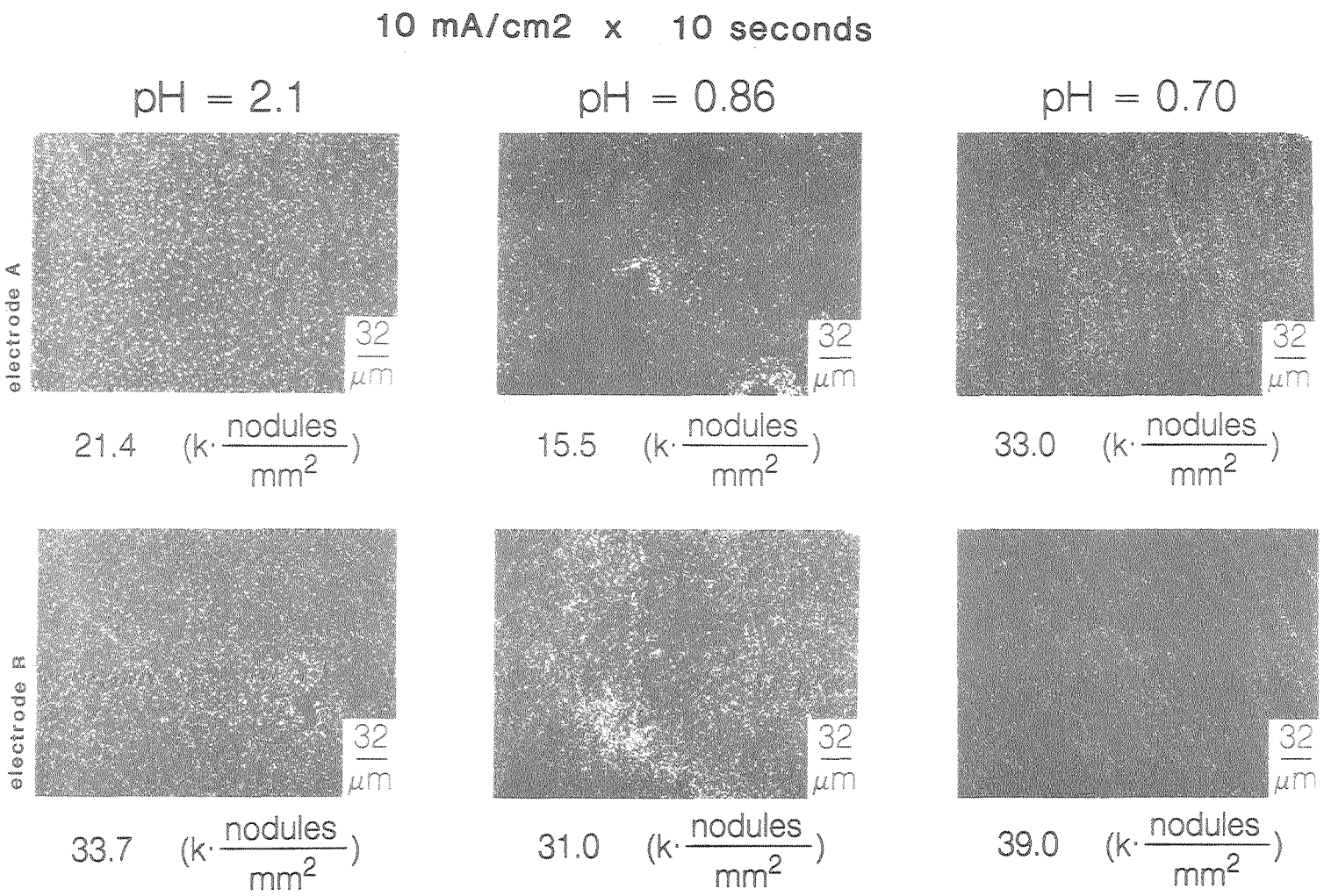

Fig. 5.50 Effect of pH on the number density of zinc nodules on Union Carbide pyrolytic graphite substrate, 1.0 M $ZnCl_2$ (Mallinckrodt reagent)

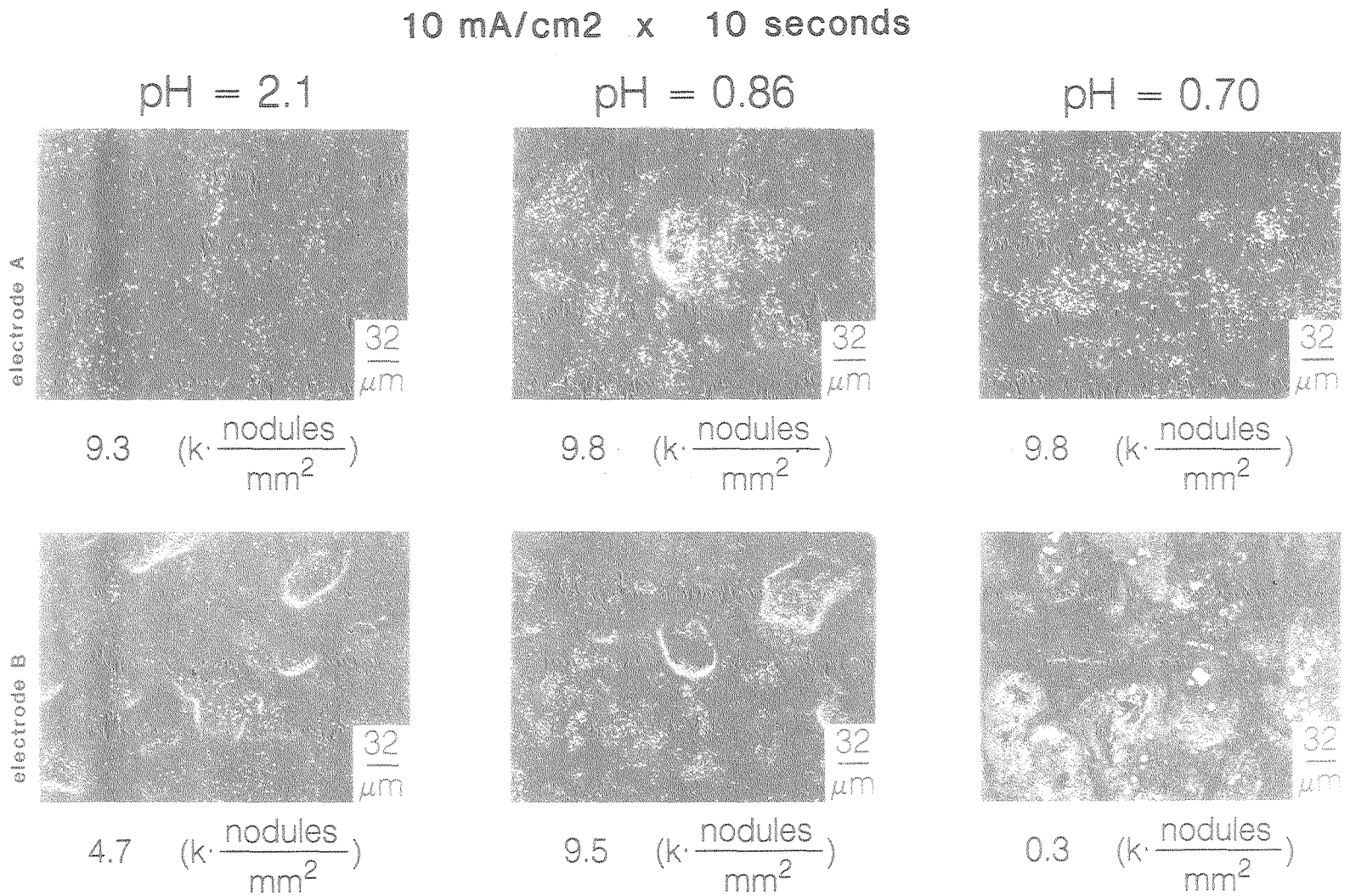

Fig. 5.51 Effect of pH on the number density of zinc nodules on Gould pyrolytic graphite substrate, 1.0 M $ZnCl_2$ (Mallinckrodt reagent)

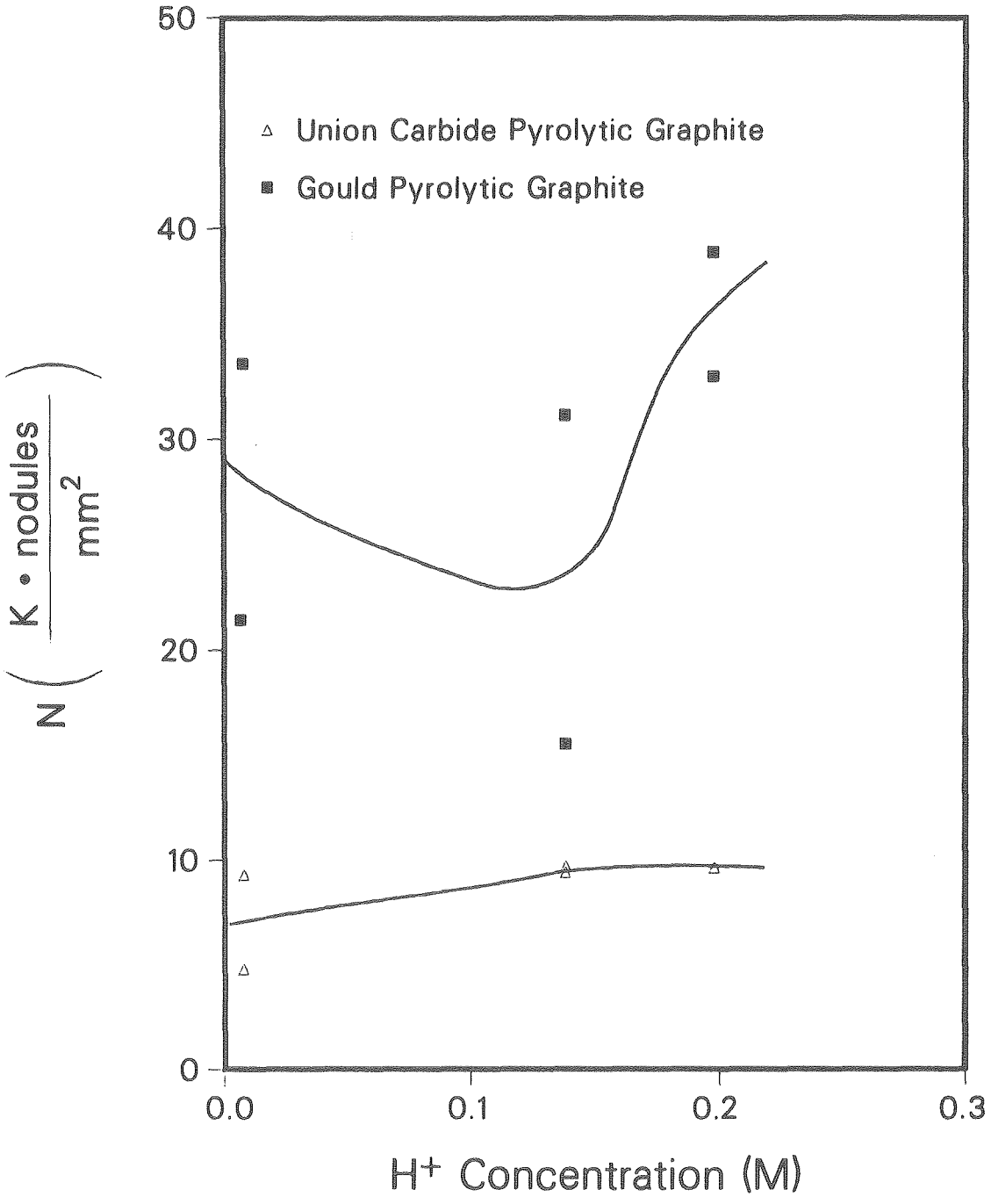

XCG 848-13285

Fig. 5.52 Effect of ionic hydrogen concentration on zinc nodule number density,
10 mA/cm^2 x 10 sec.
1.0 M $ZnCl_2$ (Mallinckrodt reagent)

VI. THE RECORDED POTENTIAL TRANSIENT

VI.A. Behavior

The potential between the working electrode and a saturated calomel electrode was monitored throughout the galvanostatic depositions. A typical response is shown in Figure 6.1. The potential maximum, which is reached during the first few seconds, is of particular note. Fleischmann and Thirsk referred to potential transients of this type as "superpolarization" in an extensive review article on metal deposition (34).

VI.B. Superpolarization*

Detection of this overpolarization is not something entirely new. As outlined in Section VI.C., many researchers have recorded such potential transients and attribute special significance to the difference between the peak and steady state potential values. In the following treatment, steady state will be arbitrarily defined as the potential at a selected average charge density.

VI.B.1. Effect of Substrate

The difference between the peak and steady state potentials should be related to the activity and number of nucleation sites available on a surface, as outlined in Section C. It should be interesting to compare such differences obtained for deposition on various substrates. Figures 6.2 and 6.3 present this potential difference for deposition from each electrolyte. In the MCB reagent, substrates in order of degree of decreasing superpolarization are: glassy carbon, Gould pyrolytic

*Fleischmann et al. translate "superpolarization" (34), originally called "Uberpolarisation" by Essin et al. (32).

graphite, platinum, and Union Carbide pyrolytic graphite. In the Mallinckrodt reagent, the order is: graphite loaded polymer, and a tie between the two types of pyrolytic graphites.

VI.B.2. Effect of Electrolyte

It has been suggested earlier (Section I.B.) that both impurities and hydrogen ions in the electrolye might have marked effects on electrodeposition kinetics. Comparisons will be made to evaluate these effects.

VI.B.2.a. pH

As in the Nodule Studies section, this investigation was limited to deposition on Gould and Union Carbide pyrolytic graphites in electrolyte prepared from Mallinckrodt reagent salt. Figure 6.4 illustrates the effect of hydrogen ion concentration on the degree of superpolarization. Here the magnitude of superpolarization is noticeably higher on the Gould than on the Union Carbide pyrolytic graphite. On both substrates the degree of superpolarization decreases by at least 20% when the pH of the electrolyte is changed from 2.1 to 0.70.

VI.B.2.b. Type of Reagent Salt

Figures 6.5 and 6.6 compare the superpolarizations of both pyrolytic graphites in the two types of electrolytes. Deposition on the Union Carbide pyrolytic graphite in the MCB electrolyte exhibited a superpolarization minima around 25 mA/cm^2. For each substrate, the superpolarization obtained in the Mallinckrodt electrolyte is higher.

VI.C. Theory and Comments

The transient signal shown in Fig. 6.1 represents a severe deviation from simple Butler-Volmer kinetics. yet similiar potential transients have been reported previously for both anodic electrocrystallization (33) and metallic electrodeposition (32,34,36,39,42) in response to galvanostatic steps. In particular, Roiter et al. and Essin et al. galvanostatically deposited zinc on single crystal zinc and copper on copper electrodes in purified solutions. In both cases potential maxima similiar to those experienced in this study were observed. Essin et al. used the term: Überpolarisation to describe this effect. Vermilyae (42) asserted that it is doubtful that these potential maxima are due to surface contamination because in such a case a shorter transient duration would be observed.

Several researchers have attempted to explain and even model this behavior. The initial ascent of the potential and the eventual decay of the resulting potential maximum can be attributed to entirely different phenomena. The current is composed initially of double layer capacitive charging, followed by faradaic current. As the double layer charges the potential increases and this process receives a decreasing fraction of the total current. This seems a reasonable explanation for the first part of the potential transient and is born out by estimates of the double layer capacity from the limiting slope of the potential transient as time tends towards zero. This interpretation is common in the literature. When the potential reaches its maximum value the double layer charging current is zero.

Vermilyae claims that the point of maximum potential corresponds to the highest rate of nucleation; this makes sense because it is at this time that the driving force, or surface overpotential, is greatest. Furthermore, Gunwardena et al. contend that nucleation occurs only during the potential rise, halting as the potential decays (36). This conclusion was reached by interrupting the galvanotatic process with potentiostatic steps at the same potential; the resulting current transient served as a diagnostic tool for indicating the number of nuclei on the surface. The eventual decay of the potential is another matter altogether.

In general, researchers attribute the decrease of the potential to enhancement of the surface, either in the form of growth sites or simply the interfacial area due to increasing roughness. A distinction should be made here between homogeneous deposition and the formation of a new phase— i.e., on a foreign substrate. Addressing the former situation, Vermilyae worked out detailed models describing a transition from step dislocations to spiral growth. His model applied to systems where the mean free path of the diffusing adatoms was much greater than the step spacing, and the current density was much greater than the exchange current density. Vermilyae predicted that an increase in the dislocation density would suppress both the magnitude and duration of the transient potential peak (42). Roiter et al., while depositing zinc onto single crystal zinc, observed an increase in surface capacitance to 2-3 times the intial value after steady state was achieved; this would indicate an increase in the electroactive area (39). Fleichmann and Thirsk attribute the potential decay for metallic electrodeposition to an

increase in the number of active sites with increasing potential and the subsequent expansion of the interface (34). For anodic electrocrystallization they give an expression for the maximum ratio between peak and steady state overpotentials from a hypothetical decrease in step dislocation spacing (33).

In this study a foreign substrate was used and, therefore, electrodeposition of zinc involved the formation of a new phase. In accordance with the hypotheses discussed above, the magnitude of the potential maximum should give some indication of the number and accessibility of the sites active for electrodeposition on the substrate.

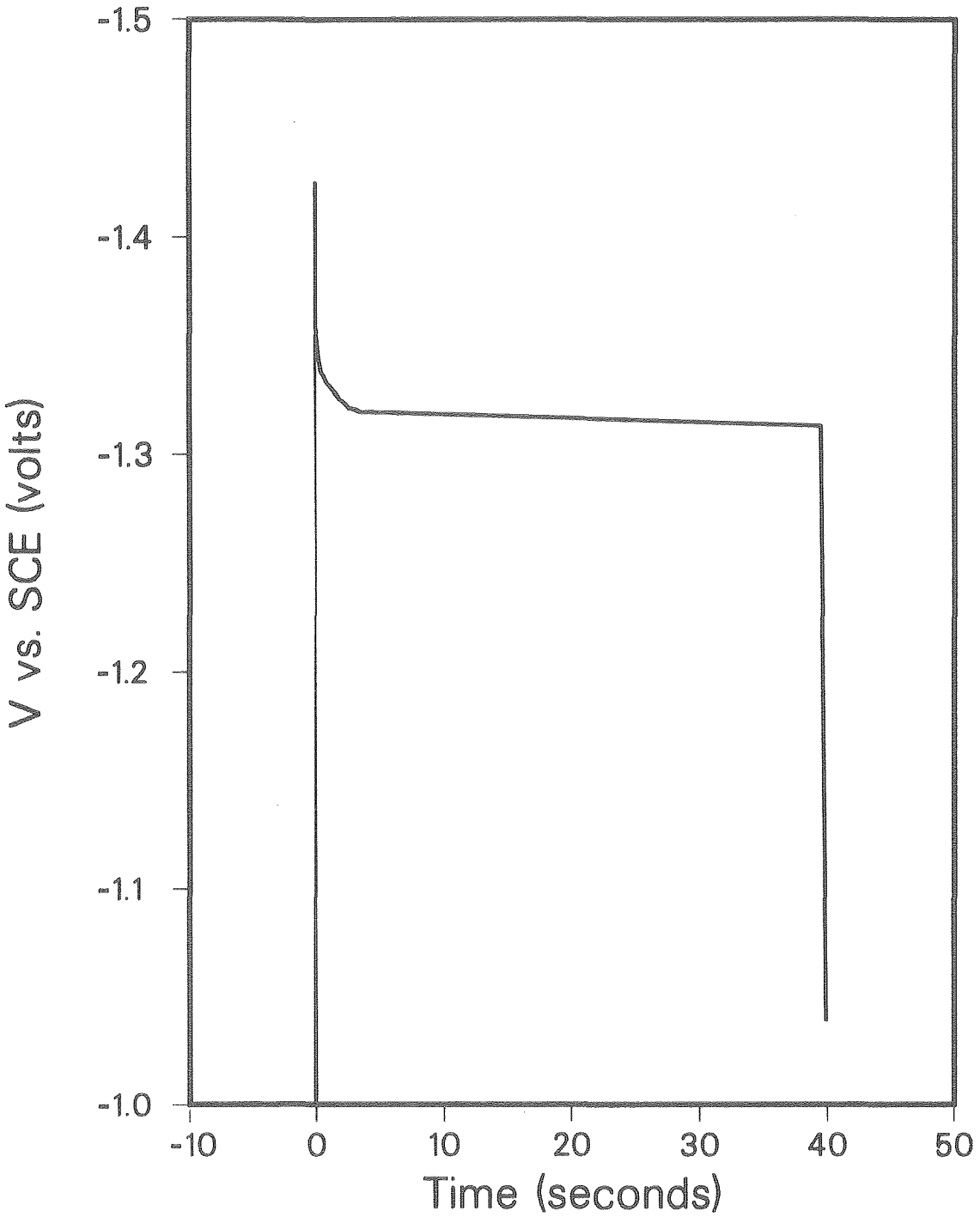

XCG 849-13292

Fig. 6.1 Typical potential transient in response to a galvanostatic step,
Union Carbide pyrolytic graphite
45 mA/cm^2 x 40 seconds
1.0 M $ZnCl_2$ (MCB reagent)

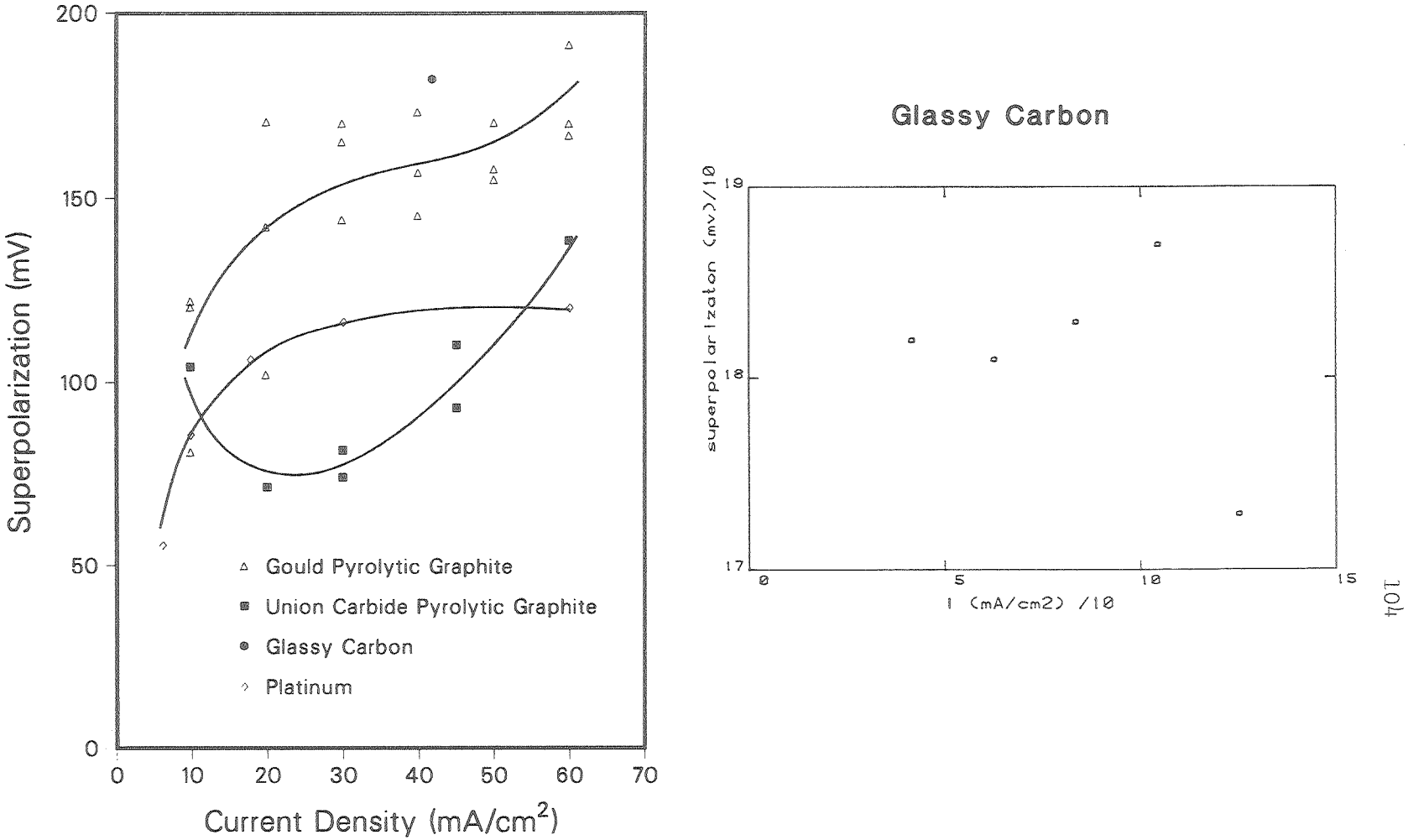

XBL 8410-4617

Fig. 6.2 Superpolarization versus current density on various substrates,
1.0 M $ZnCl_2$ (MCB reagent)

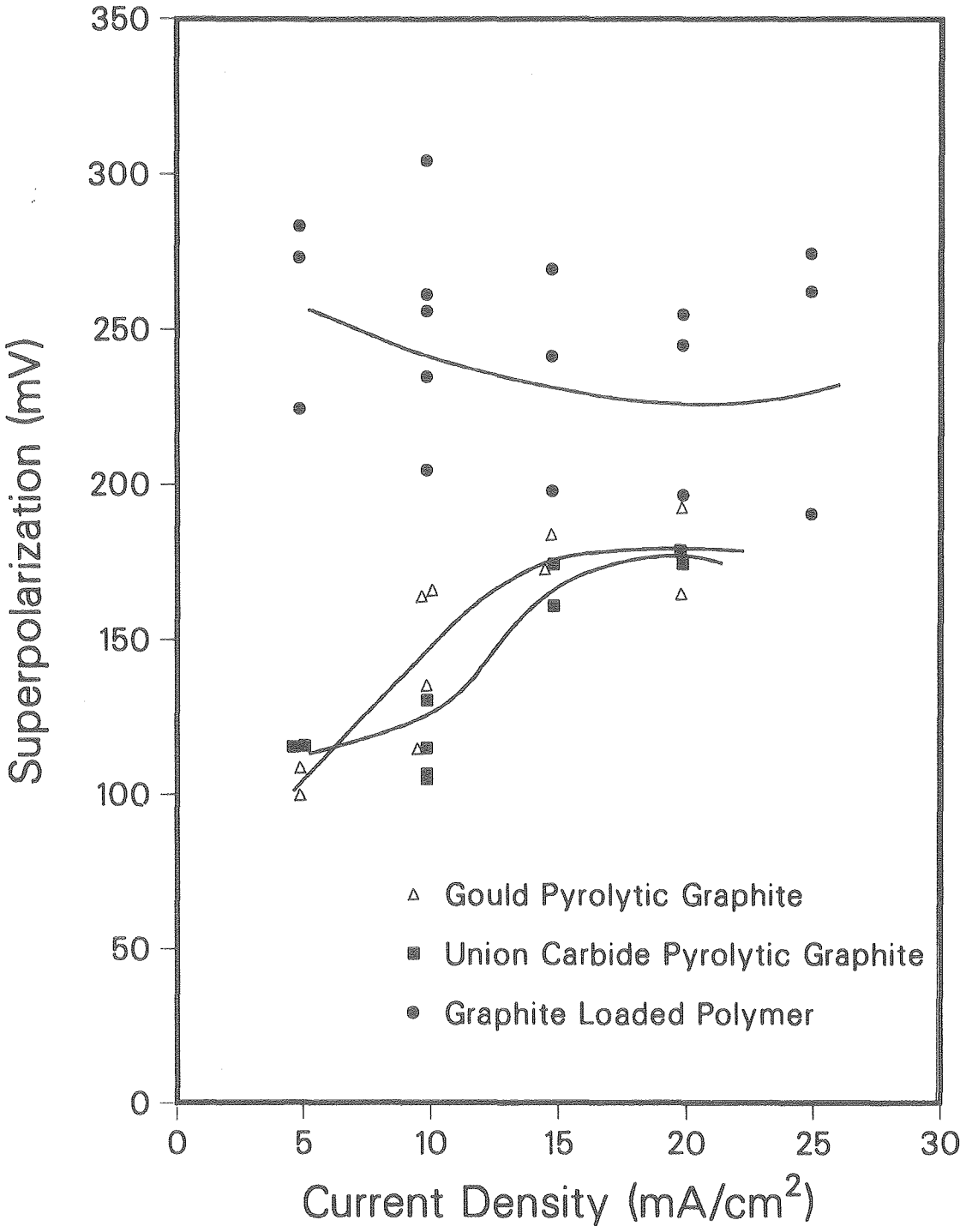

XCG 849-13287

Fig. 6.3 Superpolarization versus current density on various substrates,
1.0 M $ZnCl_2$ (Mallinckrodt reagent)

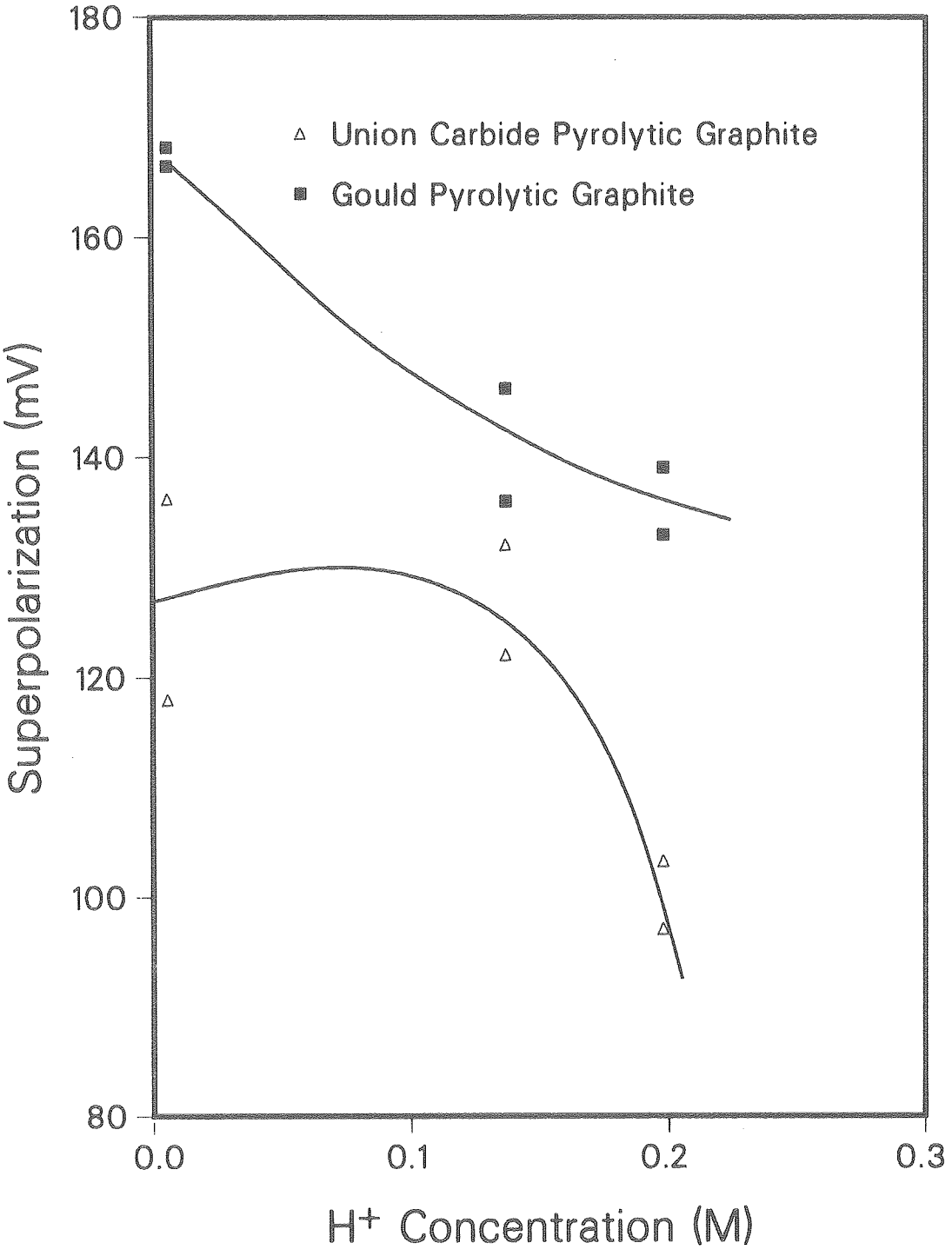

XCG 849-13291

Fig. 6.4 Effect of ionic hydrogen concentration on degree of superpolarization,
1.0 M $ZnCl_2$ (Mallinckrodt reagent)

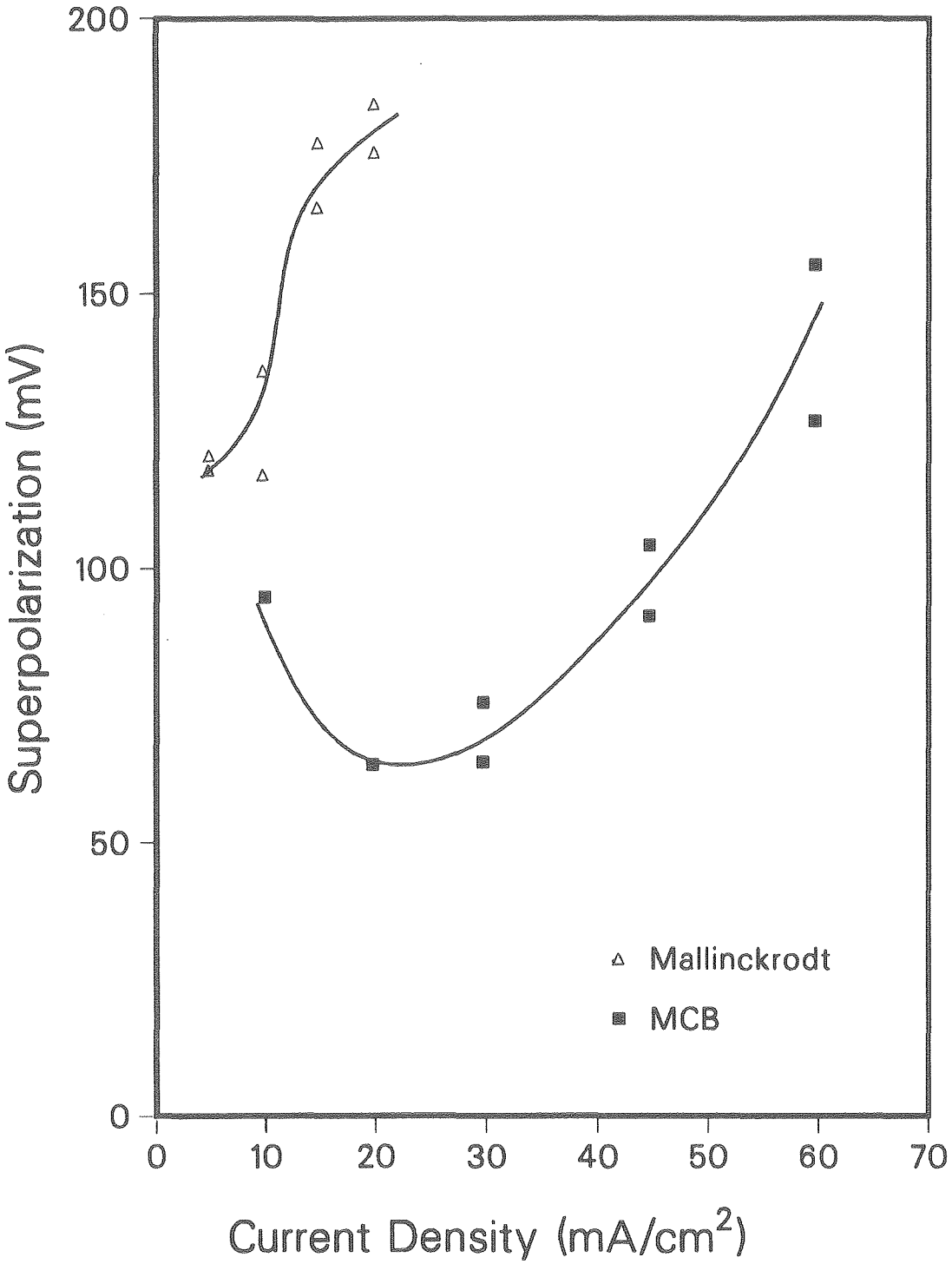

Fig. 6.5 Comparison of degree of superpolarization in two electrolytes on Union Carbide pyrolytic graphite substrate

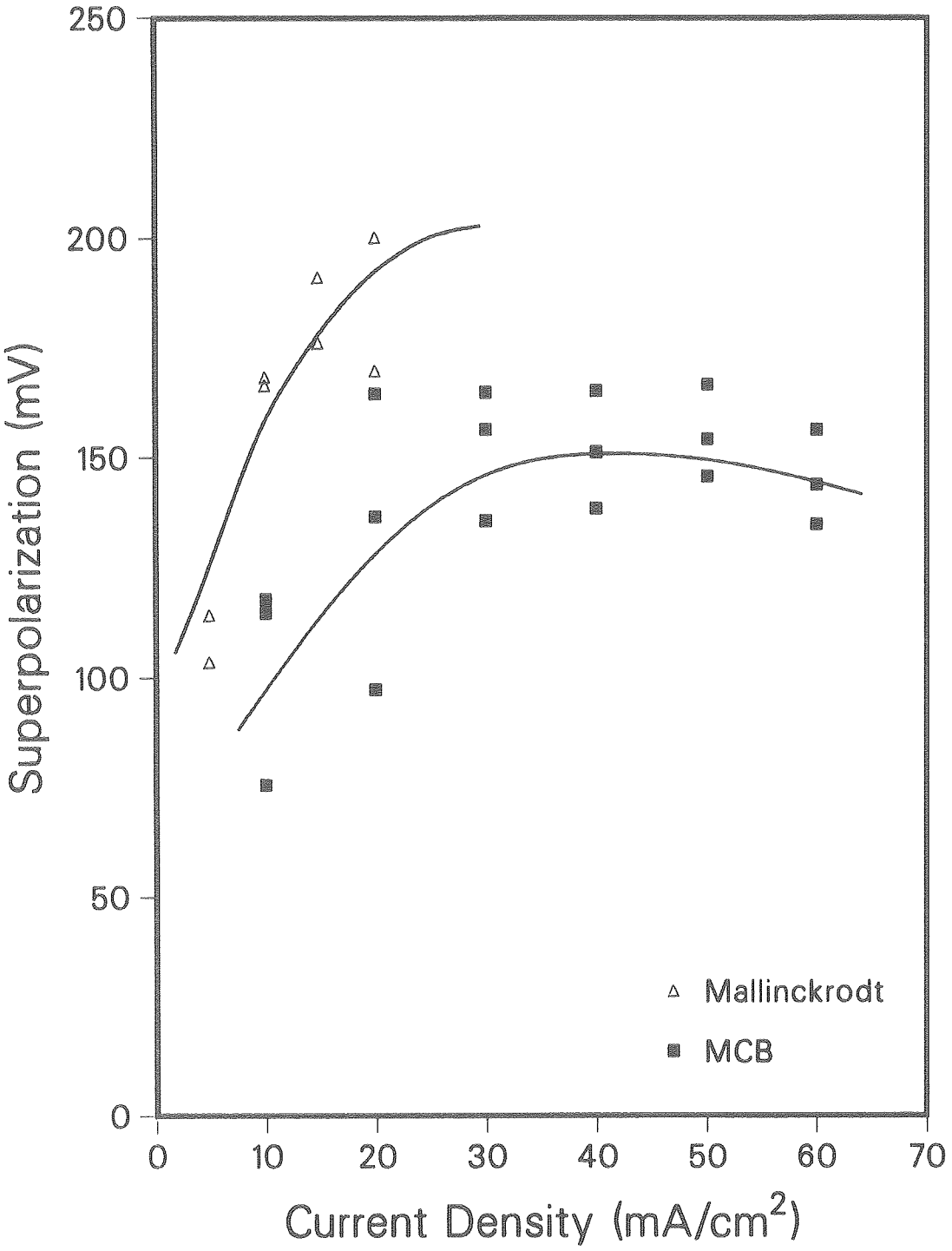

XCG 849-13290

Fig. 6.6 Comparison of degree of superpolarization in two electrolytes on Gould pyrolytic graphite substrate

VII. DISCUSSION

VII.A. Summary

The original goal of this research was to contribute to the characterization of the morphological development of electrodeposited zinc to further our understanding of the mechanisms involved in the formation of striae. This goal would be most directly realized by investigations using zinc as a substrate. Although various methods were explored (see Appendix B), the preparation of a smooth zinc electrode proved to be difficult and irreproducible. These difficulties led to placing emphasis on experiments involving the use of foreign substrates, which had the advantage of relative inertness and improved reproducibility. Two of the substrates are used in current zinc halide battery development.

The nodule densities were higher on some substrates than others, as evident in Figures 5.14 and 5.15 in Chapter 5; this ranking of substrates is given in Table 7.1. Also in this table, substrates are ranked in order of increasing degree of superpolarization, given in Chapter 6. Table 7.1 demonstrates a parallel between decreasing nodule density and increasing degree of superpolarization. This agreement between two entirely different methods means that they must each be indicative of some common phenomena.

As described in Section V.F, it is well accepted that nucleation occurs during metallic electrocrystallization and that it is dependent upon high energy sites at which to occur. The various substrates tested probably have different concentrations and activities of nucleation sites. Presumably, deposits on substrates more active to nucleation

would have higher nodule densities. It was shown in Section VI.C. that an increase in the number or activity of defect sites is predicted to result in a decrease in the degree of superpolarization. Therefore, from Table 7.1 we can list the substrates in order of decreasing activity:

- Union Carbide HOPG pyrolytic graphite
- platinum
- Gould pyrolytic graphite
- graphite loaded polymer and glassy carbon

Various investigators have reported the incorporation of codeposited hydrogen in electrodeposited zinc (10,11). Others provide evidence that adsorbed hydrogen atoms are involved in the zinc discharge reaction (49,50). In experiments on both pyrolytic graphites the degree of superpolarization decreased by as much as 20% with a decrease in pH from 2.1 to 0.70, as shown in Figure 6.4. This indicates that the surface density of sites available for electrocrystallization may increase with increasing ionic hydrogen concentration; however, nodule density measurements neither lend clear, unambiguous support to this hypothesis, nor do they contradict the possibility that hydrogen discharge plays an important role in the development of morphological features of zinc deposits.

VII.B. Application of Results

Faltemier described various hypotheses, proposed by previous researchers, which attempt to explain the formation of striae during the electrodeposition of zinc (2). The most plausible among these hypotheses proposes a mechanism for the propagation of a ridge in the

wake of a principal nodule. In the discussion that follows this mechanism is described in detail and discussed in the light of experimental evidence from this study as well as from other sources.

EFFECT OF CONVECTION ON CONCENTRATION FIELD

The effects of small (≃1 mm) shapes on localized mass transport were studied in 1975 by Carlson (44). He electrodeposited copper in a flow cell and analyzed the deposit in the region around various obstacles using photography and surface profile analysis. Figure 7.1 shows a sample photograph of the deposit and schematically depicts the effects of a conducting sphere on localized mass transport. It is of particular note that the most effective enhancement occurs upstream of the protrusion. Also, the mass transport rate to the region immediately downstream of the sphere appears to be reduced. In the development which follows, the term wake refers to the regions of enhanced mass transport depicted in Figure 7.1(b).

One might describe the effect of this enhanced mass transport in the wake of a principal nodule as a reduction of the concentration polarization near the electrode surface. Since this concentration difference is directly related to the concentration overpotential (27), the wake represents a region of attenuated concentration overpotential. In actuality, however, the concentration overpotential will vary over the area inside the wake and perhaps also with time, because the enhancement is due to eddy mixing phenomena.

COUPLING WITH SURFACE OVERPOTENTIAL

Figure 7.2 schematically depicts the relationships between the ohmic, mass transport, and kinetic impedances and resulting overpotentials. As shown, Kirchhoff's Law requires that the sums of the overpotentials inside and outside the wake should be equal. This means that the perturbed concentration overpotential in the wake results in a concomitant increase of both the surface and ohmic overpotentials in this region of the electrode. The surface and ohmic overpotentials inside the wake can be estimated if certain assumptions are made. As demonstrated in Appendix F, an 80% reduction in the concentration overpotentials at 50 ma/cm^2 could cause η_s to increase by 1 mv and enhance the current density by 4% in the wake. Once a small ridge is generated, its growth will be further enhanced because it has both ohmic and mass transport advantage over the surrounding electrode surface.

RESPONSE OF DEPOSIT MORPHOLOGY

Predicting changes in the morphology of electrodeposited zinc in response to a 1 mv increase in the surface overpotential has been the primary focus of this study. Evaluation of the first derivative of the nodule density with respect to the surface overpotential (Section V.C.) provides one assessment of this effect. To estimate this derivative, a functional relationship must be found for the data in Figures 5.30-5.36. For simplicity, a linear correlation with a non-zero intercept was used. the results are listed on Table 7.2

These experimental results are in qualitative agreement with work performed by Tsuda (6) and support the hypothesis outlined above,

although the relative insensitivity of nodule formation to surface overpotential is such that this effect alone cannot account for the formation of a ridge.

Table 7.1. Comparison of Apparent Activities of Various Substrates with Respect to Zinc Electrodeposition.

METHOD:	Nodule Formation		Superpolarization	
ELECTROLYTE:	A	B	A	B
Declining Activity	G_U	G_U	G_U	G_U
	P		P	
	G_G	G_G	G_G	G_G
		M	C	M

Key to abbreviations:

Electrolytes:
- A MCB reagent salt
- B Mallinckrodt reagent salt

Substrates:

- G_U Union Carbide HOPG pyrolytic graphite
- G_G Gould pyrolytic graphite
- P platinum
- M graphite loaded polymer from Exxon
- C glassy carbon from Pine Instruments

Table 7.2. Results of Linear Fits to Nodule Density vs Surface Overpotential Data.*

R^2	Substrate/ Electrolyte	$dN/d\eta_s$ (K nodules/$mm^2 \times mv.$)	$(1/N) \times dN/d\eta_s$ (1/mv)
84%	P / A	0.35	5.8×10^{-2}
71%	G_U / B	0.74	2.5
54%	G_G / A	0.20	2.5
52%	G_U / A	1.1	36.
49%	G_G / B	0.25	2.8
33%	M / B	0.17	11.
8%	C / A	0.24	1.2

Key to abbreviations:

Electrolytes:
- A MCB reagent salt
- B allinckrodt reagent salt

Substrates
- G_U Union Carbide HOPG pyrolytic graphite
- G_G Gould pyrolytic graphite
- P platinum
- M graphite loaded polymer from Exxon
- C glassy carbon from Pine Instruments

*Values of N are estimated for i = 10 ma/cm^2

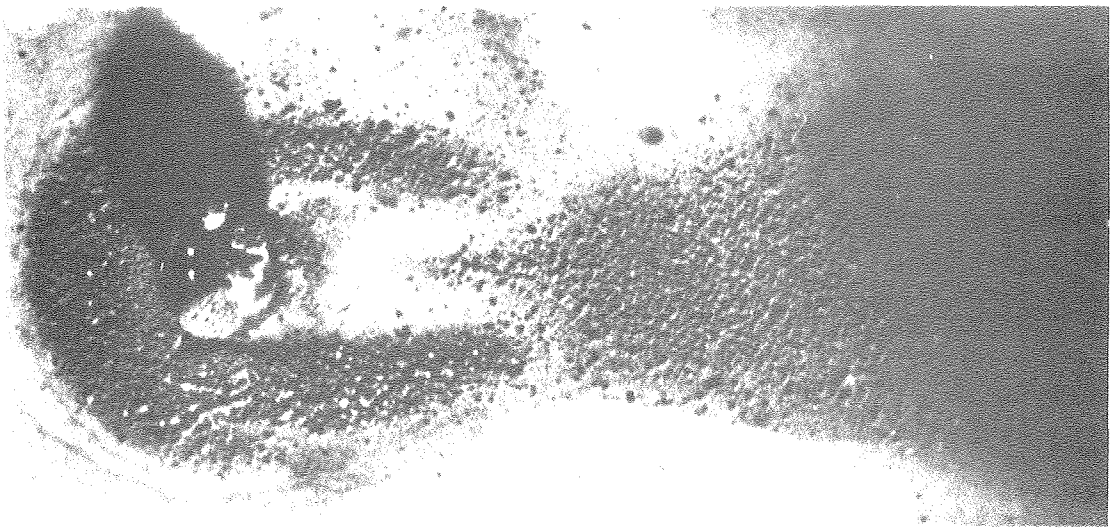

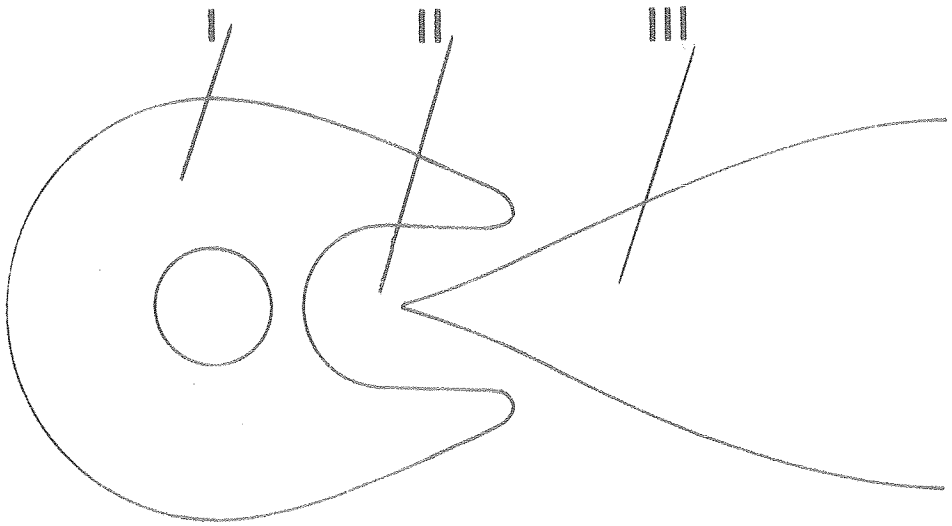

I - region of high enhancement

II - region of attenuation

III - region of moderate enhancement

XBB 840-8624

Fig. 7.1 Effect of conducting sphere on localized electrodeposition in the presence of forced convection (from experiments by Carlson)

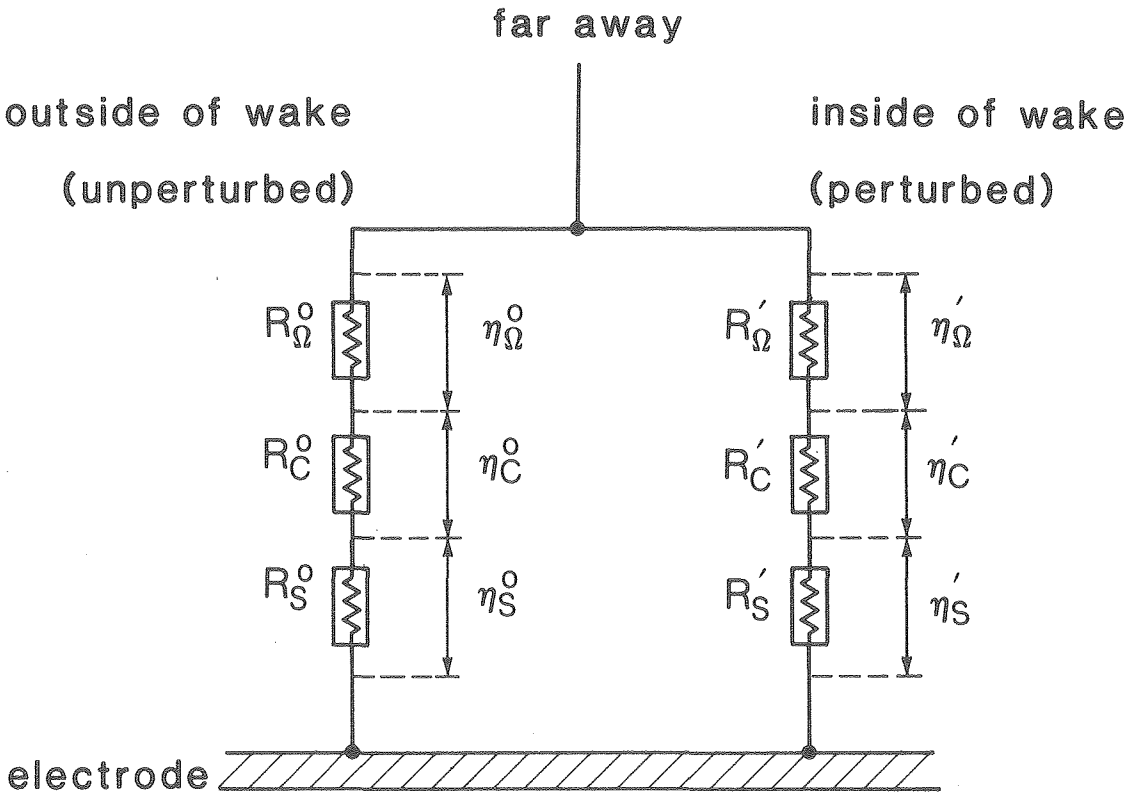

$$\eta_\Omega^o + \eta_C^o + \eta_S^o = \eta_\Omega' + \eta_C' + \eta_S'$$

Fig. 7.2 Schematic representation of the relationship between overpotentials in and outside of wake

VIII. CONCLUSION

The aim of this research was to advance our understanding of the mechanism for the development of striae during electrodeposition of zinc from chloride solutions. In this study it was quantitatively established that the nodule number density increases as the surface overpotential is increased. As a result of this work, the following conclusions can be made:

1. The exchange current density for electrodeposition of of zinc from 1.0 M $ZnCl_2$ electrolyte is on the order of 1 ma/cm^2.

2. Cyclic voltammetry experiments revealed only one discernable cathodic peak— implying only one cathodic reaction. The shape of this cathodic peak is indicative of hindered nucleation processes.

3. The density of nodules formed, and the degree of superpolarization, can both provide a reliable assessment of the relative activities of zinc deposition on various substrates.

4. Substrates ranked in order of decreasing activity towards zinc deposition from both superpolarization and nodule density measurements are as follows:

   - Union Carbide HOPG pyrolytic graphite
   - platinum
   - Gould pyrolytic graphite
   - graphite loaded polymer and glassy carbon

5. Concentration of hydrogen ions has a marked effect on the degree of superpolarization; as the pH of the electrolyte is decreased from 2.1 to 0.70 the extent of superpolarization decreases by about 20%. This can be interpreted to mean that the presence of hydrogen ions increases the number of available nucleation and growth sites. Nevertheless, experimental measurements of the number densities of nodules formed in electrolytes over the same pH range were inconclusive.

6. The nodule number density generally increases as the current density is increased. When the steady state surface overpotential is calculated from assumed kinetic parameters, it is apparent that, in the range of current densities investigated, the nodule density increases with surface overpotential at a rate in the range of 200-1000 nodules/($mm^2 \times mv$).

7. These results are in qualitative agreement with those obtained by Tsuda. Also, they support the hypothesis by which the lowering of the concentration overpotential in the wake of a principal nodule results in an increase of the current density inside the wake; the resulting modest increase of the surface overpotential causes enhanced nucleation and surface roughening. Growth of these roughness elements is increased due to both mass transfer and ohmic effects.

APPENDIX A. DRIFT OF THE OPEN CIRCUIT POTENTIAL

During the earlier part of this study it was noticed that the open circuit potential measured with polycrystalline zinc as the working electrode was unstable. Further investigation showed that after an initial sharp potential transient lasting 2-3 minutes upon immersion in the electrolyte, the potential typically rose 6 mv/10 minutes as shown in Figures A.1 and A.2. The rate of this potential drift was not affected significantly by either purging the electrolyte with nitrogen or varying the pH from 0.4 to 4.0. Photographs of a polycrystalline zinc electrode before and after immersion in electrolyte for 70 minutes are shown in Figure A.3.

Such a drift in the open circuit potential is not wholly unexpected. Several corrosion couples involving the dissolution of zinc are thermodynamically favorable in this system. The considerable pitting evident in Figure A.3 confirms that corrosion processes are occuring. The following half-reactions are of particular interest:

			E_o (Volts versus RHE)
$Zn^{++} + 2e^-$	=	Zn	- 0.7628*
$2H^+ + 2e^-$	=	H2(g)	0.0
$O_2 + 4H^+ + 4e^-$	=	$2H_2O$	1.229

Often, the last two reactions are kinetically inhibited.

The manner by which these corrosion reactions affect the monitored open circuit potential is indirect. Changes in the potential are actually caused by variations in the electrolyte composition near the

*Since in the presence of Cl^-, zinc forms a number of complexes (53), the equilibrium reduction potential should be more negative than the value indicated above.

electrode, including the formation of zinc chloride complexes (e.g., $ZnCl^{+}$, $ZnCl_2$, $ZnCl_3^{-}$, $ZnCl_4^{--}$). Furthermore, as can be seen in Figure A.2. an increase in the pH caused a decline in the potential; this is indicative of the role hydrogen plays in these corrosion reactions.

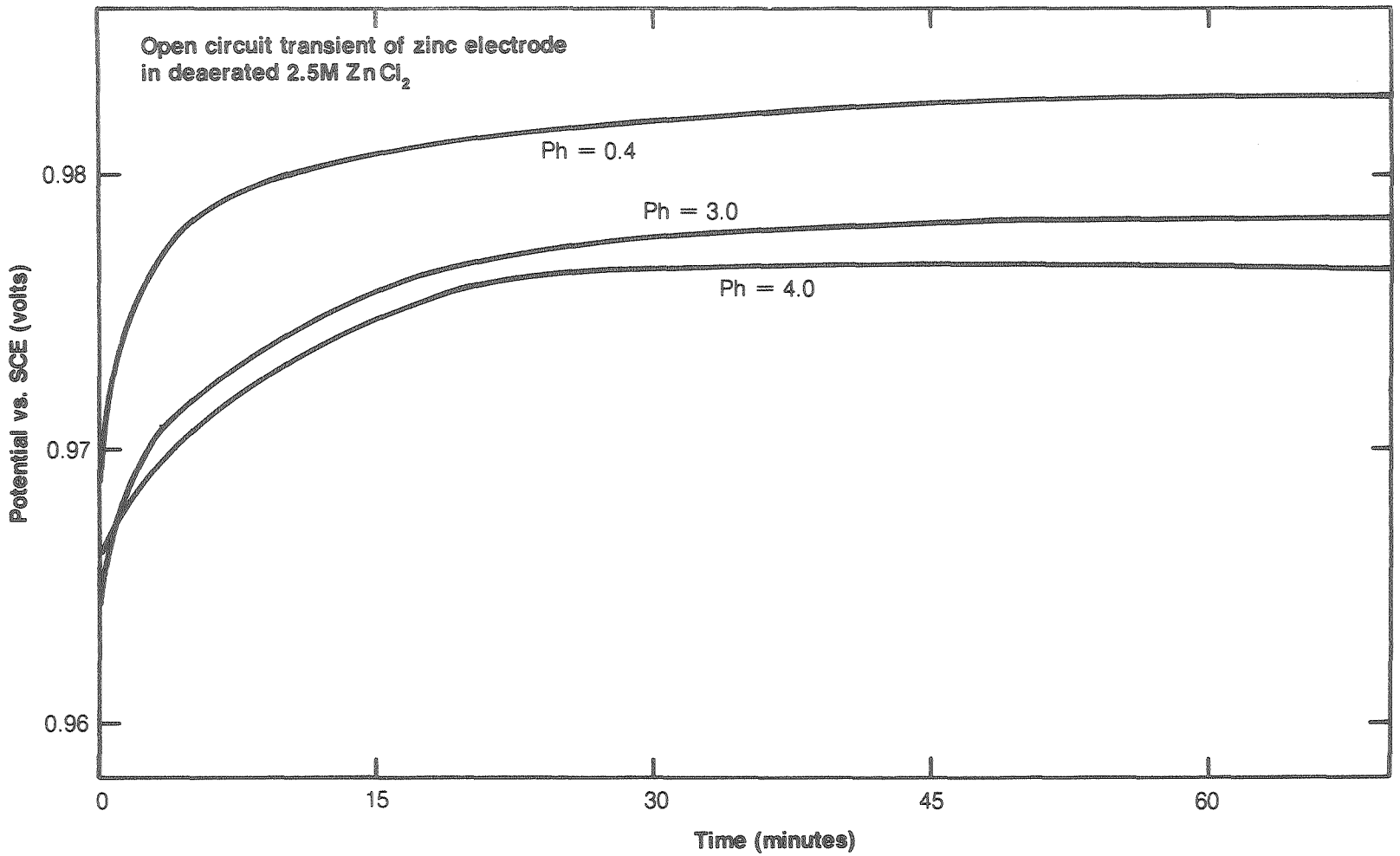

Fig. A.1 Drift of open circuit potential of polycrystalline zinc electrode versus time

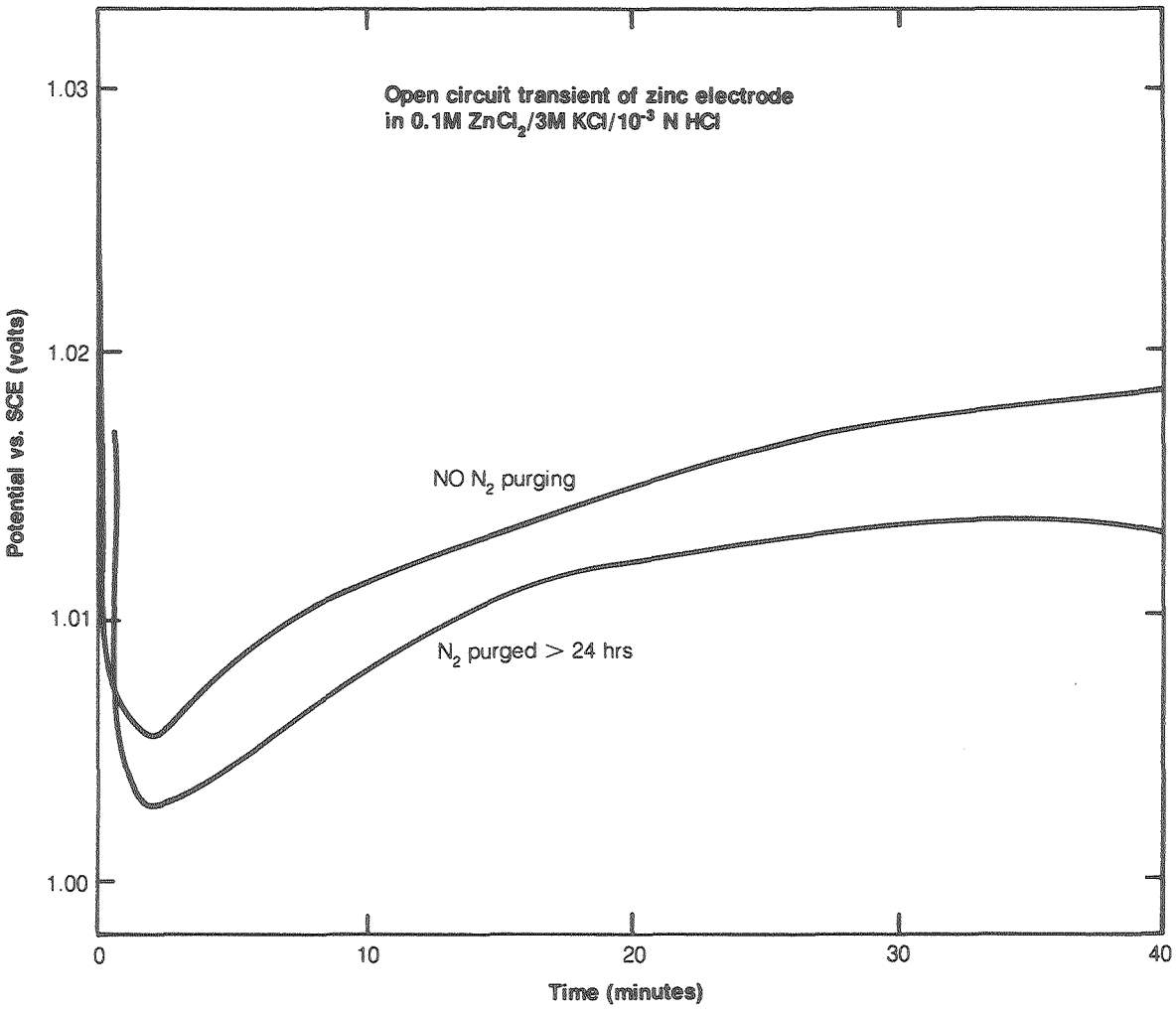

Fig. A.2 Drift of open circuit potential of polycrystalline zinc electrode versus time

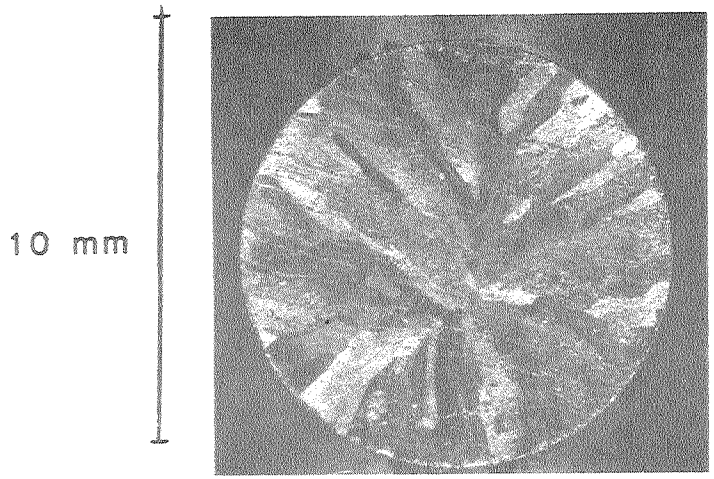

A) Polished electrode

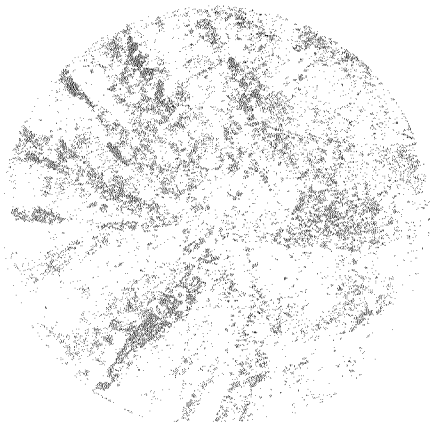

B) After exposure to 0.1 M $ZnCl_2$, 3 M KCl, and 0.001 M HCl (purged with nitrogen for 70 minutes).

XBB 840-8574

Fig. A.3 Macrophotographs of polycrystalline zinc electrode, before and after open circuit potential experiments

APPENDIX B. ZINC SUBSTRATES

The objective of this research is to gain insight about the behavior of zinc electrodeposition on a zinc substrate. Unfortunately, a well characterized reproducible zinc surface is difficult to obtain.

B.1. Polycrystalline Zinc

Polycrystalline zinc is readily available and easy to use; however, large grains become visible when the zinc is polished and these may affect the electrode's behavior. Electrodeposition on this surface results in a non-uniform deposit. A polished polycrytalline zinc electrode (1 μm diamond paste) and an SEM photograph of a subsequent electrodeposit are shown in Figure B.10.

Rough polishing (i.e., 600 grit) improves the uniformity of the electrodeposit, as shown in Figure B.11; yet, such a surface preparation method is unacceptable. First, the grooves formed during polishing probably affect the flow near the surface. Furthermore, it is unclear whether or not this surface preparation method is reproducible.

B.2. Zinc Prepared by Evaporation

Another method investigated to prepare a smooth and reproducible zinc substrate was evaporation. In this process zinc is electrically heated in a vacuum ($\simeq 10^{-2}$ torr); the evaporated metal deposits on any cold surface it strikes, including the substrate which is placed adjacent to the zinc source. This method has the unique advantage of good control over deposit purity. By using 6-9 (99.9999% purity) zinc wire as the source, impurities in the deposit were minimized.

On a platinum electrode substrate, however, the zinc did not adhere well and didn't deposit uniformly. To alleviate these problems, gold was first sputtered onto the platinum, immediately followed by zinc evaporation. An aluminum mask was in place throughout this process.

Figure B.20(a) shows an SEM photograph of a typical zinc deposit, freshly prepared by this method. Unfortunately, these deposits degraded with time. After a few hours cracks would begin to appear, as shown in Figure B.20(b); these were probably due to the formation of zinc oxides.

Galvanostatic experiments were performed on freshly prepared (1 hr.) zinc substrates. SEM photographs reveal that the resulting deposits differed sharply from those formed on foreign substrates. Figure B.21 shows some typical results of these galvanostatic experiments. The prominent features on the surface are not individual nodules but primarily needle-like or flaky fine structures. This type of deposit probably forms because of the nature of the evaporated zinc substrate. It is likely that this surface is energetically much further from equilibrium than other substrates studied, and the finer deposit results from an increase in the surface density of growth sites. This type of deposit cannot be evaluated using the same methods as in the main part of this work; therefore, zinc prepared by evaporation was not used in the nodule study experiments.

B.3. Single Crystal Zinc

A material which would seem ideal for this type of study is single crystal zinc. The grain boundaries encountered on polycrystalline zinc would be avoided. In addition, single crystal zinc can be better charac-

terized and reproducible.

Polishing single crystals of zinc is a difficult procedure. Mechanical polishing smears the first few thousand monolayers and so the electroactive surface is no longer a single crystal; consequently, electropolishing was used. The electropolishing was carried out under potentiostatic control in a 1:1 solution of 80% ortho-phosphoric acid and 1.0 M KOH (1) on a rotating disc electrode (1000 rpm). It was hoped that potentiostatic control would be more stable than galvanostatic control near the limiting current. Unforunately success was limited, a microscopically smooth surface was not obtained. Figure B.30 shows a Laue x-ray diffraction pattern and SEM photo of an electropolished single crystal zinc electrode.

Zinc was subsequently deposited galvanostatically from 1.0 M $ZnCl_2$ electrolyte on electrodes prepared using the method outlined above. Typical SEM photographs are shown in Figure B.31. As with the vacuum evaporated zinc, the fine structure of the deposit prohibited analysis by the same means used in the main section of this work (this structure might consist of nodules but they must be much smaller than those treated on other substrates). For these reasons, the single crystal zinc was not employed in the nodule studies.

B.4. Zinc Cyannide Strike

The goal of this experiment was to produce reasonably smooth, pure, and reproducible zinc deposits. Smooth zinc deposits are routinely obtained in industry from cyanide baths. In this laboratory, the following solution (52) provided the best deposit.

43 g/l ZnO

52 g/l NaOH

102 g/l NaCN

The zinc was deposited at 50 ma/cm^2 and room temperature (≃25°C) on platinum polished with 1 μm diamond paste; the disc electrode was rotated at 1000 rpm. The resulting deposits had poor uniformity and reproducibility, as is evident in Figure B.40.

A brightening dip is often used in industry after deposition to level the metal's surface and make it shiny. Figure B.41 compares the condition of one of these deposits before and after dipping in a dichromate solution for 3 seconds.

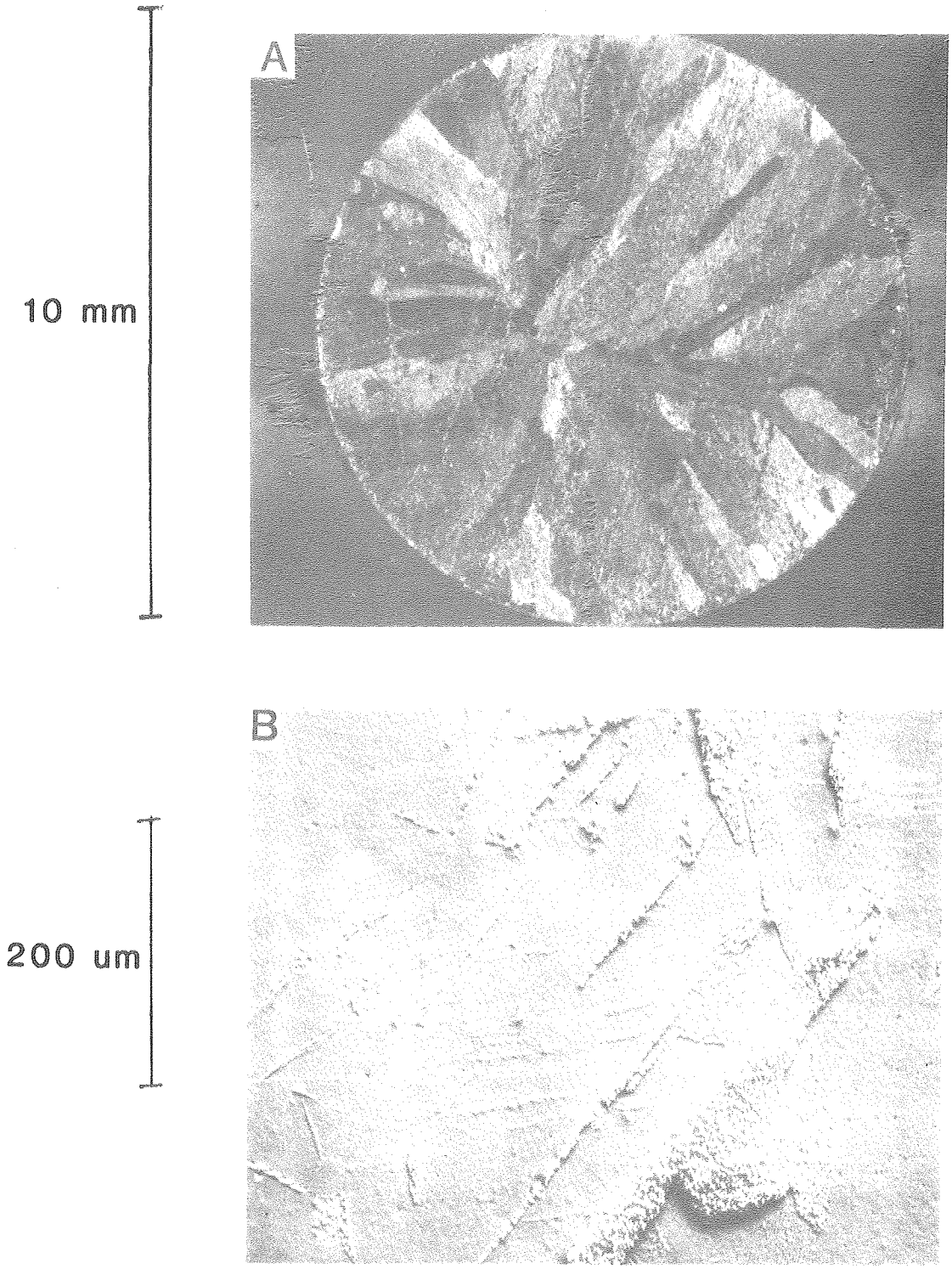

XBB 840-8636

Fig. B.10 Polycrystalline zinc electrode
a) polished (1 μm diamond paste) substrate
b) SEM photograph after deposition
2.4 mA/cm^2 x 10 minutes
1.0 M $ZnCl_2$ (MBC reagent)

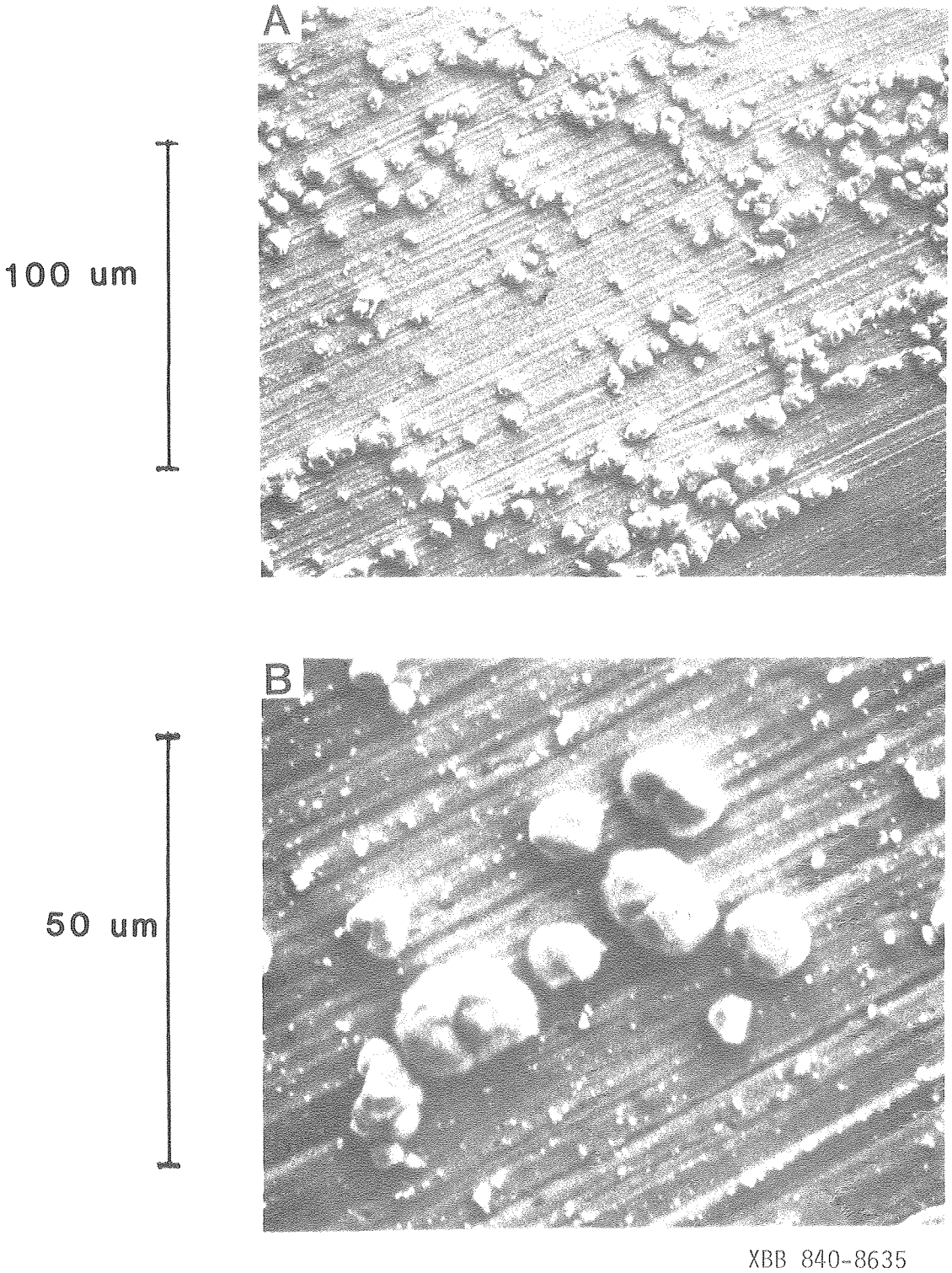

XBB 840-8635

Fig. B.11 Zinc nodules deposited on polycrystalline zinc electrode (polished with 600 grit), 36 mA/cm^2 x 30 seconds 1.0 M $ZnCl_2$ (MCB) reagent)

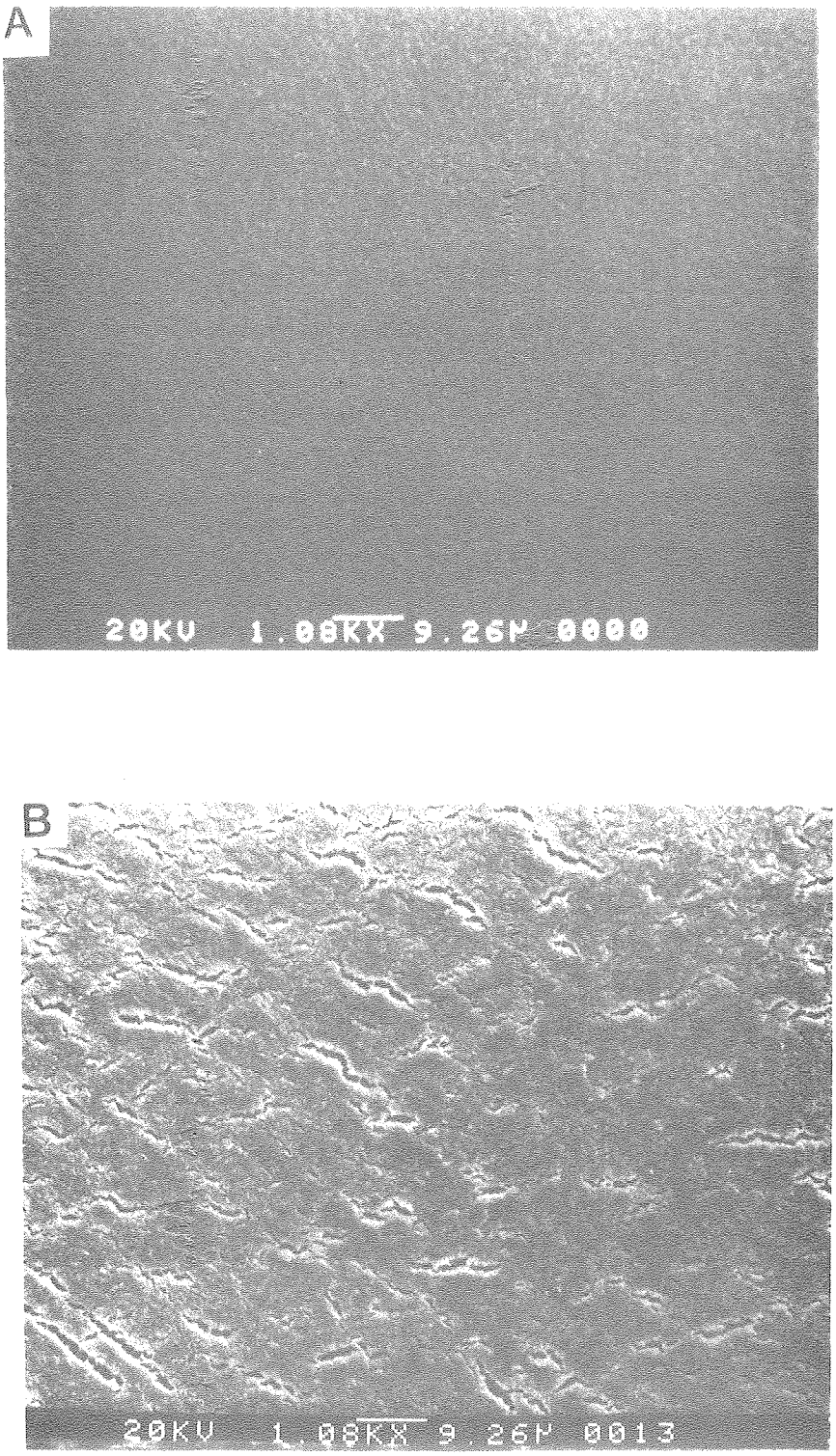

XBB 840-8637

Fig. B.20 Zinc prepared by evaporation
a) fresh
b) 8 hrs.

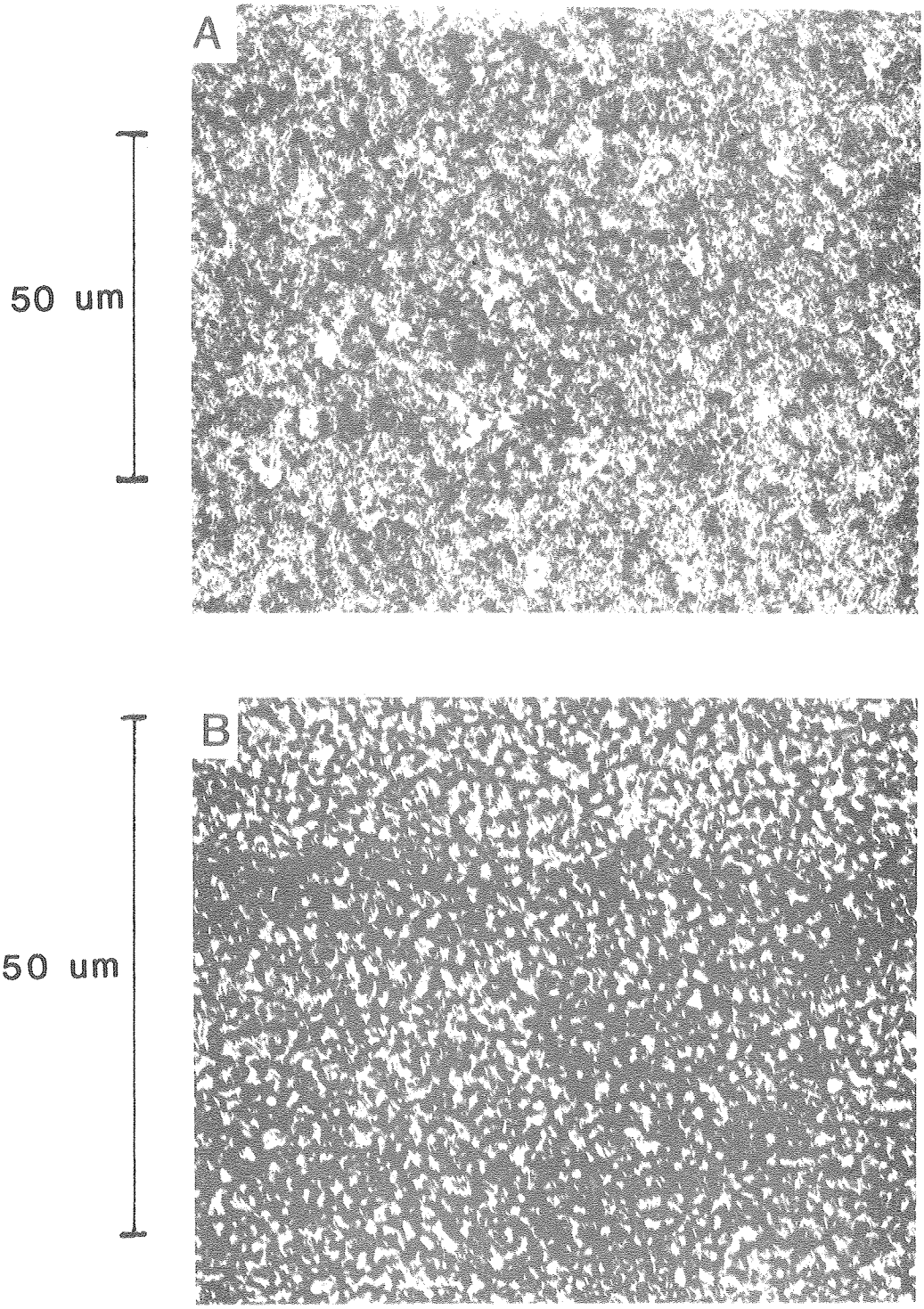

XBB 840-8626

Fig. B.21 Zinc electrodeposited on evaporated zinc
a) 36 mA/cm^2 x 30 seconds
b) 36 mA/cm^2 x 15 seconds

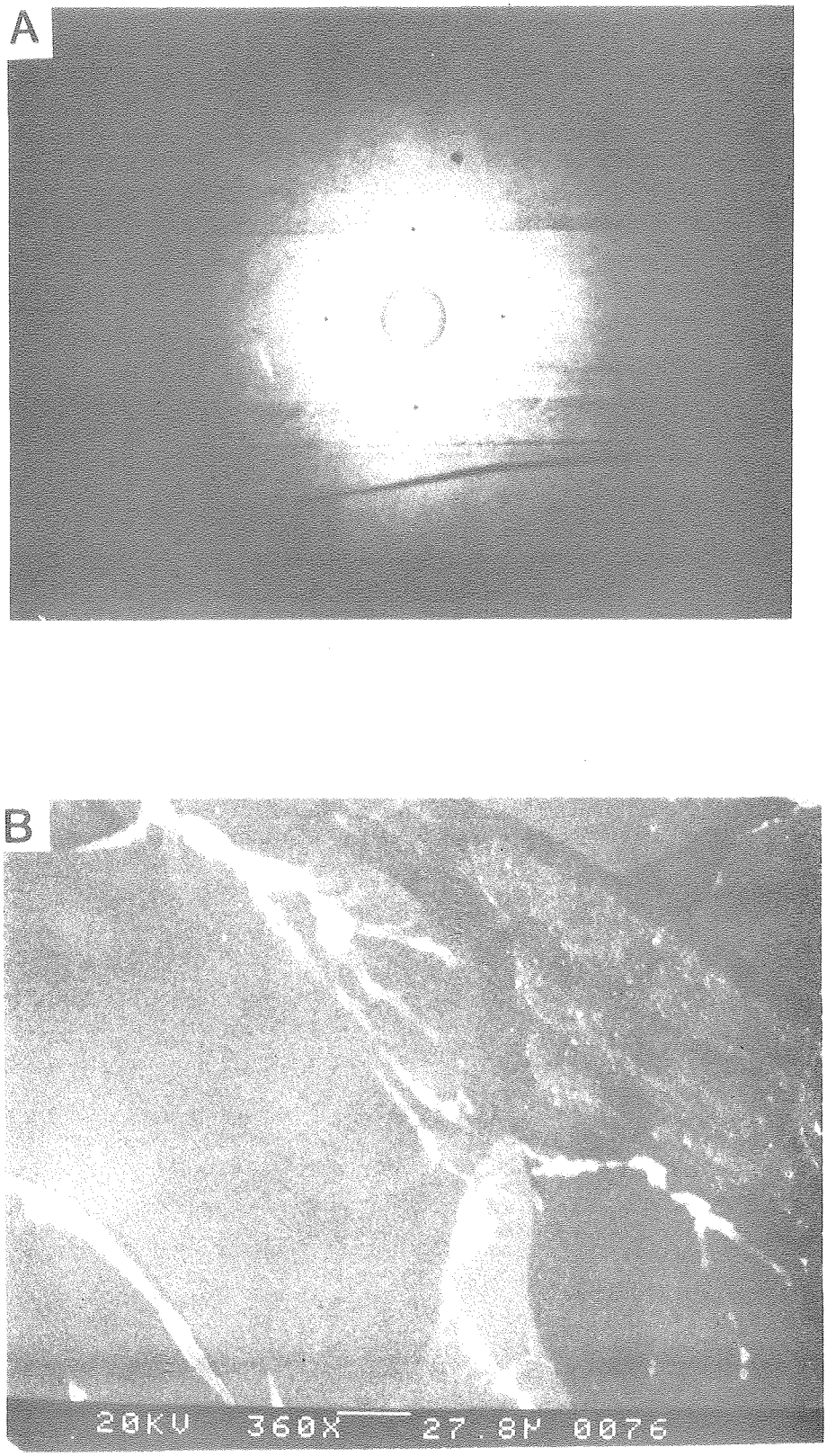

XBB 840-8640

Fig. B.30 Single crystal zinc (electropolished)
a) Laue x-ray diffraction pattern
b) SEM photograph

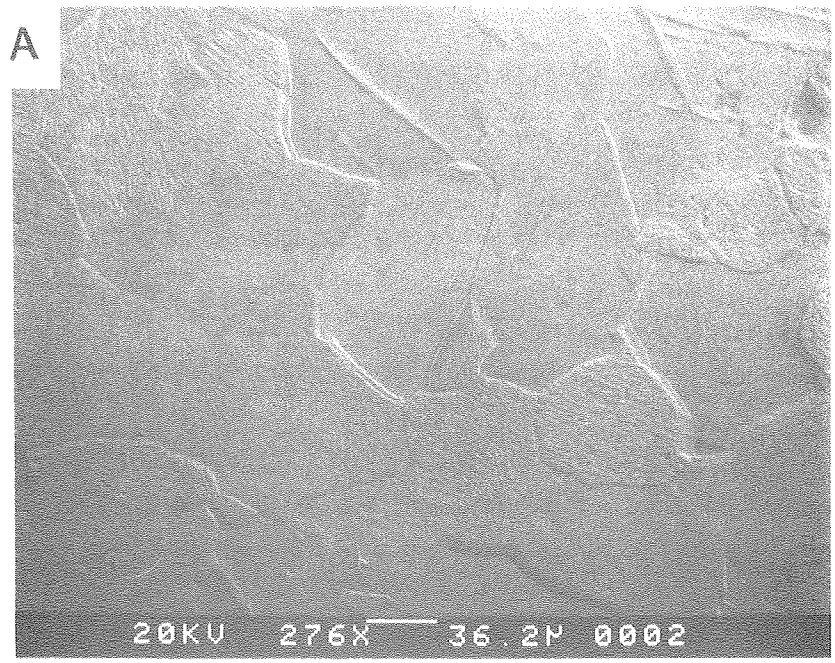

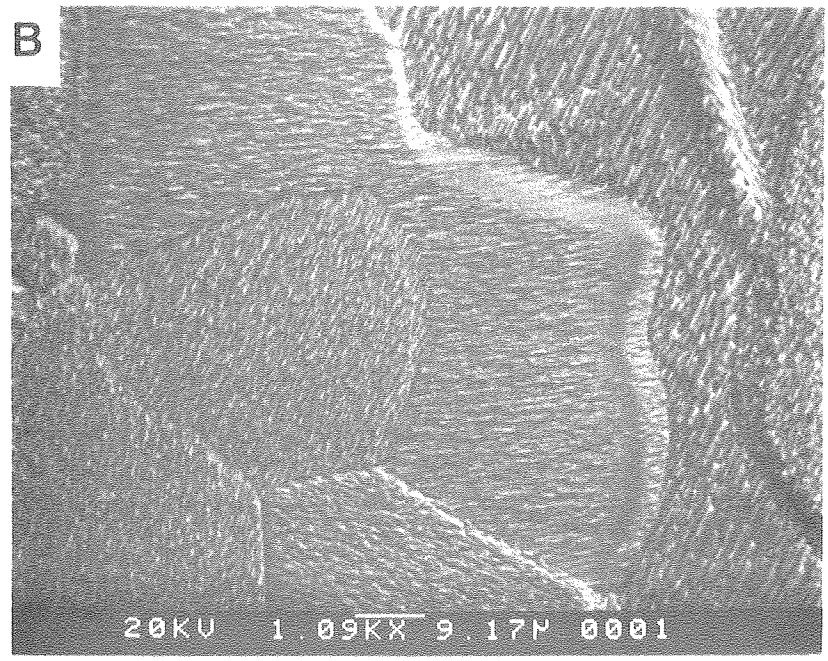

XBB 840-8639

Fig. B.31 Zinc electrodeposited on single crystal zinc
a) 30 mA/cm^2 x 42 seconds
b) 30 mA/cm^2 x 21 seconds

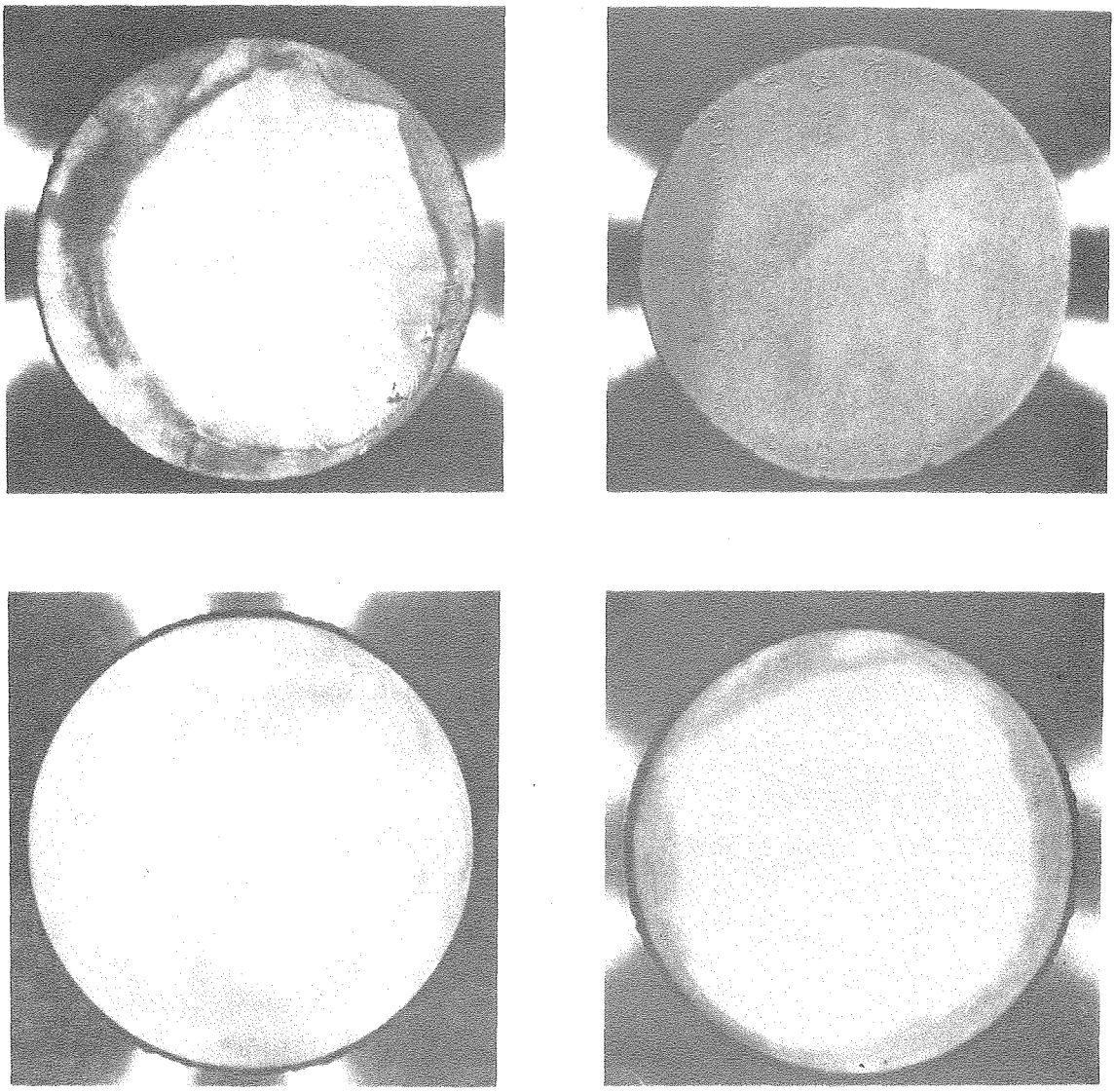

XBB 840-8633

Fig. B.40 Zinc electrodeposited from ZnCN solution

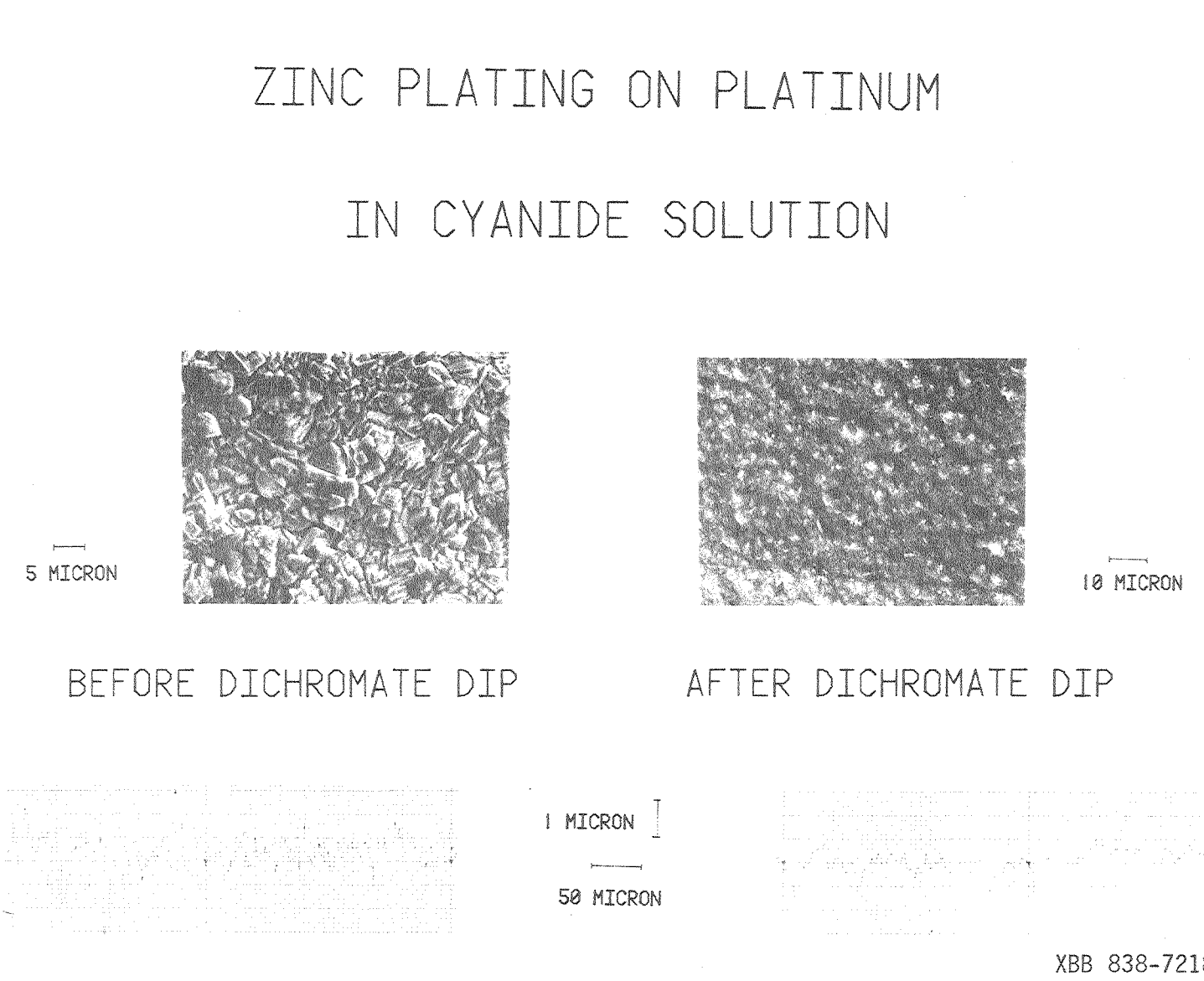

Fig. B.41 SEM photographs of zinc electrodeposited from ZnCN solution.

APPENDIX C. THE MEASURED OVERPOTENTIAL

As described in Section VI, the potential underwent a transient during galvanostatic deposition. A representative charge density, or average thickness was arbitrarily chosen for each set of experiments, at which to compare the potentials. These are outlined below.

Electrolyte	Substrate	Charge Density (milliCoulombs/cm^2)	Average Thickness (Å)
MCB	Union Carbide	500	2400
	Gould	500	2400
	platinum	500	2400
	glassy carbon	500	2400
Mallinckrodt	Union Carbide	100	470
	Gould	100	470
	graphite loaded polymer	50	240

Measured overpotential at steady state as a function of applied current density is shown for each set of experiments in Figures C.1-C.7. The potentials measured for two substrate-electrolyte combinations are particularly inconsistent. The irregular behavior of the measured potential for Gould pyrolytic graphite shown in Figure C.2 might be due to the porosity of this substrate. Also, at higher current densities (60 ma/cm^2) the potential transient is still important when q = 500 mC/cm^2.

The Exxon graphite loaded polymer substrate (Figure C.7) also exhibited inconsistent behavior, although for probably an entirely different reason. This substrate was mounted on a specially prepared replaceable substrate mount. It is not inconceivable that these electrodes may have been leaky.

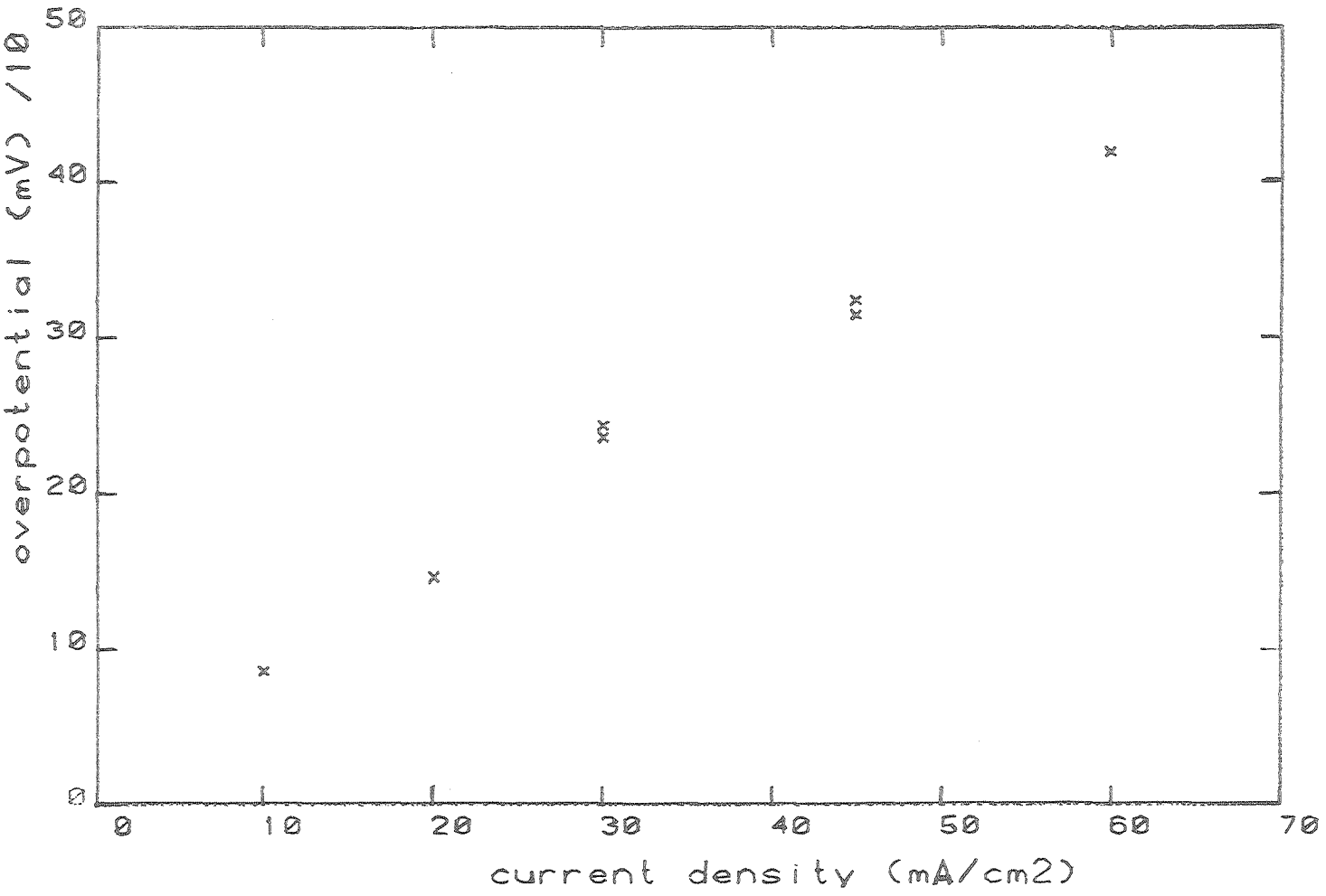

XBL 8411-4815

Fig. C.1 Overpotential measured on Union Carbide pyrolytic graphite substrate,
1.0 M $ZnCl_2$ (MCB reagent)

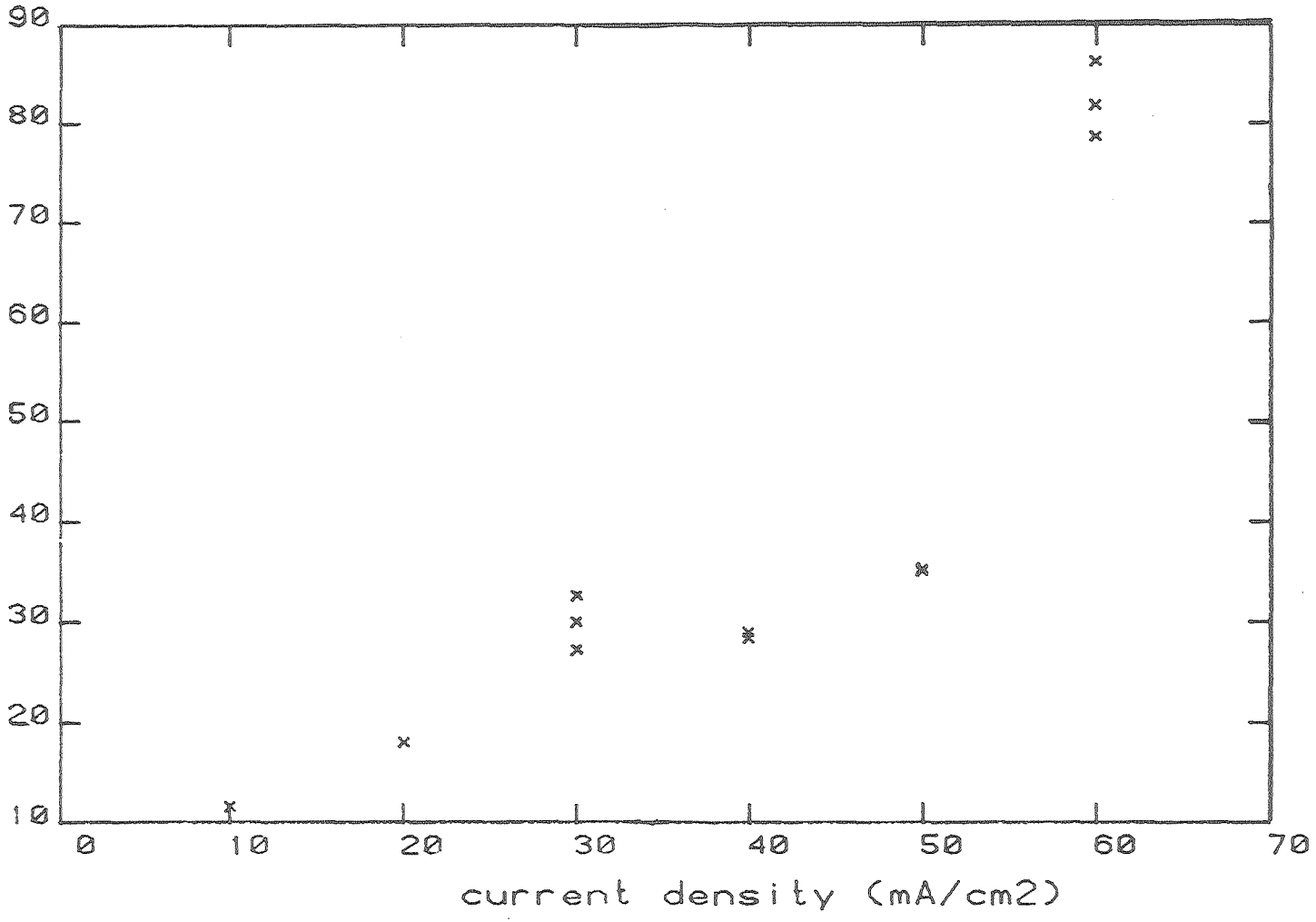

XBL 8411-4811

Fig. C.2 Overpotential measured on Gould pyrolytic graphite substrate, 1.0 M $ZnCl_2$ (MCB reagent)

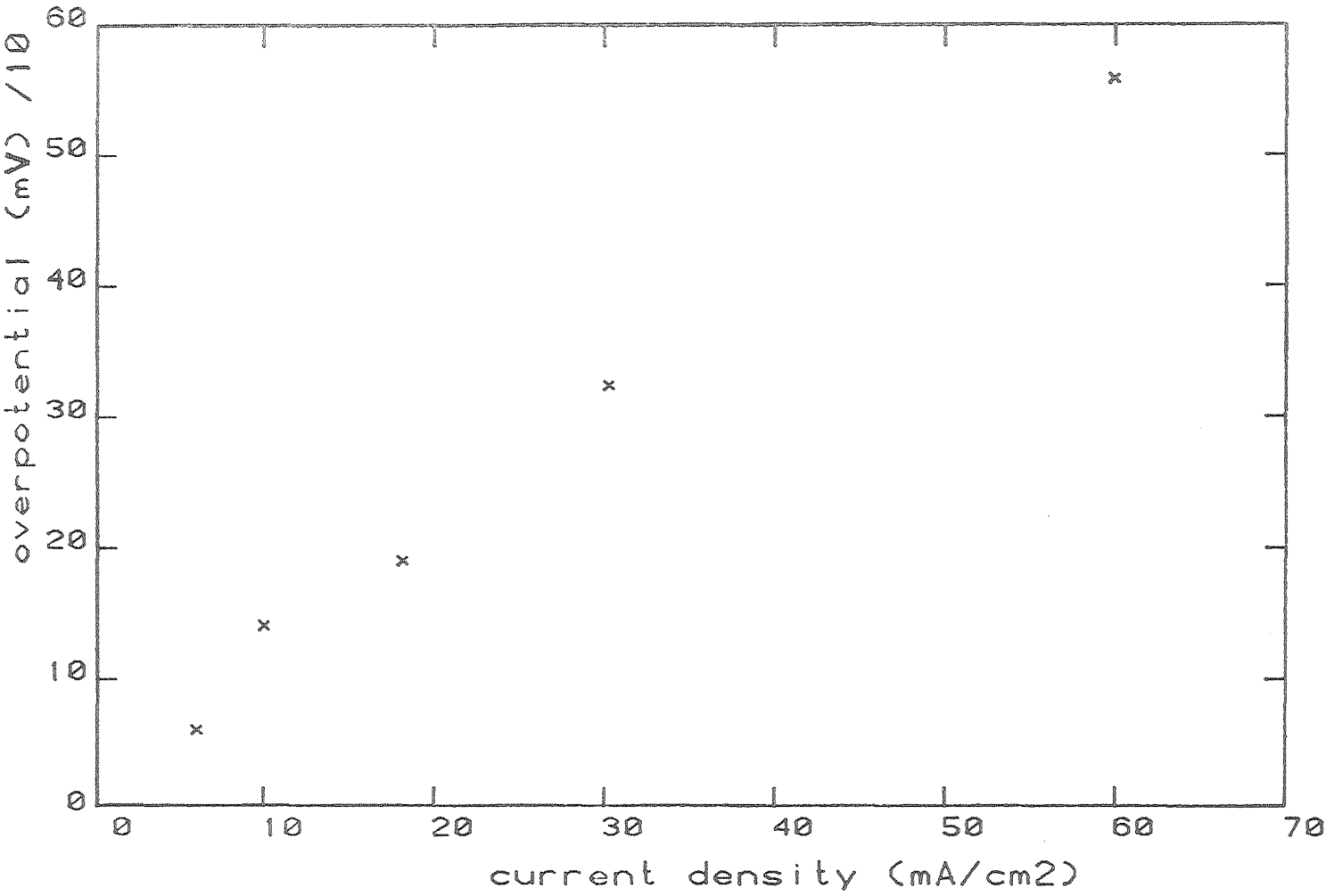

XBL 8411-4810

Fig. C.3 Overpotential measured on platinum substrate, 1.0 M $ZnCl_2$ (MCB reagent)

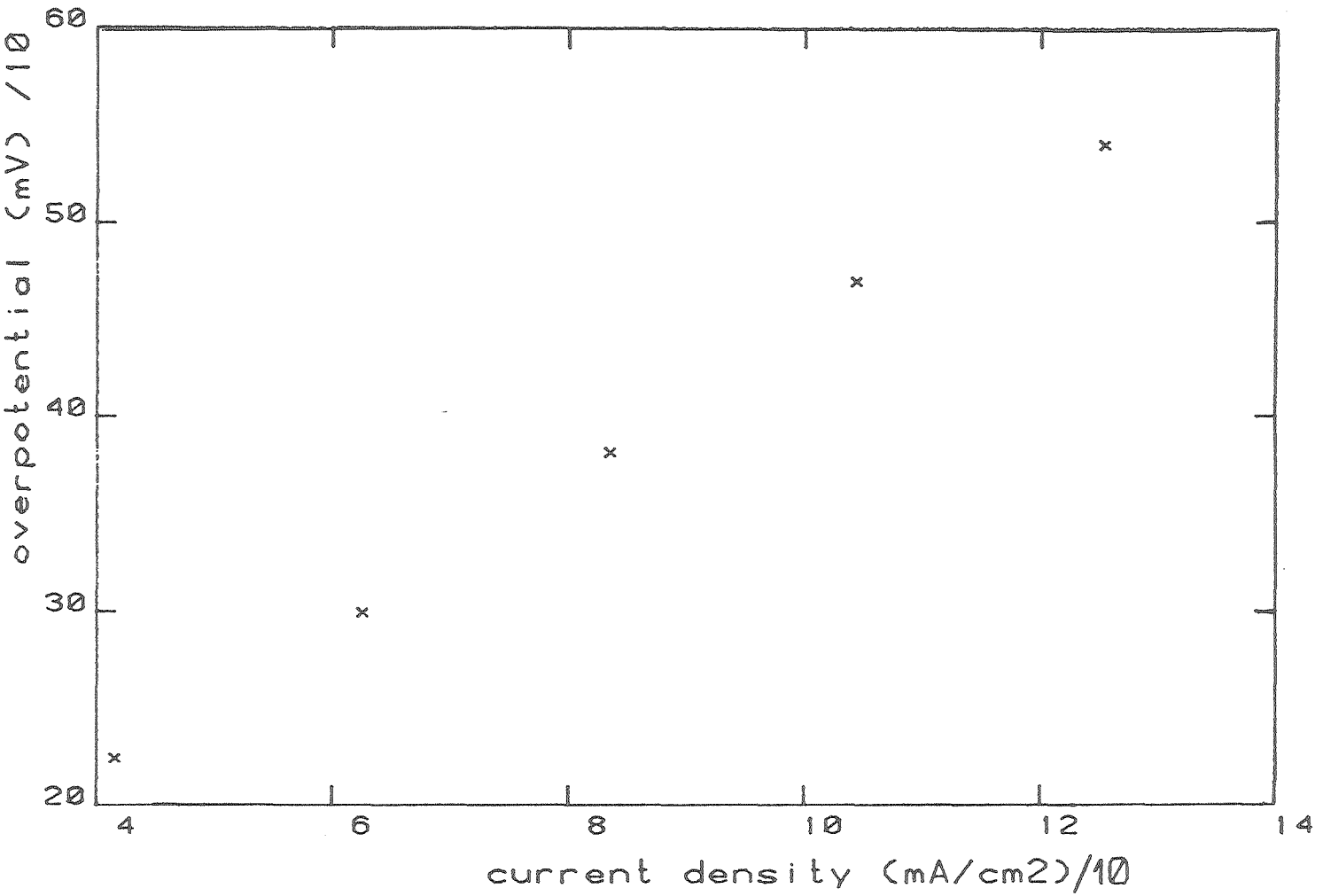

XBL 8411-4814

Fig. C.4 Overpotential measured on pine glassy carbon substrate, 1.0 M $ZnCl_2$ (MCB reagent)

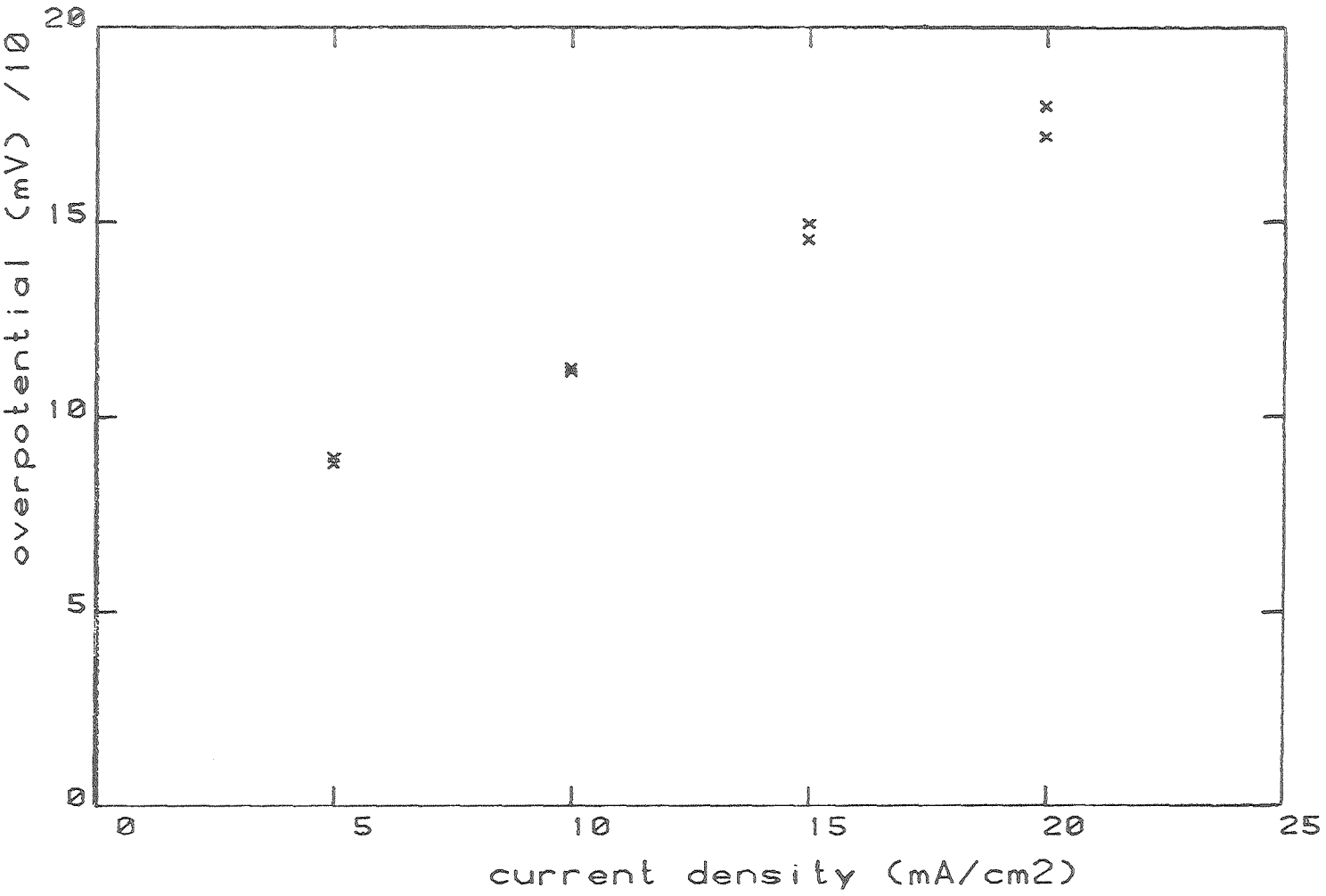

XBL 8411-4812

Fig. C.5 Overpotential measured on Union Carbide pyrolytic graphite substrate,
1.0 M $ZnCl_2$ (Mallinckrodt reagent)

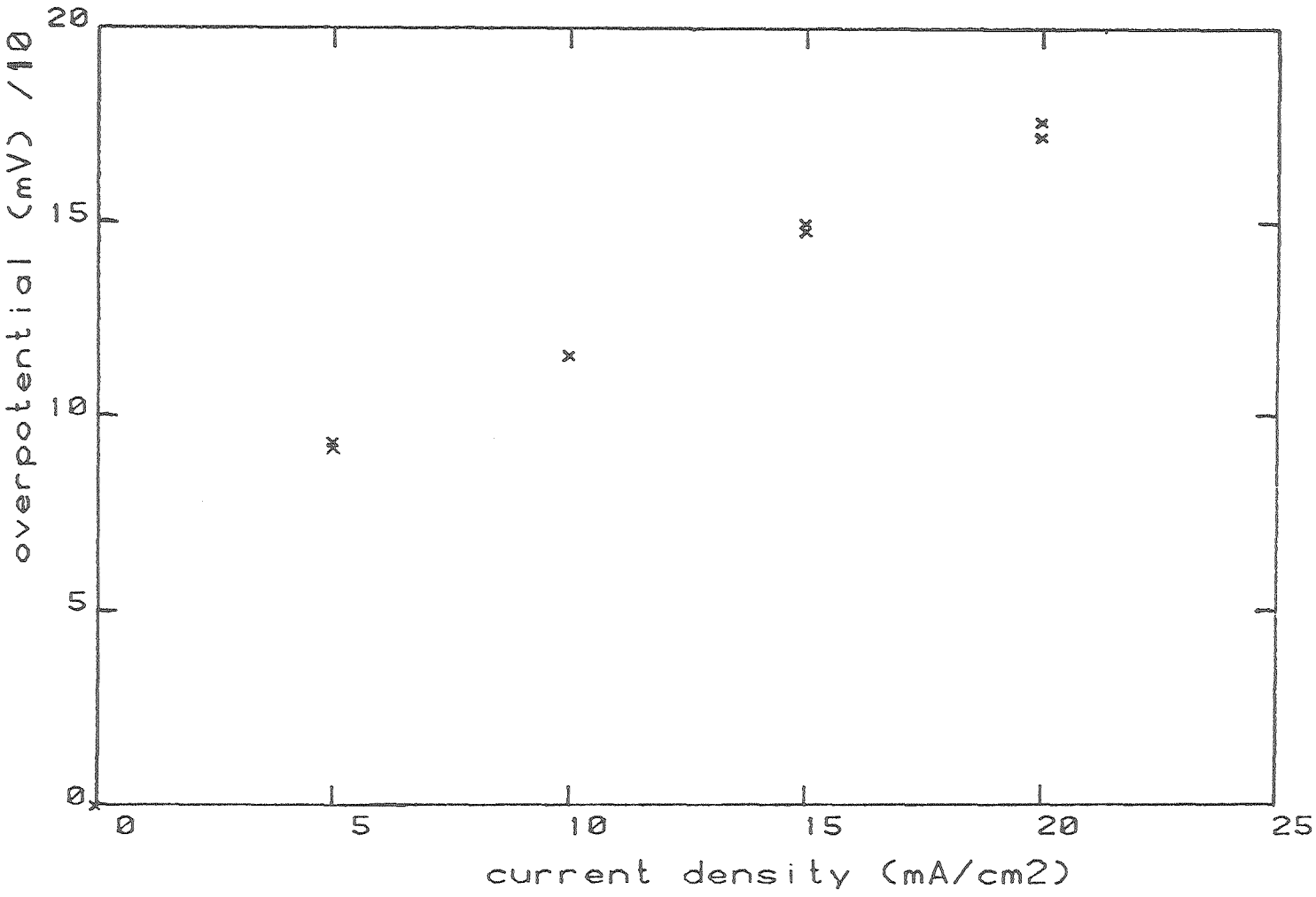

XBL 8411-4813

Fig. C.6 Overpotential measured on Gould pyrolytic graphite substrate, 1.0 M $ZnCl_2$ (Mallinckrodt reagent)

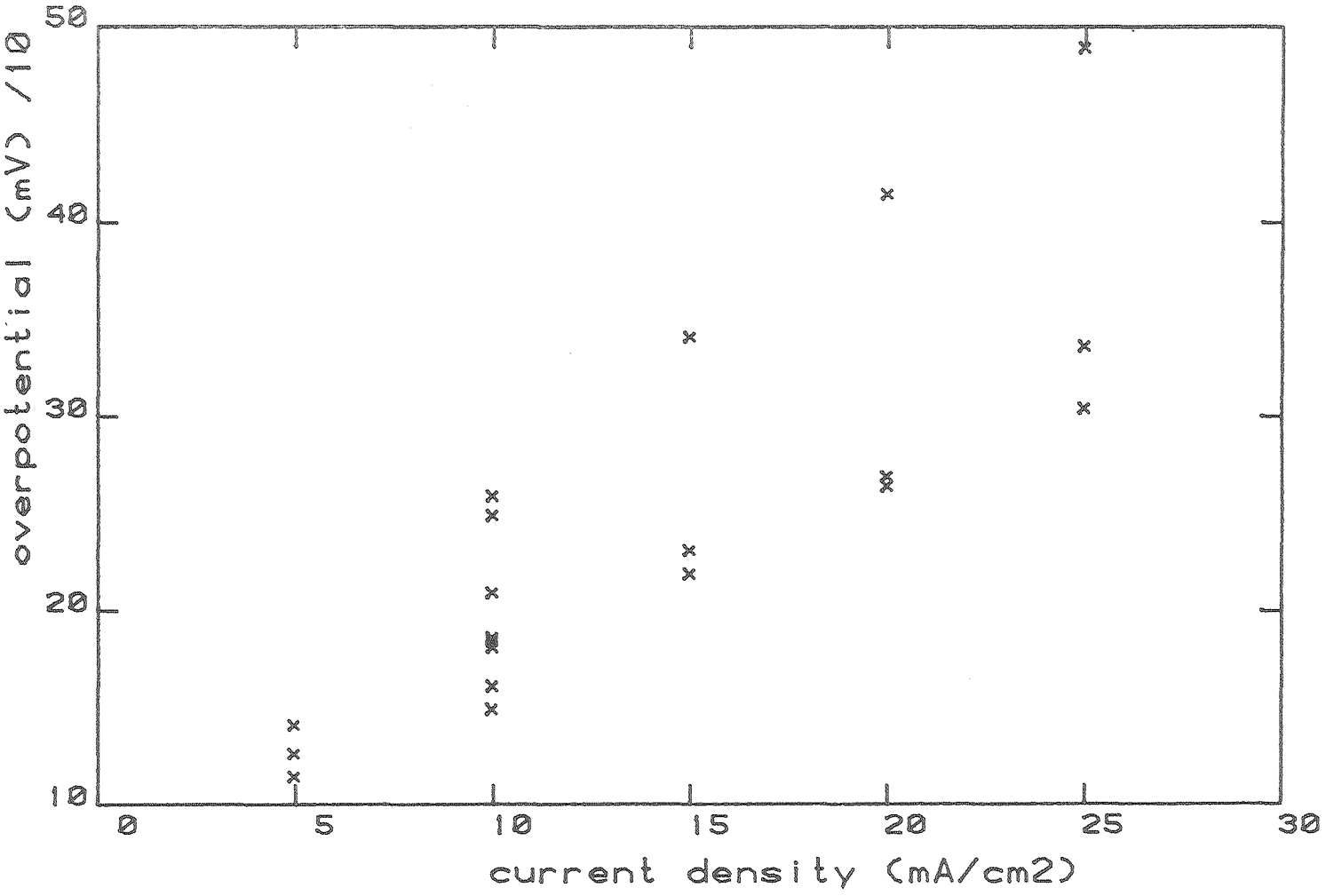

XBL 8411-4809

Fig. C.7 Overpotential measured on Exxon graphite loaded polymer substrate,
1.0 M $ZnCl_2$ (Mallinckrodt reagent)

APPENDIX D. CHOICE OF THE TERM: "NODULE"

There are innumerable references in the literature to nodules which have grown into large (1-10 μm) crystal forms. Similar formations have been referred to as "protrusions" by previous workers in this research group (6). Elsewhere, "dendrite" or "dendrite precursor" have been used (1). Since precise word usage is important in science, the relevant parts of definitions from Websters Dictionary are given below:

dendrite 1. A branching figure resembling a tree produced on or in a mineral or stone (as in the moss agate) by an oxide of manganese or other foreign mineral; also: the mineral or stone so marked. 2. A crystallized arborescent form (as of gold or silver) 3. Any of the protoplasmic processes of a nerve that conduct impulses toward the cell body and that are usually branched and comparatively short: an afferent fiber of a neuron . . .

nodule 1. A small quantity of medicinal material tied up in a bag or bit of cloth. 2. A small rounded mass of irregular shape: a little lump: as a) a small rounded bud or gemma 2) a thickening on the valve of a diatom 3) one of the swellings on the roots of a leguminous plant that contains symbiotic bacteria; c) the nodulus of the cerebellum; d) a small abnormal protuberance . . .

protrusion Protuberant: 1. Bulging beyond the surrounding or adjacent surface. PROMINANT. 2. Forcing itself into conciousness (obtrusive) . . .

Of these possibilities, the word "nodule" was chosen to best describe the phenomena studied.

APPENDIX E. EFFECT OF POOR SUBSTRATE PREPARATION ON NODULE FORMATION

Electrochemical experiments are inherently sensitive to impurities on the surface. Consequently, electrode preparation methods critically affect the character of the resulting electrodeposit. SEM photographs of a poor zinc deposit on a glassy carbon electrode are shown in Figure E.10.

Glassy carbon was the most difficult substrate on which to obtain a satisfactory deposit. This was due in part to its non-porous nature. The deposit shown in Figure E.10 was probably globular because a contaminant, acting as a surfactant, was not removed from the surface sufficiently.

The development of a reproducible preparation technique was the first major task undertaken in this study. The methods which worked best are outlined in the Experimental section in the main body of this report.

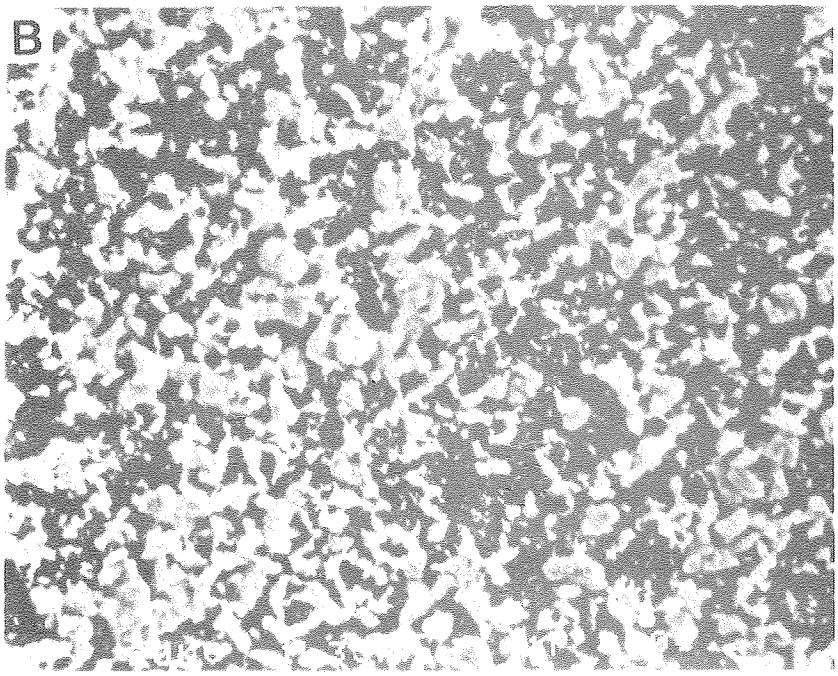

XBB 840-8638

Fig. E.10 Zinc electrodeposited on glassy carbon
42 mA/cm^2 x 22.5 seconds

APPENDIX F. ESTIMATION OF LIMITING CURRENT

Throughout this work it has been assumed that no substantial depletion of the reacting zinc species occurs at the electrode. In other words, it was assumed that the range of current densities applied in this study were well below the limiting current. In this section we will show how valid an assumption this is.

The diffusion limiting current is given by (54):

$$i_l = 0.62 \times n \times F \times (D)^{2/3} \times (\omega)^{1/2} \times (\nu)^{-1/6} \times C_b \qquad (F.1)$$

where:

n = faradays per mole of species electrolyzed

F = 96500 Coulombs/mol equiv.

D = diffusivity, cm^2/sec

w = angular velocity, rad/sec

v = kinematic viscosity, cm^2/sec

C_b = bulk concentration of electroactive species, mol/cm^3

For zinc electrodeposition on a disc electrode rotated at 1000 rpm in 1.0 M $ZnCl_2$, the following values apply.

n = 2 mol equiv/mol

$D \simeq 0.4 \times 10^{-5}$ cm^2/sec

$v \simeq 10^{-2}$ cm^2/sec

$w \simeq 105$ rad/sec

$C_b = 10^{-3}$ mol/cm^3

From these values, Equation (F.1) predicts that

$i_l = 660\ ma/cm^2$.

In this study, the current density was usually much lower than 60 ma/cm^2. This means that we operated at a current density which was less than 10% of the limiting current.

This value is, however, only an estimate. Significant complexing occurs in the $ZnCl_2$ system, where some species would migrate away from the cathode (i.e., $ZnCl_3^-$, $ZnCl_4^{--}$) (2,53). The migration of these species would reduce the value of the limiting current given above.

APPENDIX G. SENSITIVITY OF CURRENT DISTRIBUTION TO CHOICE OF EXCHANGE CURRENT DENSITY

In Section V values were presented for the local current density and surface overpotential at the center of the disc electrode. The local current density was calculated by assuming i_o = 1 ma/cm^2, $\alpha_a = \alpha_c = 0.5$, using Newman's analytical treatment of the current distribution on a rotating disc electrode (27).

The kinetic parameters indicated above are best estimates. It should be instructive to assess the sensitivity of the current distribution to the choice of these parameters. Figure G.1 relates the current density at the center of a disc electrode to the exchange current density for $\alpha_a = \alpha_c = 0.5$ at the indicated average current densities.

i average: 10 mA/cm2

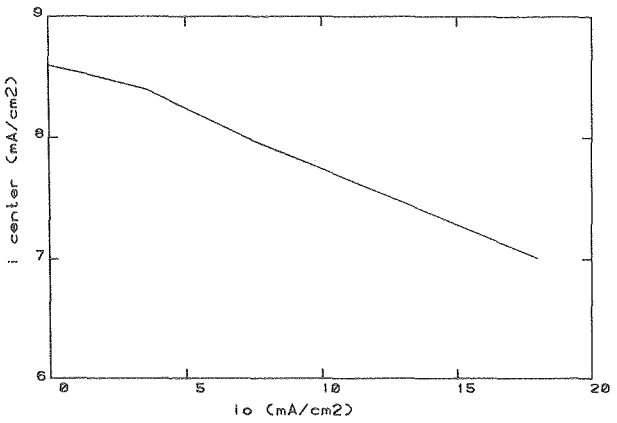

i average: 35 mA/cm2

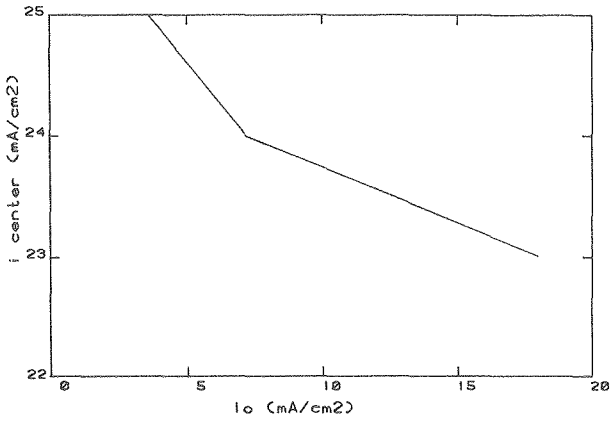

i average: 60 mA/cm2

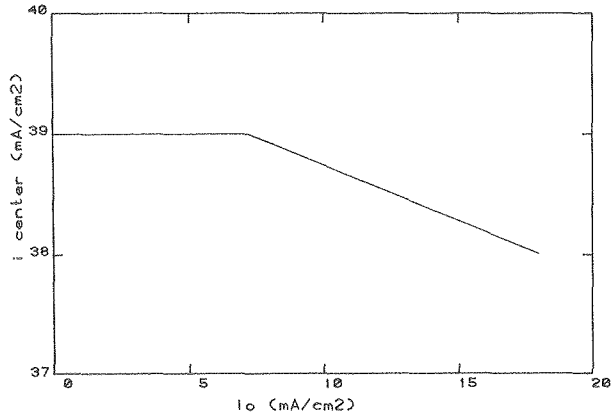

XBL 8410-4597

Fig. G.1 Effect of exchange current density on current density at center of disc

APPENDIX H. CHEMICAL ANALYSIS OF $ZnCl_2$ REAGENTS

The elemental impurity analyses were performed on a Perkin-Elmer Atomic Adsorption Spectrometer Model 360 by Tom Morrison in the Chemical Analysis Services Laboratory, College of Chemistry, University of California, Berkeley.

Table H.1* gives results of analyses on two 1.0 M $ZnCl_2$ samples prepared from the Mallinckrodt reagent salt. Results were obtained using the flame atomizer in the spectrophotometer; results from the graphite furnace atomizer, which has a higher sensitivity but lower precision, are reported only when an impurity is undetectable by the former method. The concentrations in the table are reported in units of ug/cc which are roughly equivalent to ppm.

Table H.2 gives results of an analysis of 1.0 M $ZnCl_2$ prepared from the MCB reagent salt. The considerations covered above apply to this table as well.

---

*The information presented in Table H.1 was extracted from data reported by J. Faltemier (2).

Table H.1. Chemical Analysis of 1.0 M $ZnCl_2$ Prepared from Mallinckrodt Reagent Salt.

		ug/cc		
Impurity	Test	Sample 1	Test	Sample 2
Pb	flame	0.70	gr.fur.	>0.001
Fe	gr.fur.	<0.001	gr.fur.	<0.001
Mn	flame	0.07	gr.fur.	>0.001
Ni	gr.fur.	>0.005	gr.fur.	>0.005
Cd	flame	0.47	gr.fur.	>0.0004
Sb	flame	<0.4	flame	<0.4
Co	flame	<0.04	flame	<0.04
Mo	flame	<0.4	flame	<0.4

Table H.2. Chemical Analysis of 1.0 M $ZnCl_2$ Prepared from MCB Reagent Salt.

Impurity	Test	ug/cc
Pb	flame	0.3
Fe	gr.fur.	<0.01
Sb	gr.fur.	<0.005

REFERENCES

1) U. Landau, Project Coordinator, "Zinc Electrodeposition and Dendritic Growth from Zinc Halide Electrolytes," Final Report, Electric Power Research Institute, May 1982, Report No. EPRI EM-2393.

2) James Faltemier, "The Effect of Hydrodynamic Flow on the Morphology of Electrodeposited Zinc," Ph.D. Thesis, University of California--Berkeley, Report No. LBL-16485, August 1983.

3) D.L. Douglas, "Status Review of Zinc/Chloride Batteries," Proceedings of the EPRI/LBL Workshop on the Electrochemistry of Zinc/Halogen Batteries, November 30 and December 1, 1983.

4) D.L. Douglas, Project Manager, "Development of Zinc Chloride Battery for Utility Applications," Interim Report, Electric Power Research Institute, June 1983, Report No. EPRI EM-3136.

5) K. Yee and J. Jorne, "Striated Zinc Electrodeposition on Rotating Disc and Hemisphere Electrodes," (extended abstract).

6) Tetsuaki Tsuda, "The Influence of Lead Ions on the Macromorphology of Electrodeposited Zinc," University of California--Berkeley, Report No. LBL-13057, September 1981.

7) J. McBreen and E. Gannon, "Zinc Electrode Morphology in Acid Electrolytes," Brookhaven National Laboratory, Annual Report on Subcontract P.O. #4516210.

8) J. McBreen, Personal Communication: May, 1984.

9) H.B. Alcazar and J.A. Harrison, Electrochemica Acta, 22, 627 (1977).

10) E. Raub and A. Knodler, Trans. Inst. Metal Finish, 38, 131 (1961).

11) I.N. Justinijanovic and A.R. Despic "Some Observations on the Properties of Zinc Electrodeposited from Alkaline Zincate Solutions," Electrochem. Acta, 18, 709 (1973).

12) D. Rajhenbah, J. Faltemier and C.W. Tobias, "Mass Transfer Limiting Currents for Zinc Deposition in Acidic $ZnCl_2$ and $ZnSO_4$ Solutions," Report No. LBL-15338, October 1983.

13) T. Hurlen and K.P. Fischer, "Kinetics of Zn/Zn(II) Reactions in Acidified Solutions of Potassium Chloride," J. Electroanal. Chem. 61, 165 (1975).

14) H.B. Sierra Alcazar and J.A. Harrison, "The Rate of Zinc Deposition at Zinc Amalgam and Zinc Metal," Electrochim. Acta, 22, 627 (1977).

15) J.T. Kim and J. Jorne, "The Kinetics and Mass Transfer of Zinc Electrode in Acidic Zinc-Chloride Solution," J. Electrochem. Soc., 127, 8 (1980).

16) M.A. Edmund and R.E. White, Ext. Abstr. 80-1, p. 1249, The Electrochemical Society, Princeton, N.J. (1980).

17) Allan Hauser, "The Corrosion of a Zinc Rotating Disc in 1 Molar Hydrochloric Acid," Masters Thesis, University of California--Berkeley, Report No. LBL-17461, June 1984.

18) L.W. Oeholm, Suom. Kem. Tiedon., 46, 18 (1937).

19) A. Agnew and R. Patterson, J. Chem. Soc. (Far. Trans. I), 74, 2896 (1978).

20) D. Miller and J. Rard, "Transport in Aqueous Battery Systems," Lawrence Livermore National Laboratory, Contract Final Report, December 31, 1981.

21) J. Chamberlin, "Status of Zinc/Bromine Batteries," Proceedings of the EPRI/LBL Workshop on the Electrochemistry of Zinc/Halogen Batteries, November 30 and December 1, 1983.

22) Normar Industries: Company Literature, Anaheim, CA (1983).

23) P. Grimes and K. Newby, Exxon Research and Engineering, Personal Communication, July 1983.

24) Craig Smith, "Ellipsometry of Anodic Film Growth," University of California--Berkeley, Report No. LBL-8082, August 1978.

25) S. Fletcher, R. Deutscher, C. Harvey, R. Woods, E.J. Frazer, T. Lwin, G. Nelson, and D. Gates, "Zinc Battery Electrodes," CSIRO Institute of Earth Resources, Division of Mineral Chemistry, Semi-Annual Progress Report No. 2, November 1981.

26) R. Lacmann and H. Randig, "Electrolytic Nucleation of Copper and Brass on Platinum Single Crystal Spheres," Journal of Crystal Growth, 17, 97, (1972).

27) John Newman, Electrochemical Systems, Prentice-Hall, Englewood Cliffs, NJ (1973).

28) Philip Russell and John Newman, "Experimental Determination of Passive-Active Transition for Iron in 1 M Sulfuric Acid," J. Electrochem. Soc., 130, 547, (1983).

29) William H. Tiedemann, John Newman, and Douglas Bennion, "The Error in Measurements of Electrode Kinetics Caused by Nonuniform Ohmic-Potential Drop to a Disk Electrode," J. Electrochem. Soc., 120, 256, (1973).

30) M.Y. Abyaneh and M. Fleischmann, "The Role of Nucleation and of Overlap in Electrocrystallization Reactions," Electrochimica Acta., 27 (1982), pp. 1513-1518.

31) E.B. Budevski, "Deposition and Dissolution of Metals and Alloys. Part A: Electrocrystallization", in Comprehensive Treatise on Electrochemistry, Vol. 7, B.E. Conway, et.al., eds., Plenum Publishing Co., New York, to be published.

32) Von O. Essin, L. Antropov and A. Levin, "Veranderung der Elecktrodenpolarisation mit der Zeit," Acta Physicochimica U.R.S.S. , 6 (1937), pp. 445-454.

33) M. Fleischmann and H.R. Thirsk, "Anodic Electrocrystallization," Electrochimica Acta, 2 (1960), pp. 22-49.

34) M. Fleischmann and H.R. Thirsk, "Metal Deposition and Electrocrystallization," in Advances in Electrochemistry and Electrochemical Engineering, Vol. 3, P. Delahay and C.W. Tobias, eds., Interscience, New York (1963).

35) S. Fletcher and T. Lwin, "A General Probabilistic Model of Electrochemical Nucleation," Electrochimica Acta, 28 (1982), pp. 237-243.

36) Gamini A. Gunawardena, Graham J. Hills and Irene Montenegro, "Potentiostatic-Galvanostatic-Potentiostatic Study of the Deposition of Mercury on Graphite," Faraday Symposia:

Electrocrystallization and Phase Formation, 12 (1977) pp. 90-100.

37) J.A. Harrison and H.R. Thirsk, "The Fundamentals of Metal Deposition," in Electroanalytical Chemistry, Vol. 5 , J. Bockris, ed., pp. 67-149.

38) I. Markov and D. Kashciev, "Nucleation of Active Centres," J. of Crystal Growth, 16 (1972) pp. 170-176.

39) Von W.A. Rojter, W.A. Juza and E.S. Polujan, "Elektrochemische Polarisation der Metallelektroden," Acta Physicochimica U.R.S.S. , 10 (1939) pp. 389-414 and 845-858.

40) Benjamin Scharifker and Graham Hills, "Theoretical and Experimental Studies of Multiple Nucleation," Electrochimica Acta, 28 (1983), pp. 879-889.

41) D.A. Vermilyea, "Anodic Films," Advances in Electrochemistry and Electrochemical Engineering," Vol. 3, P. Delahay and C.W. Tobias. eds. Interscience, New York (1963).

42) D.A. Vermilyea, "On The Theory of Electrolytic Crystal Growth," The Journal of Chemical Physics, 25 (1956) pp. 1254-1263.

43) T. Erdey-Gruz and M. Volmer, Z. Phys. Chem. 157, 165 (1931).

44) Eric Carlson, "Electrodeposition Around Protruding Surface Imperfections in Turbulent Flow," M.S. Thesis, University of California-Berkeley, Report No. LBL-3175, January 1975.

45) Lawrence Berkeley Laboratory, MMRD Annual Report 1976, Report No. LBL-6016, pp. 427-428.

46) Lawrence Berkeley Laboratory, MMRD Annual Report 1977, Report No. LBL-7355, pp. 509-510.

47) Lawrence Berkeley Laboratory, MMRD Annual Report 1978, Report No. LBL-8580, pp. 489-490.

48) C.H. Hamann and W. Vielstich, "Elektrochemie II", Weinheim: Verlag Chemie, 1981.

49) I. Epelboin, M. Ksouri and R. Wiart, J. Electrochem. Soc., 122, 2106 (1975).

50) I. Epelboin, M. Ksouri and R. Wiart, J. Electroanal. Chem., 58 433 (1975).

51) M. Jaksic and C.W. Tobias, "Hydrodynamic Flow Visualization by an Electrochemical Method," presented September 9, 1980 in Bochum, Germany.

52) D.A. Swalheim and R.W. Mackey, "Cyanide Zinc Plating," in Modern Electroplating, 2nd ed., F.A. Lowenheim, Ed. Wiley, New York, 1963, Chap. 16.

53) J. McBreen and E. Cairns, "The Zinc Electrode," in Advances in Electrochemistry and Electrochemical Engineering, Vol. 11, H. Gerischer and C.W. Tobias, eds., John Wiley and Sons, New York (1978).

54) V.G. Levich, Physiochemical Hydrodynamics, Prentice-Hall, Inc., Englewood Cliffs, NJ, (1962).

55) J.L. Faltemier, M.M Jaksic, T. Tsuda, and C.W. Tobias, "An Inventory of Photographs of Zinc Electrodeposited from Acid Electrolytes," Report No. LBL-16601, September 1983.

This report was done with support from the Department of Energy. Any conclusions or opinions expressed in this report represent solely those of the author(s) and not necessarily those of The Regents of the University of California, the Lawrence Berkeley Laboratory or the Department of Energy.

Reference to a company or product name does not imply approval or recommendation of the product by the University of California or the U.S. Department of Energy to the exclusion of others that may be suitable.

TECHNICAL INFORMATION DEPARTMENT
LAWRENCE BERKELEY LABORATORY
UNIVERSITY OF CALIFORNIA
BERKELEY, CALIFORNIA 94720